Theses and Dissertations   Theses, Dissertations, and Senior Projects

January 2019

Inflammation Is A Common Factor Between Central And Peripheral Neurodegeneration

Brett Anthony Mcgregor

Follow this and additional works at: https://commons.und.edu/theses

INFLAMMATION IS A COMMON FACTOR BETWEEN CENTRAL AND PERIPHERAL NEURODEGENERATION

By

Brett Anthony McGregor

Bachelor of Science, University of North Dakota, (2014)

A Dissertation

Submitted to the Graduate Faculty

of the

University of North Dakota

In partial fulfillment of the requirements

for the degree of
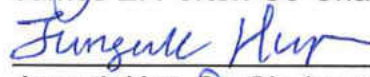
Doctor of Philosophy
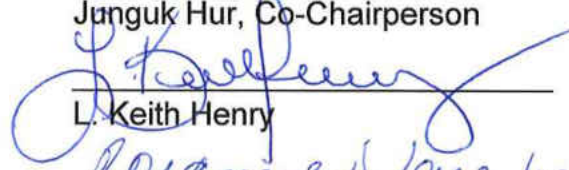
Grand Forks, North Dakota

May

2019
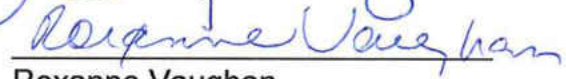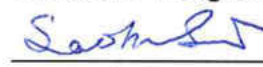
This dissertation, submitted by Brett A. McGregor in partial fulfillment of the requirements for the Degree of Doctor of Philosophy from the University of North Dakota, has been read by the Faculty Advisory Committee under whom the work has been done and is hereby approved.

_____
James E. Porter. Co-Chairperson

_____
Junguk Hur, Co-Chairperson

_____
L. Keith Henry

_____
Roxanne Vaughan

_____
Saobo Lei

_____
Peter Meberg

This dissertation is being submitted by the appointed advisory committee as having met all of the requirements of the School of Graduate Studies at the University of North Dakota and is hereby approved.

_____
Dean of Graduate School

4/24/19
_____
Date

PERMISSION

Title: Inflammation is a common factor between central and peripheral neurodegeneration

Department: Biomedical Sciences

Degree: Doctor of Philosophy

Brett A. McGregor

May, 2019

TABLE OF CONTENTS

LIST OF FIGURES

LIST OF TABLES

ACKNOWLEDGEMENTS

Jeff Boudreaux, were always there to offer advice and often took care of my dog, Addie, when I would have to work late or leave for conferences. My siblings: Chelsea Ridley, Chase Boudreaux, and Kayla Poitra as well as their families always reminded me about what really matters in times when I found myself overwhelmed. My friends Ossie Dukes, Josh Jenkins, and Adam Hesse who have been a cornerstone of my life since I was 16 were also an essential component to my success through my PhD. Although they often couldn't understand or relate to the problems I would face, they always kept me grounded and sane in difficult times. This journey would have been infinitely more difficult without the support of everyone listed above and as well as many other individuals.

ABSTRACT

The studies in this dissertation investigate neurodegenerative conditions of the central and peripheral nervous system utilizing bioinformatics and systems biology approaches. Various neurodegenerative conditions are associated with neuroinflammation or the inflammation of nervous tissue. We utilized Parkinson's disease as our system for neuroinflammation in the central nervous system and diabetic peripheral neuropathy for the peripheral nervous system. Parkinson's disease is associated with loss of dopaminergic neurons in the substantia nigra and consequent loss of dopamine signaling in the striatum of the central nervous system. Characteristics of Parkinson's Disease include symptoms such as shaking, rigidity, slowness of movement, difficulty walking, dementia, depression, anxiety, sleeping disorders, and hallmark formation of misfolded α-synuclein aggregates called Lewy bodies. Diabetic peripheral neuropathy is a microvascular complication associated with diabetes mellitus. Degeneration of the peripheral nervous system in diabetes presents as neuropathic pain in the periphery with eventual loss of sensation in a stocking and glove like pattern. The loss of sensation is an underlying cause of diabetic foot syndrome which is the leading cause of lower limb amputations.

This dissertation consists of three studies. The first study compared multiple murine models of diabetic peripheral neuropathy at different stages of

the disease against human subjects in effort to identify an underlying cause of disease using publicly available microarray transcriptomic data. Pathway and network analysis were performed in conjunction on differentially expressed genes identified by comparing healthy controls to diabetic mice and progressive to non-progressive human subjects with diabetic peripheral neuropathy. Clusters of pathways in this network were related to inflammation, degradation, apoptosis, as well as kinase and immune signaling, as conserved changes across multiple time points, models, and species of DPN. These observed pathways, commonly disrupted across progression, species, and various murine models of the disease, are likely the key responses associated with diabetic peripheral neuropathy.

The second study further investigated a single high dose streptozotocin model of type 1 diabetes mellitus by comparing tissues related to diabetic peripheral neuropathy (sciatic nerve and dorsal root ganglia) and diabetic nephropathy (renal glomerulus and cortex). RNA-sequencing identified differentially expressed genes in each complication-prone tissue between healthy controls and streptozotocin-treated mice. Genes with a conserved directional change were analyzed using network and pathway analysis. Clusters related to DNA-damage response, oxidative stress, and immune response were represented in shared genes between diabetic nephropathy and diabetic peripheral neuropathy tissue experiencing a common directional change. These cluster themes are likely key conserved disruptions in microvascular complication-prone tissue.

The third study explored neuroinflammation of the central nervous system utilizing mice overexpressing α-synuclein under the mouse thymidine1 promoter as an animal model of Parkinson's disease. This murine model exhibits parkinsonian motor and non-motor symptoms as well as α-synuclein aggregation pathology. Early activation of microglia, the resident innate immune cells of the brain, and an inflammatory response can be measured in the brains of these animals as early as one month of age. RNA and DNA were extracted from microglia isolated from these animals at 3 and 13 months of age for RNA-sequencing and reduced representation bisulfite sequencing, respectively. The time points for tissue collection involve the beginning of motor symptoms at 3 months and 13 months is immediately prior to a loss of 40% of dopamine signaling which occurs at 14 months of age. The overexpression of α-synuclein-induced both genomic methylation and gene expression changes that are indicative of an immunologically activated M1 state of microglia. Correlation between gene expression and a change in methylation status were investigated but only intronic CG rich sites held a significant correlation with observed gene expression (r=-0.15, p=0.008). Profiling the changes induced by α-synuclein provides valuable insight into the systems contributing to disease progression.

Overall, these results warrant further investigation into the role inflammation plays on the progression of neurodegenerative diseases. Our wide range of models and techniques lends strength to the notion of common immune activation pathways induced by a variety of disease insults in both the central and peripheral nervous systems.

CHAPTER I

INTRODUCTION

Preface

The topic of this dissertation is focused on bioinformatics analysis of neurodegenerative conditions in the peripheral and central nervous system and the possible contributions from interactions with the immune system. Inflammation of the nervous tissue or neuroinflammation, has been associated with many neurodegenerative conditions. However, the question of whether the immune response contributes to the cause of the disease or is an effect of the disease condition has not been determined. Elucidating the role neuroinflammation has on neurodegeneration as a cause or accelerator of disease progression would provide essential insight for understanding the pathophysiology of these debilitating conditions.

For this dissertation, three studies were conducted examining the transcriptome of both peripheral and central nervous tissue in neurodegenerative conditions. The first study compares the transcriptome of nerve biopsies from patients with diabetic peripheral neuropathy (DPN) to sciatic nerve tissue from various animal models of diabetes at different stages of DPN. This study attempts to uncover a possible shared mechanism of injury in DPN across progression of disease, types of diabetes, and species in order to identify new

therapeutic targets to treat DPN. The second study addresses the question of gene expression changes as a result of vascular complications by examining common differentially expressed genes in both DPN and diabetic nephropathy in an STZ model of Type 1 Diabetes Mellitus (T1DM). The third study provides the jump from peripheral nervous system (PNS) into the central nervous system (CNS) by examining methylation and gene expression changes in a prominent type of immune cell of the brain, microglia, from an animal model of Parkinson's Disease.

Neuroinflammation

The concept of neuroinflammation is by definition inflammation of nervous tissue often referring to the central nervous system (CNS). The CNS is considered immunologically privileged since peripheral immune cells are blocked by the blood-brain barrier (BBB). The BBB is composed of astrocytes, pericytes, and endothelial cells. The CNS has resident immune cells that play roles in homeostasis and tissue repair as well as protect from infection. These cells include microglia, astrocytes, and oligodendricites. Pio del Rio Hortaga was the first to distinguish between microglia, oligodendrocytes, and astrocytes in the central nervous system[1–3]. The inflammatory response is often initiated by microglia which become activated by sensing pathogen or damage-associated molecular patterns (PAMPs and DAMPs). Microglia then excrete cytokines and chemokines which activate astrocytes and recruit other microglia. Not only can this form a pro-inflammatory feedback loop between glia, but cytokines such as TNF-α, IL-1β, IL-1α, C1q, and IL-6 may directly induce apoptosis in resident

2

neurons and oligodendrocytes[4–8]. In most cases this inflammatory state is resolved naturally once the infection has been removed or tissue damage repaired. Sustained inflammation suggests either a persistent stimulus or a failure in resolution and may result in production of neurotoxic factors amplifying disease conditions. This sustained inflammation has been implicated in multiple neurodegenerative diseases, including but not limited to, Alzheimer's Disease (AD), Parkinson's Disease (PD), multiple sclerosis (MS), and amyotrophic lateral sclerosis (ALS)[9–12].

Cellular Response to Inflammation in the CNS

Rudolf Virchow first proposed the idea of neuroglia in 1856; however, Robert Remak is widely thought to be the first to include images of glia structures in his figures as far back as 1838[13]. Microglia are a type of glia cell that form the front line of defense as resident macrophages of the innate immune system in the brain and spinal cord. Microglia hold an essential role in the maintenance and homeostasis of tissue as well as their role in response to infection and injury. In a resting state, microglia exhibit a deactivated phenotype and produce anti-inflammatory cytokines and neurotrophic factors[14]. Microglia switch to an activated state in response to cellular injury or recognition of foreign material and in such cases, produce pro-inflammatory cytokines to induce an inflammatory response. Activated microglia recruit astrocyte's participation in the inflammatory response by secreting IL-1α, TNFα, and C1q, which together induce reactive astrocytes[15].

Astrocytes often present a star-shape with many processes extending from the cell body and are commonly identified by their expression of glial fibrillary acidic protein (GFAP)[16]. These cells are involved in a wide variety of brain functions such as BBB maintenance, axon guidance during development, provisioning of nutrients, and the repair process in response to injury or inflammation[17]. The role of astrocytes in CNS regeneration are not well understood, but upon injury, they will fill the space to form a glial scar, which is required for regeneration to occur[18]. However, reactive astrocytes during inflammation lose their neuroprotective status and instead induce death in both oligodendrocytes and neurons[15].

Oligodendrocytes surround the axons of neurons with their processes similar to a Schwann cell in the PNS. Their main function is to insulate and support axons by creating the myelin sheath which increases impulse speed and decreases ion leakage[19]. Oligodendrocytes also contribute to the local cell environment by producing glial cell line-derived neurotrophic factor (GDNF), brain-derived neurotrophic factor (BDNF), and insulin-like growth factor (IGF-1). However, these cells still play an active role during inflammation by secreting cytokines as well as communicating with other glial cells[20,21]. These cells are vulnerable to an inflammatory environment, which can lead to apoptosis of oligodendrocytes affecting myelination of neurons as well as the cellular microenvironment[21].

Neurons are electrically excitable cells that receive, process, and transmit information using electrical and chemical signals transmitted through specialized

connections called synapses. The communication between neurons is how all information in the CNS is processed, including motor, sensory, and cognitive information. This communication can be either electrical neurotransmission, between two neurons at the electrical synapse, or chemical neurotransmission, where neurotransmitters cross the synaptic cleft between neurons and act as a chemical messenger[22]. An inflammatory environment can disrupt plasticity and excitability in neurons and interfere with endoplasmic reticulum stress pathways. Cell recruitment through inflammation has been shown to increase the progression of neurodegenerative diseases. In PD multiple inflammatory mediators such as reactive oxygen species, nitrous oxide, tumor necrosis factor-α, and interleukin-1β, have all been shown to modulate the progression of dopaminergic cell loss[23,24]. Further evidence supporting the role an inflammatory response can have in PD is the lipopolysaccharide (LPS)-induced model of PD, which displays dopaminergic neurodegeneration[25].

Parkinson's Disease

Parkinson's Disease (PD) is the second most common neurodegenerative disease appearing in nearly 1% of the population over 50 years old[26]. James Parkinson first described what would become known as Parkinson's Disease in his *Essay on the Shaking Palsy* back in 1817[27]. PD is a neurodegenerative condition demonstrating intraneuronal protein aggregates referred to as Lewy bodies and early death of dopaminergic neurons in the substantia nigra which leads to a dopamine deficiency in the basal ganglia[28]. This deficiency leads to a movement disordered characteristic of PD with tremors, bradykinesia, rigidity,

and postural instability[29]. The onset of these symptoms is typically not apparent until approximately 80% of dopamine has been depleted and 60% of dopaminergic neurons in the substantia nigra are already lost[30–32]. Non-motor symptoms are also recognized with PD such as executive dysfunction, increased risk of dementia, difficulty with impulse control, hallucinations, depression, and anxiety[33]. PD is diagnosed based on medical history, signs and symptoms, and a neurological examination while successful improvements under medication often confirm the diagnosis[34].

Lewy bodies (LBs) are not only associated with PD but can also be seen in patients with dementia with LBs, multiple systems atrophy, and some other disorders[35]. These protein aggregates are composed of α-synuclein, ubiquitin, neurofilament, alpha B crystalline, and sometimes Tau[36]. LBs are mainly thought to be in dopaminergic neurons in the substantia nigra of PD patients. However, at late stages of disease they can also be found in noradrenergic, serotonergic, and cholinergic systems as well as the cerebral cortex, olfactory bulb, and autonomic nervous system[37]. The role LBs have in PD is not fully understood. They have served as prediction sites for neuronal loss and proposed as a major correlative factor in cognitive impairment[38]. However, recent studies have also suggested that the fibrillary aggregates may be protective against the toxic oligomer and protofibril forms of α-synuclein[39–41].

Treatments and Proposed Causes

Treatments for PD aim to replace the loss of dopamine. Carbidopa-levodopa is the most commonly prescribed treatment. Levodopa provides the

dopamine precursor so that more dopamine may be produced while carbidopa inhibits the peripheral metabolism of levodopa so that it may be delivered to the brain[42]. This is often given with an inhibitor to monoamine oxidase B (MAOB) and catechol O-methyltransferase (COMT) to slow the metabolism of active dopamine. Dopamine agonists have also been used to treat the symptoms of PD and while they often aren't as effective as levodopa they may last longer and help to reduce the on-off effect of levodopa[33]. Deep brain stimulation has been an effective surgical treatment providing advanced stage patients with sustained benefit[43]. Non-motor symptoms are also targeted by pharmacological agents used for their associated symptoms, such as erectile dysfunction being treated with sildenafil citrate or isosmotic macrogol treating constipation[44]. Current treatments involve targeting symptoms of PD rather than slowing or stopping the progression of the disease since the cause and contributing factors are not well defined.

The current hypotheses concerning causative factors in PD revolve around environmental toxins, genetic factors, and oxidative stress. The environmental hypothesis proposes that exposure to dopaminergic neurotoxins lead to PD related neurodegeneration. This began when it was found that people using 1-methyl-4-phenyl-1,2,3,6-tetrahydropyridine (MPTP) develop a condition very similar to PD[45]. Other insecticides and herbicides such as rotenone or paraquat can also act as a dopaminergic neurotoxin[46,47]. This review outlines studies that have shown living in a rural environment with greater exposure to these chemicals increases the risk for developing PD[48]. Environmental factors

7

that play a protective role from PD have also been identified such as smoking cigarettes, drinking coffee, non-steroidal anti-inflammatory drug use, and use of calcium channel blockers[49,50]. While exposure to various environmental factors modify susceptibility to PD, genetic mutations or familial forms of the disease have also been observed[51–57].

The first gene associated with autosomal dominant PD was alpha-synuclein (SNCA) in 1997[51], which encodes the α-synuclein protein found aggregated within LBs. The most common risk factor mutations involve leucine-rich repeat kinase (LRRK) and parkin (PRKN) genes, while the greatest genetic risk for developing PD are mutations to the GBA gene, encoding β-glucocerebrosidase[52,53]. Overall, multiple genetic association studies have been conducted in PD and over 24 loci have been identified as increasing the risk factor of developing PD[41,58–60]. Genetic mutations in SNCA have also been shown to modify environmental risk factors affecting the risk for PD development associated with head injury[54]. Interestingly, multiple PD associated genes are involved in the ubiquitin-proteasome pathway[55]. While inherited or familial forms of PD are not as common as the idiopathic form, the discovery of PD-associated genes has been critical to PD research through the development of animal models of the disease widely used in research today[52,53]. Overall, studies in both toxin and inherited forms of PD suggest mechanisms that contribute to the loss of dopaminergic neurons such as misfolding and aggregation of proteins, mitochondrial dysfunction and associated oxidative stress, including oxidized dopamine species[36,56,57].

Animal Models of Parkinson's Disease

Many studies examining PD have used chemically induced models of the disease including MPTP[61], rotenone[62], paraquat[46,47], amphetamine model[63], and 6-OHDA[64]. These neurotoxin models of PD are best used to test degeneration of nigrostriatal dopaminergic neurons, but they often possess their own drawbacks as well. Degeneration in these models usually progresses very quickly over a couple days, while PD progression takes place over years in humans[65]. The MPTP and 6-OHDA models do not present the characteristic LB formations in neurons[66–68]. Both the rotenone and paraquat models have had high mortality rates and variable cell death or loss of striatal dopamine[69,70]. Models using methamphetamine (METH) or 3,4-methylenedioxymethamphetmaine (MDMA) also demonstrate serotonergic toxicity and are often used in conjunction with other toxins to influence the progression of symptoms[71–75]. The challenge of inducing a PD phenotype into a mouse model has led to a variety of models that demonstrate the death of dopaminergic neurons along with unique sets of symptoms and abnormalities for each model.

Genetic models of PD are also often used to study familial forms of the disease with the idea that similar phenotypic changes indicate common mechanisms in the more common, sporadic form of PD. The most commonly studied PD genes: α-synuclein, LRRK2, PINK1, PRKN, and Protein Deglycase (DJ-1) can all be linked to the ubiquitin-proteasome pathway[30]. The most fundamental drawback to many of these disease models is that they do not demonstrate a significant loss of dopaminergic neurons[76–79]. The knockout (KO)

mice for PINK1, PRKN, and DJ-1 all have similar phenotypes with decreased locomotor activity and slightly decreased dopamine levels but without loss of dopaminergic neurons[80–85]. LRRK2-mutated mice typically experience mild disruption of nigrostriatal dopaminergic neurons without neuropathological symptoms, but they do display α-synuclein or ubiquitin accumulation[77,86–88]. There are many different α-synuclein transgenic models. While some have behavioral impairments and lowered dopamine levels, there is usually not a significant amount of neurodegeneration[89–92]. Overexpression models of α-synuclein can display neurodegeneration and behavioral alterations depending on the promoter used[93,94].

The mouse thymidine 1 promoter (m-Thy1) is used to drive overexpression of full-length human wild-type α-synuclein in the C57B16/DBA2 background mouse as a PD model[95]. This model shows progressive changes in both motor and non-motor symptoms, striatal dopamine levels, α-synuclein pathology, and inflammation typically observed in PD[96]. These mice overexpress the α-synuclein protein at 1.5-3.4 fold higher than wild-type littermates in most regions of the brain, which is similar to levels observed in patients with gene triplication of α-synuclein associated with a familial form of PD[96]. These mice rapidly lose 40% of striatal dopamine between 12 and 14 months of age, but there is no reduction in the amount dopaminergic neurons[97]. At 14 months, this model also fails many motor tests such as decreased locomotion and slowness in sensory motor tests without motor neuron pathology. These deficits can both be reversed with levodopa treatment, suggesting they are more reflective of

human PD[95,97–99]. This model also shows early innate inflammation in the brain and late peripheral inflammation similar to PD patients[100–102]. Microglia can be found activated in the striatum as early as 1 month and in the substantia nigra at 5-6 months along with increased tumor necrosis factor-α[100,103]. One PD hallmark this model does not demonstrate is the loss of dopaminergic neurons; however, a progressive process of terminal loss has been observed, which suggests this system as a model of early stages of PD prior to neuronal cell death[104].

Peripheral Inflammation

Inflammation is the body's response to pathogens, damaged cells, and irritants. This process utilizes immune cells and molecular mediators to eliminate the cause of cell injury or clear out damaged cells/tissue and initiate tissue repair. When microorganisms invade the body they are usually destroyed by lysozymes or phagocytosis with intracellular digestion as the typical mechanisms of the innate immune system[105]. The first component of the innate immune system encountered by a pathogen after breaching the body is generally neutrophils and residential cells trying to neutralize intruders by either ingestion by phagocytosis, degranulation with anti-microbials, or by trapping with neutrophil extracellular traps (NETs)[106]. This is closely followed by a response of the complement system[107] as a collection of proteins in bodily fluid, which coat the pathogen in complement proteins to assist phagocytic cells[108,109]. The cells involved in the innate immune system consist of macrophages, dendritic cells, mast cells, innate lymphoid cells, neutrophils, natural killer cells, basophils, and eosinophils[107]. Natural killer cells and eosinophils are responsible for destroying host cells

11

infected by a virus or parasite[110]. Macrophages, dendritic cells, mast cells, and neutrophils are all characterized as phagocytes which protect the body by ingesting foreign particles, bacteria, and dead cells. Phagocytes have specialized receptors on their surface called pattern recognition receptors (PRRs) to detect harmful objects not normally found in the body making them critical for fighting infection and maintaining healthy tissue[111].

PRRs are germline-encoded host sensors that identify PAMPs, such as microbial pathogens, or DAMPs which are endogenous stress signals[112]. These receptors can be grouped into toll-like receptors (TLRs), c-type lectin receptors (CLRs), NOD-like receptors (NLRs), and RIG-I-like receptors (RLRs)[113]. The resultant signaling from these various families of receptors interact in a complex system to promote the appropriate immune response to neutralize the current inflammatory stimulus. Often, multiple families of PRRs are activated at the same time with signaling pathways that can be both inhibitory and facilitatory to each other resulting in a dynamic system of regulation to engage immune activation at a cellular level[114].

If the innate immune system is unable to clear the inflammatory stimulus after four to seven days then the adaptive immune response may be activated[115]. The adaptive immune response is a learned response to a specific pathogen that offers long term protection. The cells that carry out the adaptive immune response are B cells and T cells. Plasma cells (fully differentiated B cells) secrete antibodies, while T cells control intracellular infections by playing various roles in the inflammatory response. T cells can secret mediators to activate other cells

and enhance defense mechanisms such as when T helper cells activate B cells in the presence of antigens[116]. T cells can also become a cytotoxic type of T cell which kill the target organism[117].

Communication and recruitment of both adaptive and innate immune cells is conducted using small soluble molecules called cytokines including chemokines, interleukins, growth factors, and interferons. These proteins regulate the amplitude and duration of the immune response and require tight regulation, since they can be highly active at low concentrations. The specific action of each cytokine is dependent on the stimulus, cell type and other mediators and receptors. For example, cytokines can serve as a means of communication between the peripheral nervous system and immune system by increasing membrane excitability in nociceptor neurons[118–120]. In chronic inflammatory cases, it is not uncommon for tissue and cellular death to occur as a result of cytotoxic defense mechanisms of the immune system[121–123]. Anti-inflammatory cytokines play a crucial role in limiting these potentially dangerous inflammatory effects[124]. Successful resolution of the inflammatory process relies on shifting the balance of pro and anti-inflammatory cytokines toward anti-inflammatory expression.

Diabetic Peripheral Neuropathy

Diabetes mellitus or, diabetes, is a metabolic disorder, in which blood sugar control is lost due to either a lack of insulin or the body becoming insulin insensitive. There are three types of diabetes with type 1 diabetes mellitus (T1DM) being associated with an insulin deficit due to a loss of pancreatic beta

cells[125]. Type 2 diabetes mellitus (T2DM) is characterized by insulin resistance usually associated with obesity. Type 3 is termed gestational diabetes, occurring in women during pregnancy. This family of conditions is associate with acute complications such as ketoacidosis, hyperosmolar hyperglycemic state, and death as well as long-term complications including nephropathy, retinopathy, cardiovascular disease, and neuropathy[126]. Diabetic peripheral neuropathy (DPN) is the most common complication of diabetes, presenting with numbness, tingling, and pain in the extremities[127]. This, in conjunction with damaged blood vessels, can lead to skin damage, which is associated with diabetic foot ulcers as well as muscle atrophy and weakness[128].

Current treatments for DPN are limited to tight blood glucose control and pain management. Most common medications prescribed include anticonvulsants, antidepressants, and opioids to help manage pain. Glucose control is significantly more effective as a treatment for patients with DPN in T1DM than T2DM[129,130]. This leaves the majority of patients with DPN resigned to pain medication.

The major mechanisms thought to influence DPN involve hyperglycemia, dyslipidemia, and disrupted insulin signaling. Hyperglycemia leads to increased oxidative stress through increase flux pathway activity and overwhelming the electron transport chain to generate reactive oxygen species (ROS)[131–133]. Chronically high blood sugar can also increase production of advanced glycation end products (AGEs) that bind extracellularly to the receptor for AGE (RAGE), which initiates an NF-kB inflammatory pathway and generates ROS[134–136].

14

Dyslipidemia, which is thought to be critical in T2DM, has been linked to DPN progression through high levels of free fatty acids (FFAs), oxysterols, low-density lipoproteins (LDLs)[137]. FFAs have been shown to directly injure Schwann cells and promote proinflammatory cytokine release from surrounding immune cells. LDLs modified by either oxidization or glycation can bind to toll-like receptor (TLR) and RAGE[136,138,139]. The insulin resistance (T2DM) or deficiency (T1DM) that disrupts normal insulin signaling increases mitochondrial stress within neurons[140]. There is some evidence that insulin can may have a neurotrophic effect which is lost in diabetes. Removing the native neurotrophic effect that insulin has on neurons may also contribute to DPN progression[141]. All of these mechanisms result in various cell stress processes creating a damaging environment for all resident cells. This can trigger the recruitment of macrophages engaging a feedback loop of inflammatory cell stress and death with a persistent stimulus related to the diabetes phenotype[142,143]. The insight into these contributing mechanisms has largely been obtained through the study of multiple animal models of diabetes used in scientific studies.

Animal Models of Diabetic Peripheral Neuropathy

Several animal models of diabetes have been developed for both T1DM and T2DM, which demonstrate varying levels of DPN. While the models that have been developed demonstrate a diabetic phenotype along with mild neuropathy, they do not reflect the severity of the human disease[144–146]. This dissertation contains studies utilizing the single high dose (SHD) streptozotocin (STZ), leptin receptor mutated (*db/db*), and leptin knockout (*ob/ob*), which we will

focus on while discussing some advantages and disadvantages for these and alternative models.

The mouse models of T1DM are either chemically induced using STZ or genetic models of the disease. The chemically induced model utilizes STZ to target the pancreatic β cells where it interferes with glucose transport and induces DNA double strand breaks[147,148]. Two different dosing regiments of STZ are commonly used to induce β cell death in this model, either a SHD or multiple low doses (MLD). The changes in dosing assist with the severe toxicity and post injection mortality observed in the SHD, but the MLD model will often show moderate to no signs of neuropathy dependent on the strain. The genetic models of T1DM include the non-obese diabetic (NOD) and B6Ins2[Akita] mice. NOD mice have an immunodeficiency similar to that seen in humans with T1DM[149]. NOD mice experience the onset of diabetes around 12 to 14 weeks[150,151], but very little neuropathy characterization has been done in this model besides the observation of hyperalgesia at 8 weeks and hypoalgesia at 12 weeks[152,153]. The B6Ins2[Akita] is induced through a point mutation in the Ins2 insulin gene which impairs insulin secretion and results in hyperglycemia[154]. This model demonstrates a diabetic phenotype by 7 weeks of age and neuropathy around 16 weeks of age[155]. However, there has been some conflicting studies suggesting that there were no significant impairments in nerve conduction velocities at 24 weeks of age[156]. While further characterization of DPN in the B6Ins2[Akita] model is required, their ability to respond to insulin treatments is unique[157].

16

Models of T2DM are either genetic or diet-induced and here we will focus on models characterized with a neuropathy phenotype[158]. Genetic models were generated by identifying a spontaneous mutations disrupting leptin signaling through either a leptin receptor mutation (*db/db*[159]) or leptin knockout (*ob/ob*[160]). The *db/db* mouse develops diabetes at 4 weeks, hyperalgesia at 8 weeks, then allodynia and hypoalgesia after 12 weeks[144,161–163]. This along with deficits in motor and sensory nerve conduction velocities make the *db/db* mouse a robust model of DPN. However, there is some strain variability with the C57BL/6 mice only having limited or no neuropathy while C57BKS mice have a robust phenotype[144,158,163,164]. The *ob/ob* mouse is not as well studied in DPN, but as a model of mild T2DM, decreased neuron conduction velocity can be observed at 11 weeks of age along with other measurements of neuropathy[165].

Diet-induced models involve a high-fat diet (HFD), which will develop diet-induced obesity in the mice through a gradual onset of metabolic imbalances characteristic of human T2DM[138,166–168]. This model also allows a unique examination of prediabetes which has been shown to be a contributing factor to neuropathy in nondiabetic patients[169]. These obese HFD mice do not demonstrate elevated glucose levels and never fully develop diabetes, although other phenotypic changes have been observed[168]. The hallmarks of DPN have been observed after 16 weeks of age in HFD mice characterized as prediabetic[170]. Strain variability has also been observed in this model with different amounts of vulnerability to diet-induced obesity, but most DPN studies have been conducted using the C57/BL6 background[171]. One unique feature of

this model is the ability to observe DPN reversal by switching HFD mice back to a standard diet[168]. This finding could allow further insight into restorative mechanisms.

Dissertation Research Objective

The objective of this dissertation is to characterize transcription signatures associated with central and peripheral inflammation, with an emphasis on Parkinson's disease and diabetic peripheral neuropathy. Our wide range of models and techniques lends strength to the notion of common immune activation pathways induced by a variety of disease insults.

CHAPTER II

CONSERVED TRANSCRIPTIONAL SIGNATURES IN HUMAN AND MURINE
DIABETIC PERIPHERAL NEUROPATHY

Abstract

Diabetic peripheral neuropathy (DPN) is one of the most common
complications of diabetes. In this study, we employed a systems biology
approach to identify DPN-related transcriptional pathways conserved across
human and various murine models. Eight microarray datasets on peripheral
nerve samples from murine models of type 1 (streptozotocin-treated) and type 2
(*db*/*db* and *ob*/*ob*) diabetes of various ages and human subjects with non-
progressive and progressive DPN were collected. Differentially expressed genes
(DEGs) were identified between non-diabetic and diabetic samples in murine
models, and non-progressive and progressive human samples using a unified
analysis pipeline. A transcriptional network for each DEG set was constructed
based on literature-derived gene-gene interaction information. Seven pairwise
human-vs-murine comparisons using a network-comparison program resulted in
shared sub-networks including 46 to 396 genes, which were further merged into
a single network of 688 genes. Pathway and centrality analyses revealed highly
connected genes and pathways including LXR/RXR activation, adipogenesis,
glucocorticoid receptor signaling, and multiple cytokine and chemokine
pathways. Our systems biology approach identified highly conserved pathways

19

across human and murine models that are likely to play a role in DPN pathogenesis and provide new possible mechanism-based targets for DPN therapy.

Introduction

According to the United States Centres for Disease Control and Prevention (CDC), more than 29 million Americans, over 9% of the United States population, are living with diabetes and another 86 million have prediabetes[172]. The most common microvascular complication of diabetes is diabetic peripheral neuropathy (DPN) which occurs in approximately 60% of patients and is the leading cause of non-traumatic lower-limb amputations[173,174]. DPN is characterized by distal to proximal degeneration of peripheral nerves which results in symptoms such as numbness, pain, and weakness[175]. Other than glucose control, there are no disease-modifying treatments for DPN. Understanding DPN pathology and identifying the underlying mechanisms of peripheral nerve degeneration are therefore critical to the development of new mechanism-based therapies for DPN.

Over the past decade with the advent of high-throughput gene expression profiling assays such as microarrays and RNA-Seq, we and others have examined genome-wide gene expression changes from the peripheral nerve tissues of various diabetic murine models[176–180] and human subjects[181,182] with diabetes. Bioinformatics analyses of these high-throughput datasets identified numerous genes in human and murine peripheral nerves that are significantly dysregulated by diabetes. Suggested mechanisms of injury such as

20

inflammation, oxidative stress, lipid and carbohydrate metabolism, regulation of axonogenesis, mitochondrion, and peroxisome proliferator-activated receptor (PPAR) signaling were also reported during diabetes onset and progression[177,178,180,181].

Yet, one limitation of the previous studies, including ours, is that the analyses didn't account for the differences in species, strains, procedure of diabetes induction, and diabetes duration. Another critical issue that hasn't been addressed thus far is the identification of common injurious pathways and networks conserved across various mouse models of diabetes as well as between mouse and human. In this study, we reanalyzed previously published DPN-related microarray datasets from human and multiple murine models using a unified analysis pipeline. Compared with the existing literature, this study provides a unique opportunity to uncover a possible common mechanism of injury shared across DPN stages, types of diabetes, and species. Such mechanisms could unravel new important therapeutic targets to treat DPN.

Research Design and Methods

Microarray Data

All datasets used were gathered from the University of Michigan Diabetic Neuropathy Microarray Knowledge-Base (DNMKB; http://hurlab.med.und.edu/DNMKB/). The data from the type 1 diabetes mellitus (T1DM) model were originally generated from male DBA/2J mice treated with streptozotocin (STZ) at 10 weeks that were terminated at 34 weeks[180]. The two type 2 diabetes mellitus (T2DM) models included BKS.Cg-Lepr$^{db/db}$ (*db/db*) mice

and BTBR.Cg-Lep*ob/ob* (*ob/ob*) mice. The male *db/db* mice were 8, 16, and 24

weeks[176,178,183], while male *ob/ob* mice were 5 and 13 weeks of age[177]. A female

ob/ob dataset was also available from 26 weeks old BTBR.Cg-Lep*ob/ob* mice[184].

Each dataset was originally generated using sciatic nerve samples on the

Affymetrix Mouse Genome 430 2.0 array platform. As previously reported each

model displayed the features typical of diabetes by the termination of their

respective studies as well as the hallmarks of DPN[176,177,184]. The human sural

nerve data used was generated using the Affymetrix Human Genome U133 Plus

2.0 array platform[178]. As previously reported these samples were evaluated for

features of DPN and were separated into progressive and non-progressive

groups based on the myelinated fibre density lost over a 52 week period[178].

Study Design

Figure 1 illustrates the overall workflow of the current study, designed to

reanalyse these microarray data from sciatic nerve (SCN) samples taken from

our T1DM and T2DM murine models when compared to controls and the human

microarray data from sural nerve biopsies, from patients with progressive and

non-progressive DPN. The original datasets were separated into these groups

(either diabetic vs healthy or progressive vs non-progressive) and were

compared using ChipInspector (Genomatix Software GMBH,

http://www.genomatix.de) to identify the differentially expressed genes (DEGs)

between groups. The DEG lists identified from each murine model were

converted to the human orthologue equivalent when possible using the

Genomatix annotation orthologue database. These DEG lists of human gene IDs

were then compared across datasets to identify the conserved DEGs between the different murine models and human. Each DEG set was also analyzed using Ingenuity Pathway Analysis (IPA; http://www.ingenuity.com) from Qiagen (Hilden, Germany) and the identified pathways were compared across models and species to identify the commonly disrupted pathways. To identify gene networks common between models, networks were generated from these DEG datasets using SciMiner[185]. The networks generated were analyzed for common network nodes and disrupted pathways using IPA.

Transcriptome Profiling

Transcriptomic data generated from Affymetrix GeneChips were analyzed using BioConductor (https://www.bioconductor.org/) and their Affymetrix QC packing in R (http://www.arrayanalysis.org/). All data passing our quality threshold were then analyzed using ChipInspector and up-to-date gene annotation. Expression signals from the microarray image files were analyzed at the single probe level. Significant transcripts were defined using a minimum of five significant probes and a false discovery rate of <1% by the Significance Analysis of Microarrays algorithm using exhaustive comparisons between control and diabetic mice. Eight datasets of DEGs were generated based on significant transcripts between control and diabetic groups for each murine model (8, 16, and 24 week *db*/*db*; 5, 13, 26 week *ob*/*ob*; and 34 week STZ) as well as between progressive and non-progressive groups for the human dataset[176–178,180,181,183,184].
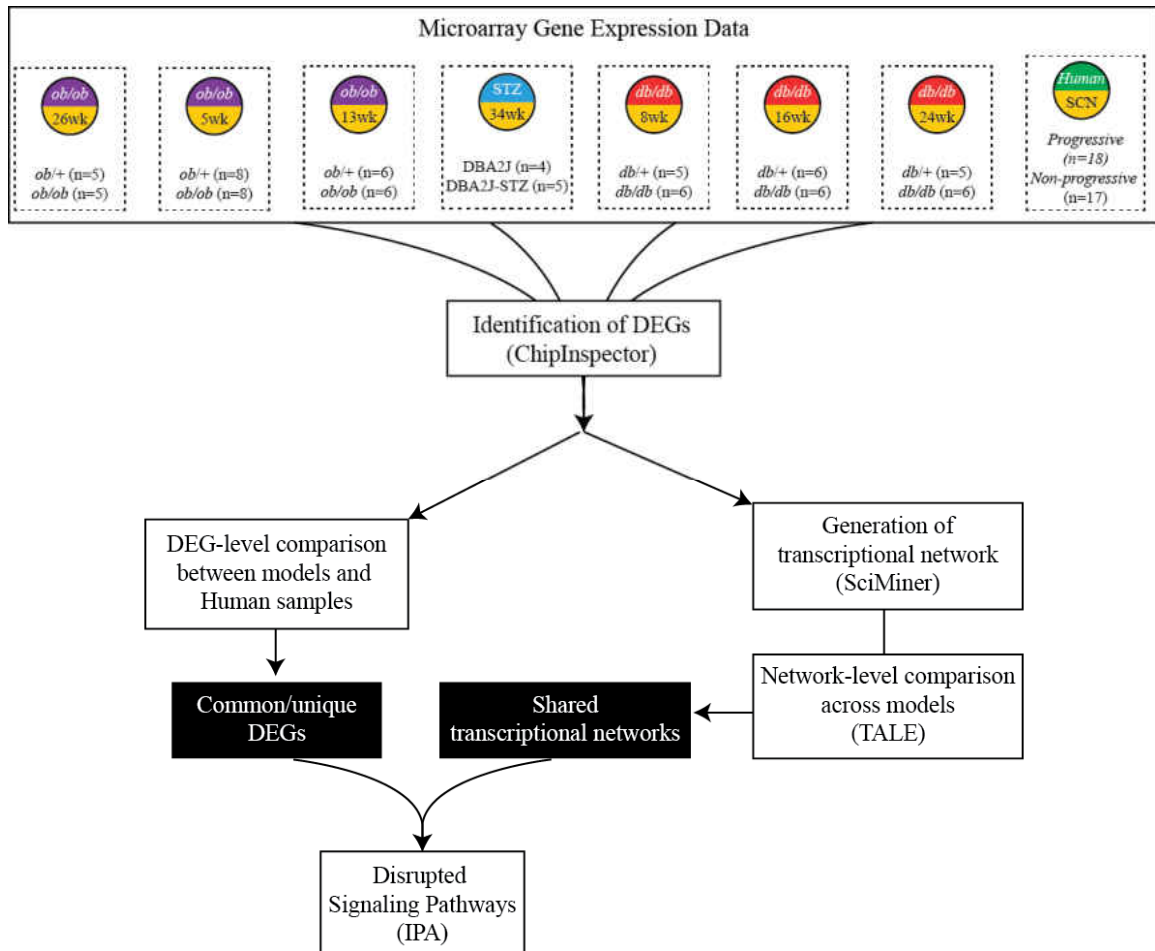
Figure 1. Model and Network DEG Comparison Workflow. Previously published microarray datasets were reanalyzed using ChipInspector to identify DEGs at various time points from murine models of type 1 diabetes (STZ), type 2 diabetes (*db*/*db* and *ob*/*ob*), and human patients. DEG datasets from all murine models were generated by comparing diabetic to healthy control mice. The human samples were grouped into progressive and non-progressive groups to determine the DEG dataset used. All DEG datasets were compared in order to find the DEGs shared across models and stages of DPN. These shared DEGs were analyzed using IPA to identify possible disrupted signaling pathways. Seven pairwise comparisons were performed to determine the shared networks between each murine dataset with our human dataset. These DEGs were then analyzed using IPA to identify possible disrupted signaling pathways.

Diabetes- and Age- Comparisons of DEGs Sets

The eight DEG sets were compared to find shared DEGs between species, stages of neuropathy, and diabetes type at a gene and network level. Each dataset was assessed in previous publications for characteristics of DPN and defined as a specific stage of DPN[176–178,180,183,184]. All DEG sets were examined for overlap to identify the conserved pathways or genes responsible for the underlying cause of DPN in the different murine and human samples.

Transcriptional Network Comparison

Each DEG set was used to generate transcriptional networks based on gene-gene associations that were identified from biomedical literature using SciMiner[185]. SciMiner is our in-house literature mining system that analyses over 24 million abstracts in PubMed to automatically extract potential gene-gene interactions based on their co-occurrence at the sentence level. The network for each of the eight DEG sets were constructed individually following mouse gene to human gene orthologue conversion according to the Geomatics annotation orthologue database. Cytoscape version 3.3.0 (http://www.cytoscape.org)[186], an open-source platform for visualizing complex networks, was used to visualize SciMiner-generated transcriptional networks.

Each mouse DEG network was compared to the human DEG network in a pairwise manner, using a Tool for Approximate Subgraph Matching of Large Queries Efficiently (TALE)[187]. TALE compares network structure and extracts overlapping conserved relationships between two networks. The mismatch parameter used allows 10% mismatch when generating seed gene nodes and

extended networks as in our previous studies[188,189]. Conserved nodes across

networks were then examined and analyzed for overlapping pathways using IPA.

Functional Enrichment Analysis

IPA was used to identify enriched pathways within each of the eight DEG

sets as well as the seven TALE generated network comparison datasets

(comparing each mouse DEG set to our human DEG set). These pathways for

the eight DEG sets were compared to identify conserved disrupted pathways that

may indicate an underlying cause to DPN. The disrupted pathways observed in

our TALE datasets were also compared in order to identify a possible central

pathway based on nodes and subnetworks generated from our transcriptional

network comparison. The background list of genes used for this analysis was the

Affymetrix Human Genome U133 Plus 2.0 Array.

Construction of Merged Human-Mouse-Conserved Transcriptional
Network and Network Centrality Analysis

Eight TALE networks were combined using the merge function in

Cytoscape. Edges supported by less than three citations according to SciMiner

were removed from the network. The merged human-mouse-conserved

transcriptional network was examined to identify the most central genes in the

network. Using package '*sna*', tools for social network analysis, in R

(https://CRAN.R-project.org/package=sna), four centrality metrics (degree,

eigenvector, closeness, and betweenness) were computed to identify the most

important nodes (*i.e.*, genes) in the merged transcriptional network. These four

different centrality metrics measures different aspects of node

26

characteristics[190,191].

Briefly, the degree centrality is the number of nodes that are its first neighbors (*i.e.*, directly connected to the given node). The more connections a node has, the more central it is, based on degree centrality. In eigenvector centrality, a node contributes to the centrality of another node proportionally to its own centrality. A node is more central, if it is connected to many central nodes. The other two metrics (closeness and betweenness) is dependent on the position of a node in the network. Closeness centrality is based on the distance of a node to the other nodes in the network. The closer a node is to the other nodes, the more important it is considered to be. Betweenness centrality is based on the number of shortest paths connecting two nodes that pass over the given node. A node is more central, if it acts like a bridge in the network, *i.e.*, lies on many shortest paths. In the current study, we defined the top 10 or 50 most central genes, belonging to the ranks of the genes using each metric. These gene sets were further examined for their enriched biological functions using IPA.

The validity of the central genes was examined by comparing against the average centrality scores from randomly generated transcriptional networks. We generated 1,000 gene sets for each of the eight DEG sets containing the same number of genes randomly selected from all the genes available on the microarray platform. These random gene sets were processed in the same exact way as the real data sets, which resulted in 1,000 merged shared networks. The four centrality scores were measured for each gene in the networks and were

used as the background distribution for a Z-test of the centrality scores from the real data.

Results

Identification of Changes in Gene Expression

Gene expression profiles were generated using eight published datasets from sciatic nerve samples from both T1DM and T2DM murine models with DPN as well as human sural nerves from patients with T1DM and T2DM[176–178,180,181,183,184]. Metabolic and neuropathy phenotyping on all animal models as well as human subjects are summarized in Table 1 based on the published reports. Briefly, T2DM mouse models (*ob*/*ob* and *db*/*db*) were significantly heavier and displayed higher levels of fasting glucose levels and glycosylated hemoglobin, when compared with age-matched non-diabetic controls (*ob*/+ and *db*/+, respectively). Triglyceride levels were significantly increased in T2DM mice. STZ-induced T1DM mice had significantly reduced body weight and higher fasting blood glucose and glycosylated hemoglobin levels relative to non-diabetic controls. Motor and sensory nerve conduction velocities (NCVs) were significantly lower in diabetic mice at all stages of diabetes. Intra-epidermal nerve fiber density (IENFD) was significantly decreased in *ob*/*ob* mice at 9 and 13 weeks compared with age-matched control littermates. Similar changes were observed in the *db*/*db* mouse model at 16 and 24 weeks of age. Both IENFD loss and reduced NCVs confirm the development of DPN in murine models of disease[192]. In the human subjects, there was a change in myelin fibre density (MFD) over the course of the 52-week study between subjects with progressive

versus non-progressive neuropathy[181]. However, other factors, including gender, age, insulin treatment, triglyceride levels, glycosylated hemoglobin and body mass index (BMI), were not significantly different between the two groups.

ChipInspector was used to reanalyze each dataset and identified between 438 – 5,757 DEGs within each dataset (Table 2). Gene expression profiles were based on a healthy control vs DPN comparison for each murine model while the human sural nerve comparison was based on comparing patients with progressive versus non-progressive DPN[181]. Across all eight datasets, over 11,000 genes were identified with at least 2,100 being shared across at least 3 datasets. Most murine models displayed a similar expression pattern while our T1DM model (STZ-treated) showed a distinct pattern (Figure 2). Some of the most common genes identified across these models include interleukin 1 receptor antagonist (IL1RN)[193,194], complement component 3a receptor 1 (C3AR1), macrophage scavenger receptor 1 (MSR1)[195,196], and matrix metallopeptidase 12 (MMP12)[197], which have been implicated in the pathogenesis of DPN. Table 3 illustrates the enrichment levels of the most frequently enriched pathways identified in at least five DEG sets in these datasets by IPA. These pathways include many genes related to lipid metabolism, extracellular matrix homeostasis, and immune signaling, which have all been implicated in the pathogenesis of DPN[177,178,180,182–184,188,198,199].

Published Datasets Included	*db/db* 8 wks (M)[183]	*db/db* 16 wks (M)[178]	*db/db* 24 wks (M)[176]	*ob/ob* 5 wks (M)[177]	*ob/ob* 13 wks (M)[177]	*ob/ob* 26 wks (F)[184]	DBA2J-STZ 34 wks (M)[180]	Human DPN[181]
Metabolic measures								
Body weight	↑	↑	↑	↑	↑	↑	↓	BMI: N/S
Fasting glucose	↑	↑	↑	↑	↑	N/A	↑	N/A
Triglycerides	N/A	↑	↑	↑	↑	↑	N/A	N/S
% Glycosylated hemoglobin	↑	↑	↑	↑	↑	↑	↑	N/S
Neuropathy phenotype measures								
Hindpaw latency	N/S	↑	↑	↑ *	N/A	N/A	↑	N/A
Motor nerve conduction velocity	↓	↓	↓	↓ *	↓	↓	↓	N/A
Sensory nerve conduction velocity	↓	↓	↓	↓ *	↓	↓	↓	N/A
Intra-epidermal nerve fiber density	N/S	↓	↓	↓ *	↓	↓	N/A	N/A
Myelinated fiber density changes over 52 wks	N/A	N/A	N/A	N/A	N/A	N/A	N/A	↓

Table 1. Metabolic and neuropathy phenotypic measures of microarray datasets. The previously published datasets included in this study have all been tested for measurements of metabolic disturbances and neuropathic phenotyping independently. The increase (+) or decrease (-) indicates the changes observed in diabetic animals compared to their respective non-diabetic controls and between the progressive and non-progressive human patients. Not all studies underwent the same testing and measurements not included are indicated by an N/A, while non-significant results (p>0.05) are indicated by N/S. The superscript numbers in the header row correspond to the reference numbers in the manuscript. BMI: body mass index; M: male; F: female. wks: weeks. * indicates that measurements taken at 9 weeks in the published study.

Dataset	Number of Control Samples	Number of Diabetic Samples	DEGs identified by ChipInspector
8wk *db*/*db*	6	5	2,955
16wk *db*/*db*	6	6	871
24wk *db*/*db*	6	6	5,068
5wk *ob*/*ob*	8	8	2,096
13wk *ob*/*ob*	6	6	723
Female 26wk *ob*/*ob*	5	5	482
34wk DBA2J-STZ	4	5	3,022
Human sural nerve	17 non-progressive	18 progressive	5,757

Table 2. Study 1 Dataset Summary. The number of samples for both control and diabetic samples within each dataset is represented in the 2nd and 3rd column. The human dataset rather than being healthy versus diabetic samples were grouped into non-progressive and progressive groups based on myelin fibre density lost. The amount of DEGs identified by ChipInspector ranged from 482 to 5,757 for each dataset.

8wk dbdb

24wk dbdb

13wk obob

5wk obob

16wk dbdb

F26wk obob

34wk DBA2J-STZ

Human
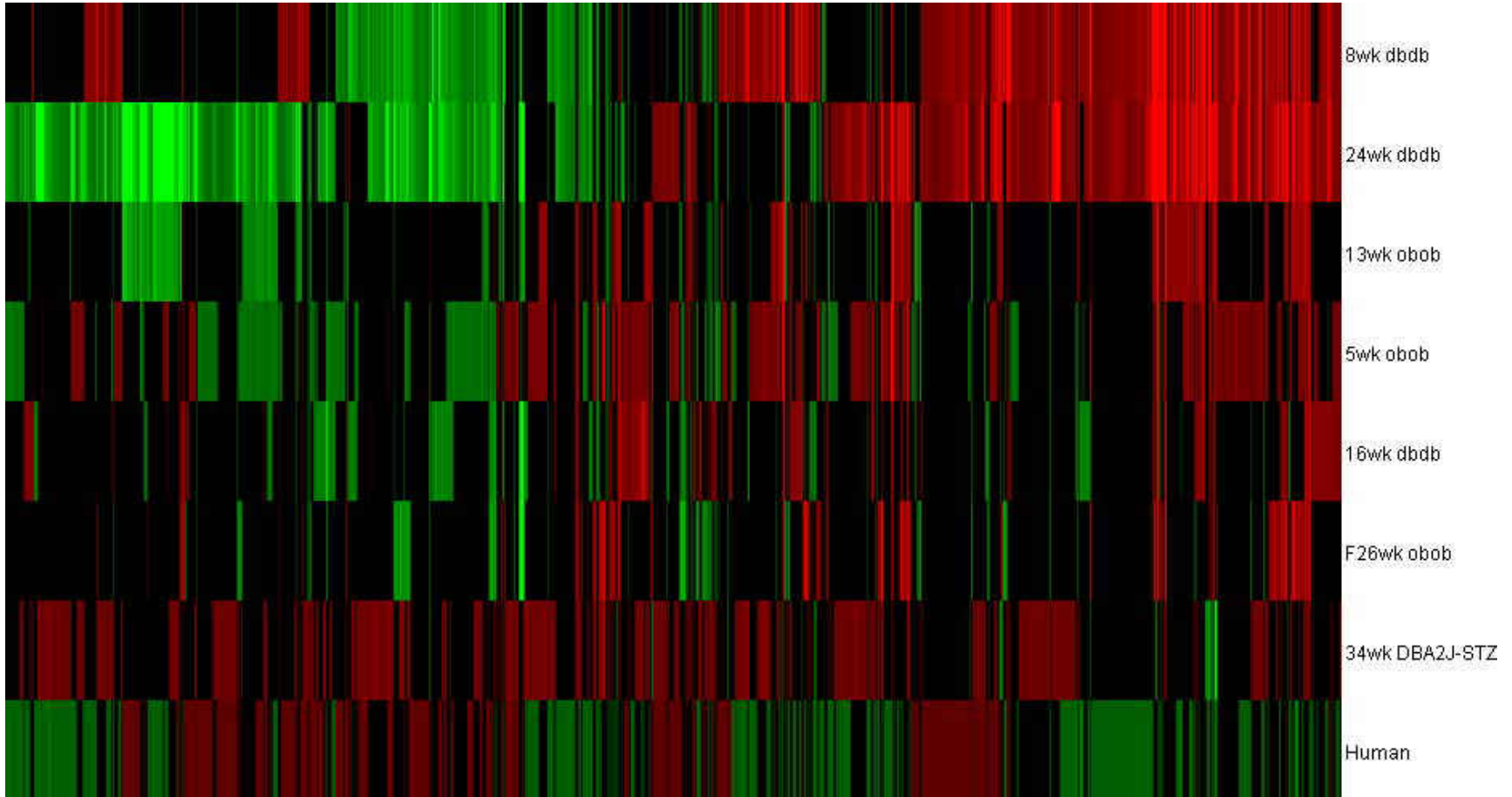
Figure 2. DEG patterns in study 1 DPN models. Over 11,000 genes were identified and at least 2,100 were shared across a minimum of 3 datasets. This heat map shows the pattern of distribution for DEGs across models to display how similar or different each model used in this analysis appeared to be on a transcription level.

pathway	count	8wk_dbdb	16wk_dbdb	24wk_dbdb	5wk_obob	13wk_obob	F26wk_obob	34wk DBA2J-STZ	Human
Role of Osteoblasts, Osteoclasts and Chondrocytes in Rheumatoid Arthritis	7	3.32	2.45		3.50	1.42	1.75	4.98	1.95
Clathrin-mediated Endocytosis Signaling	7	2.72	2.05	1.92	3.90	2.27	2.19	1.53	
Hepatic Fibrosis / Hepatic Stellate Cell Activation	6	3.42	6.24		8.70	1.97		3.09	2.12
Growth Hormone Signaling	6	2.48	1.46		2.23		1.55	1.32	1.55
Atherosclerosis Signaling	6	2.15	2.17		11.50	2.22	3.14	5.67	
LXR/RXR Activation	6	1.33	5.79		7.11	1.36	1.99	4.63	
Axonal Guidance Signaling	6	3.27		1.61	3.62	3.32	3.83	2.59	
Inhibition of Matrix Metalloproteases	6	1.58	1.57	1.93	3.36	1.83	4.44		
Leukocyte Extravasation Signaling	6	1.74	1.30		4.95	2.91	3.00	5.76	
Production of Nitric Oxide and Reactive Oxygen Species in Macrophages	6	1.59	1.82	2.01	6.53	2.01		2.91	
Type II Diabetes Mellitus Signaling	6	1.44	1.53	2.41	1.80	1.53		1.75	
PPARγ/RXRα Activation	5	1.50	2.50	2.06	3.85				2.65
Calcium Signaling	5		1.73	3.02			2.05	2.15	2.29
Glioma Invasiveness Signaling	5	4.15		2.12			1.87	1.68	2.26
Paxillin Signaling	5	1.59		2.28			1.95	1.60	2.19
Renin-Angiotensin Signaling	5	1.38		1.34	1.68			1.42	2.04
Aryl Hydrocarbon Receptor Signaling	5	2.73			5.05		1.32	1.61	1.67
Reelin Signaling in Neurons	5	2.43		2.04		1.95		3.10	1.65
Role of JAK1 and JAK3 in Î³c Cytokine Signaling	5	1.73			1.99		1.78	1.50	1.62
MSP-RON Signaling Pathway	5	1.35			2.08		2.26	2.55	1.37
Angiopoietin Signaling	5	2.06	3.22	1.63	2.08			1.86	
ERK/MAPK Signaling	5	1.64		1.46	2.15	2.30	1.79		
IL-8 Signaling	5	5.19	2.43	2.57	4.30			2.22	

Table 3. Most frequently dysregulated canonical pathways in study 1 datasets identified by Ingenuity Pathway Analysis (IPA). Each dataset was analyzed using IPA for canonical pathway enrichment then compared to determine the most frequently enriched pathways across datasets. The numbers and color gradient within the table are -log (p values) to represent significant enrichment within each column.

Transcriptional Network Analysis

Our network analysis refines the datasets by examining the connections between identified DEGs to allow prioritization of possibly centrally influential genes or pathways. Prior to pathway analysis with IPA, transcriptional networks are generated based on gene-gene associations, among DEGs, that are identified for each dataset using SciMiner[185]. These networks were then compared in a pairwise manner between murine and human datasets using TALE with a 10% mismatch parameter to limit the shared network[187]. Networks ranging from 46 – 396 genes were identified as shared between each murine set of DEGs and the progressive human set of DEGs (Table 4; Figure 3). The top network DEGs identified as shared across datasets within the compared networks are presented in Table 5. Among these shared DEGs there is a large number of immune factor genes such as CD44, Interleukin 1 receptor antagonist, and macrophage scavenger receptor 1.

Other notable genes identified in this shared network include dipeptidyl peptidase 4 (DPP4), a serine peptidase that modulates the levels of incretin hormones, major regulators of glucose homeostasis[200]. The antidiabetic action of DPP4 inhibition has been associated with a partial amelioration of NCV deficit in T1DM rats as well as a reduction in nerve fiber loss[201,202]. The identification of the immune genes previously described as well as other target genes associated with DPN suggests that our network approach can successfully narrow the focus of transcriptomic data.

Dataset	Number of control samples	Number of diabetic samples	DEGs identified by ChipInspector	Orthologue mapped Human Gene IDs	Genes included in the literature-derived network
db/db 8 wks (M)[183]	6	5	2,955	2,782	2,194
db/db 16 wks (M)[178]	6	6	871	794	579
db/db 24 wks (M)[176]	6	6	5,068	4,743	3,762
ob/ob 5 wks (M)[177]	8	8	2,096	1,910	1,535
ob/ob 13 wks (M)[177]	6	6	723	685	509
ob/ob 26 wks (F)[184]	5	5	482	438	338
DBA2J-STZ 34 wks (M)[180]	4	5	3,022	2,482	1,932
Human DPN[181]	17 non-progressive	18 progressive	5,757	5,757	4,232

Table 4. Summary of the microarray datasets. The number of samples for both control and diabetic samples within each dataset is represented in the 2nd and 3rd column. The human dataset rather than being healthy versus diabetic samples were grouped into non-progressive and progressive groups based on myelin fiber density lost. The amount of DEGs identified by ChipInspector ranged from 482 to 5,757 for each dataset. The superscript numbers in the header row correspond to the reference numbers in the manuscript. wks: weeks.
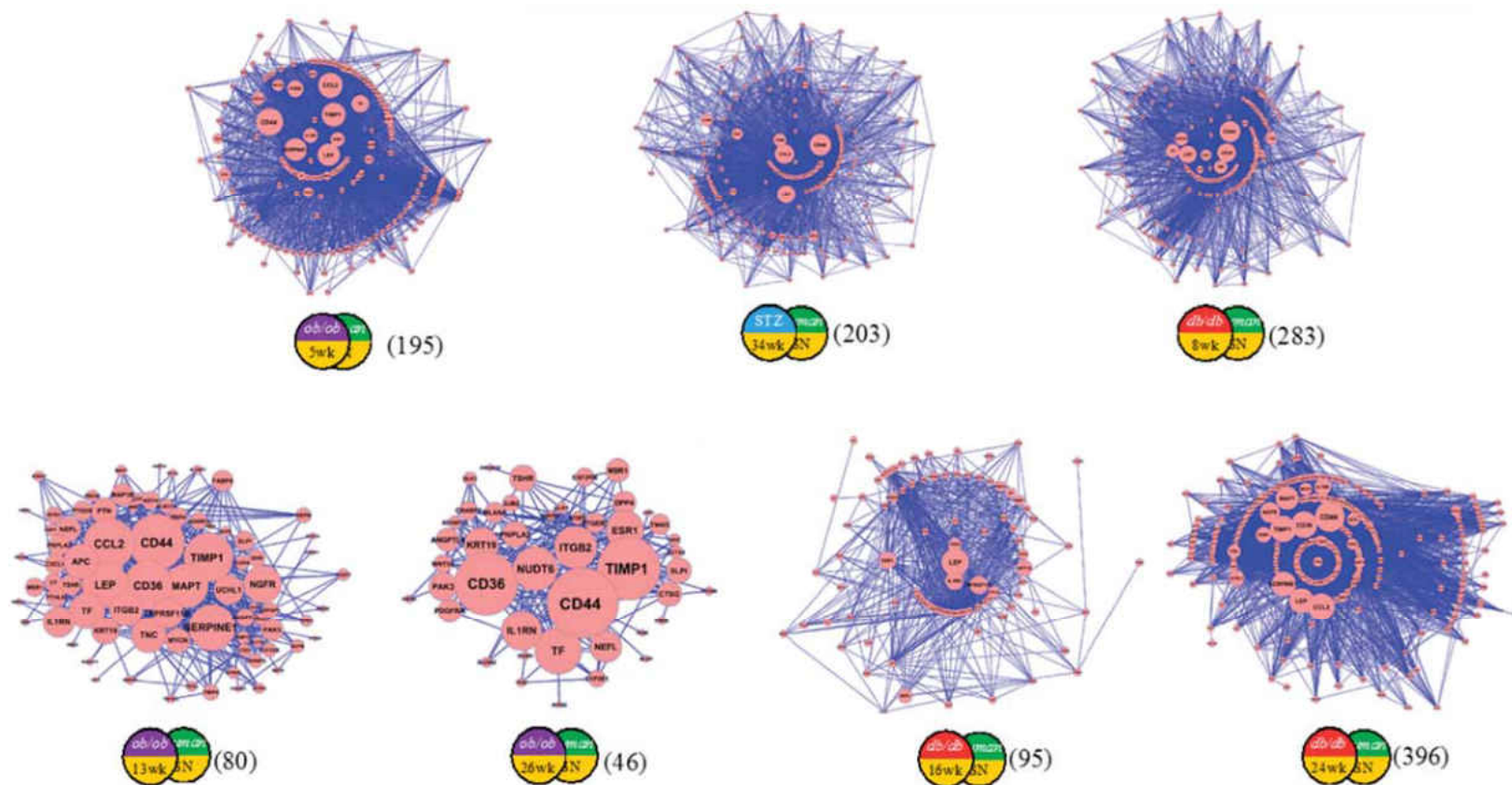
Figure 3. Shared transcriptional networks between murine and human datasets identified by TALE, a graph matching software. Using a graphical matching software (TALE), each network generated using the murine datasets were examined for overlap with the human gene network. The resulting networks are below with the number in parenthesis representing the total genes within the network. Node size indicates amount of degree relative to the size of the network.

ID	Symbol	Description	count	8wk db/db	16wk db/db	24wk db/db	5wk ob/ob	13wk ob/ob	F26wk ob/ob	34wk DBA2J-STZ	Human
3557	IL1RN	interleukin 1 receptor antagonist	8	3.50	3.01	4.98	4.74	3.05	2.54	1.29	-1.07
4481	MSR1	macrophage scavenger receptor 1	8	1.83	1.58	2.25	1.91	1.78	2.00	1.31	-1.09
6590	SLPI	secretory leukocyte peptidase inhibitor	7	3.03		3.41	1.78	2.69	3.23	1.53	1.27
2099	ESR1	estrogen receptor 1	7	-1.67	-1.70	-1.77	-1.36		-1.84	1.27	-1.10
7253	TSHR	thyroid stimulating hormone receptor	7	3.06		2.86	1.35	2.24	1.77	-2.53	-1.12
960	CD44	CD44 molecule (Indian blood group)	7	1.70		2.13	2.18	1.53	1.86	1.40	-1.16
6423	SFRP2	secreted frizzled-related protein 2	7	-1.95	-3.41	-3.53	-2.03	-1.78	-2.48		-1.22
3952	LEP	leptin	7	2.57	2.25	4.14	2.23	2.77		-5.86	-1.88
3880	KRT19	keratin 19	6		1.55		1.42	1.97	1.84	1.28	1.42
1382	CRABP2	cellular retinoic acid binding protein 2	6	1.80			1.42	1.85	2.39	1.45	1.28
1803	DPP4	dipeptidyl-peptidase 4	6	-1.96	-1.62	-2.30	-1.35		-2.00		1.21
5063	PAK3	p21 protein (Cdc42/Rac)-activated kinase 3	6		-1.43	-1.99	1.36	-1.66	-1.58		1.21
6638	SNRPN	small nuclear ribonucleoprotein polypeptide N	6	2.08		-2.67	-1.24	-1.72		1.28	1.14
4043	LRPAP1	low density lipoprotein receptor-related protein associated protein 1	6	1.48	1.41		1.51	1.46		1.28	1.10
6530	SLC6A2	solute carrier family 6 (neurotransmitter transporter, noradrenalin), member 2	6	-2.59	-2.25	-2.30	-1.26		-2.00		-1.09
51129	ANGPTL4	angiopoietin-like 4	6		2.10	3.39	1.42	2.39	2.19		-1.24
7079	TIMP4	TIMP metallopeptidase inhibitor 4	6	2.92		3.51	1.47	1.89		-2.51	-1.54

Table 5. The most commonly dysregulated differentially expressed genes among the shared transcriptional networks. Shared network genes between each murine dataset and human dataset were identified. The fold change for each dataset is represented by the value in each cell and the color displays the relative change within the table, with red being an increased fold change and blue being a decreased fold change. Many of the represented DEGs are directionally consistent across murine models but not necessarily between the human and murine comparison.

Cytoscape was then used to visualize each shared TALE network. Each individual shared network based on the TALE comparison between the human dataset and each murine dataset is visualized in Figure 3. Networks were merged using the merge network feature in Cytoscape in order to identify the most connected DEGs (Figure 4). The top five most highly connected genes, based on degrees within the merged network, were PIK3CA, MPAK8, CD44, MAPK1, and CREB. These most connected genes are not biased by the amount of dataset in which they appear, but instead depend on the connections that each node has within the network. The majority of highly connected genes do appear in four or more datasets and all genes are observed in our human data.

The genes in the shared transcriptional networks between human and each murine model were analyzed for pathway enrichment using IPA. Over 380 pathways were found to be significantly enriched and the top pathways shared across each network are shown in Table 6, which displays a fold change based on the average fold change of the pathway genes identified by IPA. The directionality is indicated by color (with red being an increase and blue being a decrease) based on the percentage of genes involved that have increased or decreased expression levels. These pathways were often directionally similar to our human dataset, unlike the originally described DEGs. The T1DM STZ model used in our study does display consistent up-regulation of the subset of enriched pathways identified as shared across models in Table 6. The top pathways shared across each network included LXR/RXR activation, agrin interactions at

A
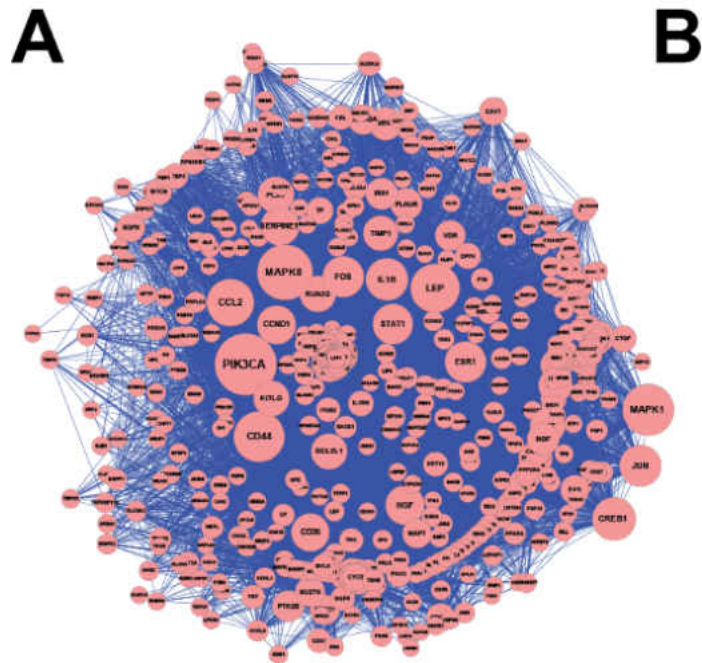
B

Gene Symbol	Description	Degree	8wk db/db	16wk db/db	24wk db/db	5wk ob/ob	13wk ob/ob	F26wk ob/ob	34wk DBA2J-STZ	Human
PIK3CA	phosphoinositide-3-kinase, catalytic, alpha polypeptide	304	1.43		1.24				1.28	1.10
MAPK8	mitogen-activated protein kinase 8	261	1.42		-1.35				1.29	-1.01
MAPK1	mitogen-activated protein kinase 1	234			-1.10					1.14
CD44	CD44 molecule (Indian blood group)	228	1.70		2.13	2.18	1.53	1.86	1.40	-1.16
LEP	leptin	216	2.57	2.25	4.14	2.23	2.77		-5.86	-1.88
CCL2	chemokine (C-C motif) ligand 2	206			3.01	2.22	1.78		1.33	1.17
CREB1	cAMP responsive element binding protein 1	177	1.60		1.49	-1.21				1.12
IL1B	interleukin 1, beta	172				1.85			1.52	1.21
JUN	jun proto-oncogene	167			-1.37					1.16
ESR1	estrogen receptor 1	164	-1.67	-1.70	-1.77	-1.36		-1.84	1.27	-1.10
FOS	FBJ murine osteosarcoma viral oncogene homolog	163				1.39			1.49	1.39
STAT1	signal transducer and activator of transcription 1, 91kDa	157		-1.36	-1.45	-1.28				-1.12
HGF	hepatocyte growth factor (hepapoietin A; scatter factor)	149	1.81		1.58					-1.13
CCND1	cyclin D1	146	-1.49			-1.27				1.11
SERPINE1	serpin peptidase inhibitor, clade E (nexin, plasminogen activator inhibitor type 1), member 1	144			5.13	1.88	2.01			-1.24
CD36	CD36 molecule (thrombospondin receptor)	143	1.71		2.06		1.90	1.61		-1.49
RUNX2	runt-related transcription factor 2	131	1.74		1.92	1.35			1.25	1.09
PLAT	plasminogen activator, tissue	130	-1.78		-1.59	-1.33				-1.15
BCL2L1	BCL2-like 1	129				1.39	1.35		1.35	1.11
KITLG	KIT ligand	125	1.43			-1.27			1.29	-1.10

Figure 4. Highly connected DEGs across TALE networks. (A) TALE networks were combined using the merge network feature in Cytoscape. Node size is based on the degree of connections and organized as a radial tree. (B) This table shows the fold changes of the most highly connected genes in each dataset with red coloring being an increased fold change and blue being a decreased fold change. A total of 688 genes were included in the network with the degree of connections between genes ranging from 304 and 1. Each connection between genes were supported by a minimum of 3 citations as defined by SciMiner.

Pathway	Count	8wk db/db	16wk db/db	24wk db/db	5wk ob/ob	13wk ob/ob	F26wk ob/ob	34wk DBA2J-STZ	Human
Agrin Interactions at Neuromuscular Junction	8	-2.1	-1.44	-2	1.82	-2	-1.76	1.3	-1.14
Role of Osteoblasts, Osteoclasts and Chondrocytes in Rheumatoid Arthritis	8	-1.7	-1.96	-1.9	1.77	-1.9	-2.06	1.34	-1.14
Hepatic Fibrosis / Hepatic Stellate Cell Activation	8	-1.8	-1.69	-2.1	1.62	2	1.92	1.75	-1.17
Colorectal Cancer Metastasis Signaling	7	-1.6	1.6	-1.8	-1.3		-1.72	1.32	-1.14
Acute Phase Response Signaling	7	-1.9	-1.91	-1.8	1.67	-1.9	2.36	1.34	
Adipogenesis pathway	7	-1.8	-1.62	-1.8	-1.4	1.97		2.24	-1.18
Wnt/ß-catenin Signaling	7	1.66	-1.81	-1.7	-1.5	-1.6	-1.98	1.34	
LXR/RXR Activation	7	-2.3	1.8	2.32	1.97	1.95	2.13	1.37	
Glucocorticoid Receptor Signaling	7	-1.7	-1.66	-1.9	-1.6	2.38	2.54	1.34	
Paxillin Signaling	7	-1.8	-1.44	-1.7	1.85		-1.76	1.32	-1.13
Role of Macrophages, Fibroblasts and Endothelial Cells in Rheumatoid Arthritis	7	-1.7	-2.07	-1.8	1.66	-1.9	-2.21	1.36	
Ovarian Cancer Signaling	7	-1.6	1.5	-1.5	-1.4		1.68	1.31	1.14
Hepatic Cholestasis	7	-1.8	1.91	-2.3	1.79	-2.1	1.98	1.32	
Atherosclerosis Signaling	7	-2.4	2.11	2.18	2.14	2.17	2.03	1.34	
MSP-RON Signaling Pathway	7	-2.2		1.75	2.62	2.17	1.87	1.32	-1.15
eNOS Signaling	7	-1.6	-1.6	1.48	-1.3		1.73	1.31	-1.13

Table 6. Disrupted Pathways Based on TALE DEGs. The most frequently perturbed pathways within each shared network are represented in the table. The cell value indicates the average change in fold change for the genes involved in this pathway while the color indicates the overall direction of the genes. Red indicates that more genes involved in the pathway have increased expression while blue indicates the genes involved have decreased expression values. The most common theme among these pathways are inflammation with multiple interleukin signaling pathway as well as some autoimmune pathways commonly found in rheumatoid arthritis.

neuromuscular junctions, hepatic fibrosis, and role of osteoblasts, osteoclasts, and chondrocytes in rheumatoid arthritis. The common themes that underlie these enriched pathways are lipid metabolism, extracellular matrix, and disrupted inflammation.

Merged Transcriptional Network and Centrality Analysis

Seven human and murine shared networks were merged into a single network, consisting of 688 genes that interacted with up to 304 other genes in the network (Figure 4A). Using the *sna* package in R, this merged network was analyzed to identify the most central and influential genes within the network. The four measures of centrality used included closeness, betweenness, degree, and eigenvector values. Table 7 lists the 14 most central genes that are ranked among top 10 in each centrality measure. While these genes exhibit overlap with Figure 4B, they also represent a more thorough and analytical measure of gene influence within the network, while the previous figure assists in clarifying the complex merged network. These genes include interleukin 1 beta (IL1B), hepatocyte growth factor (HGF), c-c motif chemokine ligand 2 (CCL2), CD36, FOS, and JUN. While transcription factors such as FOS and JUN are likely to be central to a network as regulators of many genes, the inclusion of cytokine and chemokines such as IL1B, HGF, and CCL2 further supports the involvement of the immune system in DPN[198,203–205].

The 14 most central genes were also used as input to IPA in order to identify enriched pathways represented by these influential genes. The top 20 canonical pathways are shown in Table 8 with $-\log_{10}$(p-value) as a measure of

significance; the ratio represents the proportion of the 14 central genes to all the genes involved in the canonical pathway. Ratio values in this case are expected to be low since our input gene list was only the 14 genes identified as most central within the network. The most significant pathways include HMGB1 signaling and Glucocorticoid receptor signaling.

We further extended our pathway enrichment analysis to the 64 most central genes, belonging to the top 50 in at least one centrality measure. Based on gene overlap and shared directionality among pairs of these pathways, we constructed a contextual similarity network in Figure 5, where edges from the top 25% similarity scores are included. InfoMap[206], a network clustering algorithm, was used to identify sub-networks or clusters that are highly interconnected. These clusters shared common functional themes, and the largest cluster of canonical pathways was associated with immune response and inflammation (in green in Figure 5).

Symbol	Description	Degree (p-value)	Closeness (p-value)	Betweenness (p-value)	Eigenvector (p-value)
PIK3CA	phosphoinositide-3-kinase, catalytic, alpha polypeptide	406 (p=1.8E-08)	0.00081 (p=6.4E-01)	43246.5 (p=0.0E+00)	0.16 (p=2.9E-03)
MAPK8	mitogen-activated protein kinase 8	372 (p=3.8E-07)	0.00078 (p=6.6E-01)	30937.8 (p=0.0E+00)	0.15 (p=6.3E-03)
CD44	CD44 molecule (Indian blood group)	349 (p=1.3E-08)	0.00075 (p=6.6E-01)	32129.4 (p=0.0E+00)	0.13 (p=7.3E-03)
MAPK1	mitogen-activated protein kinase 1	280 (p=3.5E-03)	0.00074 (p=6.5E-01)	19719.2 (p=1.7E-03)	0.13 (p=3.9E-02)
CREB1	cAMP responsive element binding protein 1	283 (p=1.2E-08)	0.00073 (p=6.4E-01)	15524.7 (p=0.0E+00)	0.12 (p=3.0E-03)
LEP	leptin	301 (p=8.7E-10)	0.00072 (p=6.6E-01)	22639.7 (p=0.0E+00)	0.12 (p=5.6E-03)
CCL2	chemokine (C-C motif) ligand 2	276 (p=3.3E-03)	0.00071 (p=6.9E-01)	13595.3 (p=4.5E-03)	0.12 (p=1.0E-01)
JUN	jun proto-oncogene	232 (p=5.9E-03)	0.00071 (p=6.7E-01)	11905.8 (p=1.2E-02)	0.12 (p=4.3E-02)
ESR1	estrogen receptor 1	269 (p=4.7E-09)	0.00071 (p=6.6E-01)	17433.2 (p=0.0E+00)	0.11 (p=5.8E-03)
FOS	FBJ murine osteosarcoma viral oncogene homolog	229 (p=3.1E-03)	0.00070 (p=6.4E-01)	21885.2 (p=2.5E-07)	0.10 (p=7.4E-02)
CD36	CD36 molecule (thrombospondin receptor)	247 (p=5.0E-07)	0.00070 (p=6.5E-01)	11865.1 (p=6.5E-13)	0.11 (p=7.2E-03)
IL1B	interleukin 1, beta	224 (p=6.5E-03)	0.00070 (p=6.6E-01)	12492.5 (p=3.4E-03)	0.09 (p=1.6E-02)
HGF	hepatocyte growth factor (hepapoietin A; scatter factor)	213 (p=9.4E-06)	0.00069 (p=6.6E-01)	8254.8 (p=2.6E-07)	0.12 (p=4.6E-03)

Table 7. Centrality Analysis Gene Results. Centrality analysis was conducted using the Cytoscape plug-in CentiScaPe and four centrality metrics (degree, eigenvector, closeness, and betweenness) to identify the most important nodes (*i.e.*, genes) in the merged transcriptional network. The top 10 ranked genes in each perspective centrality metric is included in the table and indicate the most influential genes within the network. The centrality scores of each node were compared against the background distribution of centrality scores that were obtained from randomly generated 1,000 random merged networks. P-values were calculated using z-test to examine the significant difference between the real and random networks.

Ingenuity Canonical Pathways	-log$_{10}$(p-value)	Genes	Ratio
HMGB1 Signalling	14.2	FOS, PIK3CA, JUN, CCL2, MAPK1, MAPK8, IL1B, PLAT	0.06
Glucocorticoid Receptor Signalling	13.6	FOS, PIK3CA, JUN, CCL2, MAPK1, CREB1, MAPK8, IL1B, ESR1	0.03
GDNF Family Ligand-Receptor Interactions	11.3	FOS, PIK3CA, JUN, MAPK1, CREB1, MAPK8	0.08
Neurotrophin/TRK Signalling	11.3	FOS, PIK3CA, JUN, MAPK1, CREB1, MAPK8	0.08
Estrogen-Dependent Breast Cancer Signalling	11.2	FOS, PIK3CA, JUN, MAPK1, CREB1, ESR1	0.08
LPS-stimulated MAPK Signalling	11	FOS, PIK3CA, JUN, MAPK1, CREB1, MAPK8	0.07
HGF Signalling	10.2	FOS, PIK3CA, JUN, MAPK1, HGF, MAPK8	0.05
Renin-Angiotensin Signalling	10.1	FOS, PIK3CA, JUN, CCL2, MAPK1, MAPK8	0.05
IL-6 Signalling	9.92	FOS, PIK3CA, JUN, MAPK1, MAPK8, IL1B	0.05
Aryl Hydrocarbon Receptor Signalling	9.66	FOS, JUN, MAPK1, MAPK8, IL1B, ESR1	0.04
Role of Macrophages, Fibroblasts and Endothelial Cells in Rheumatoid Arthritis	9.38	FOS, PIK3CA, JUN, CCL2, MAPK1, CREB1, IL1B	0.02
IL-2 Signalling	9.37	FOS, PIK3CA, JUN, MAPK1, MAPK8	0.08
UVB-Induced MAPK Signalling	9.3	FOS, PIK3CA, JUN, MAPK1, MAPK8	0.08
IL-10 Signalling	9.23	FOS, JUN, MAPK1, MAPK8, IL1B	0.07
EGF Signalling	9.23	FOS, PIK3CA, JUN, MAPK1, MAPK8	0.07
Acute Phase Response Signalling	9.17	FOS, PIK3CA, JUN, MAPK1, MAPK8, IL1B	0.04
Chemokine Signalling	9.14	FOS, JUN, CCL2, MAPK1, MAPK8	0.07
Toll-like Receptor Signalling	9.05	FOS, JUN, MAPK1, MAPK8, IL1B	0.07
CD40 Signalling	8.93	FOS, PIK3CA, JUN, MAPK1, MAPK8	0.06
Dendritic Cell Maturation	8.86	PIK3CA, LEP, MAPK1, CREB1, MAPK8, IL1B	0.03

Table 8. Top 20 IPA Canonical Pathways Based on the Most Central Genes.
The 14 genes identified by CentiScaPe to be the most central genes within the merged network based on the four centrality measures were used as input for IPA to analyze pathway enrichment. This table represents the enriched pathways based on these genes with –log$_{10}$(p-value) as a significance measure and the ratio as the proportion of significant DEGs measured over the total genes within the pathway. HMGB1 signaling, Glucocorticoid receptor signaling, as well as the various interleukin pathways indicate disrupted inflammation as a central influence within the cross-species shared network. The ratio represents the proportion of the 14 central genes to all the genes involved in the canonical pathway.
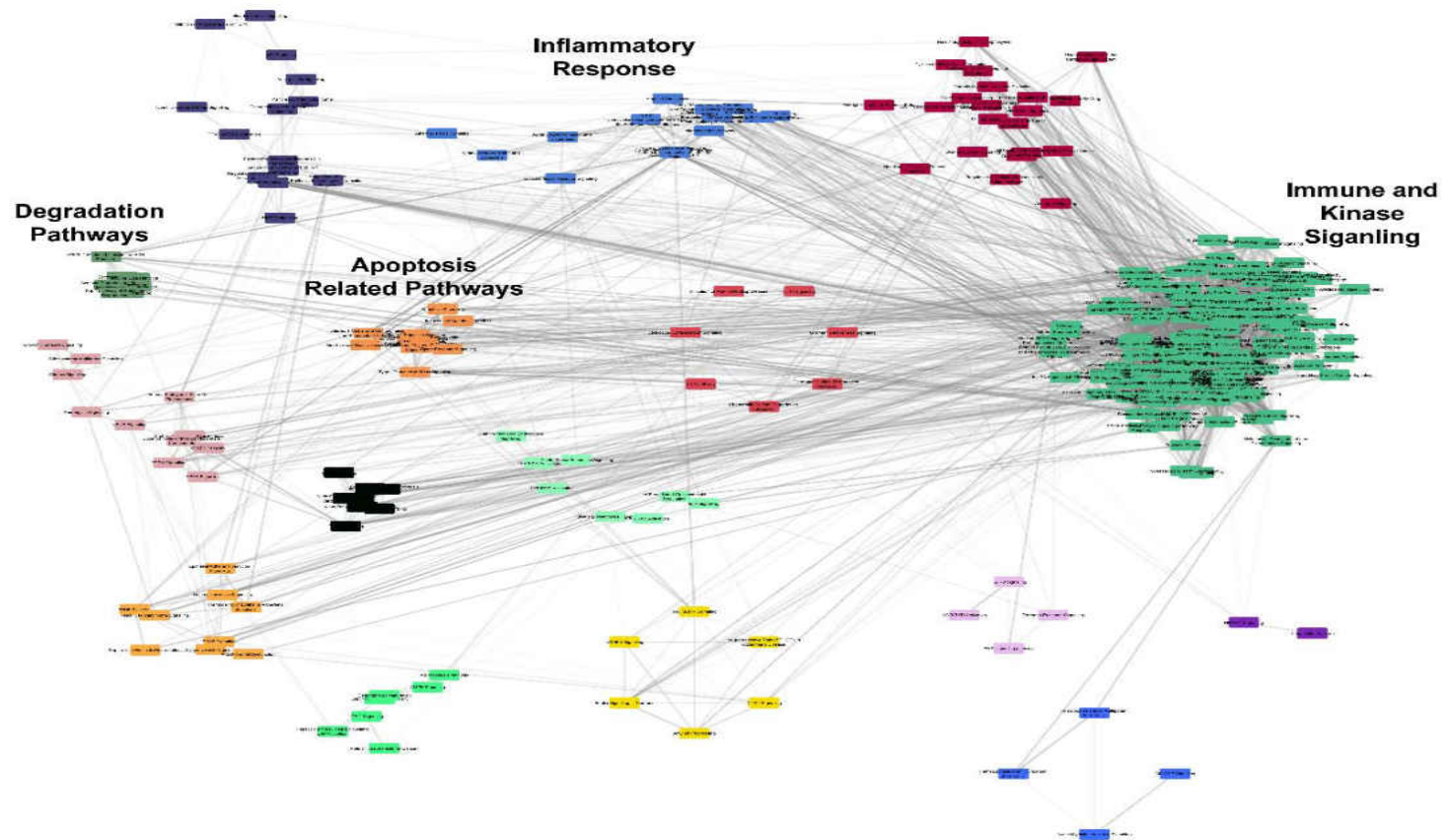
Figure 5. IPA Enriched Pathway Clustering. The pathways found to be enriched by IPA based on the top 64 most central genes, belonging to the top 50 in at least one centrality measure, within the merged network. 272 canonical pathways determined significantly enriched by IPA were examined for their similarity in terms of gene content and shared directionality among the pathways. Edges, connections between pathways, are only included if their similarity scores were among the top 25%. InfoMap[206], a network clustering package in R, was used to identify clusters, which are represented in different colors. These clusters shared common functional themes, which are noted in the figure. The largest cluster of canonical pathways were associated with immune response and inflammation (in green). Colors of the node denote the clusters identified by InfoMap.

Discussion

In our first study, we compared transcriptomic changes in peripheral nerves isolated from humans and mouse models of T1DM and T2DM at various stages of DPN to identify potential molecular pathways contributing to disease. We previously examined these changes during the development of DPN in both mouse models and human patients[177,178,180,181] and determined critical genes and pathways that play an important role in DPN. However, no systematic comparison of these transcriptomics datasets has been made. In the current study, using our published datasets, transcriptomic changes were compared in multiple mouse models of diabetes at different stages of the disease as well as in human subjects with DPN. Changes in one human and seven murine microarray datasets - at both the gene and pathway level – were examined using a single unified analysis pipeline to identify common pathways involved in the development of DPN. In total, we identified over 380 pathways that were enriched across all data sets, providing new insights into DPN pathogenesis.

Many of the pathways that were dysregulated in our previous reports were similarly dysregulated when compared across the seven murine models and human samples, including pathways associated with immune system, cellular development and cellular survival[176,178,181,188,199]. In addition, we show that key pathways governing lipid metabolism (LXR/RXR, adipogenesis and PIK3CA) and extracellular matrix homeostasis (chondrocytes, paxillin, and fibrosis), that have been highlighted in our previous study, were also altered in the current setting[178]. Consistent with previous reports, transcriptional changes associated with

estrogen signaling were observed, as sex-specific risk levels for diabetic complications have been well documented in human[207] and mouse[184,208] models.

In agreement with our previous studies[176–178,182–184,199], we observed transcriptomic and functional pathway changes in multiple immune-related pathways in all of the data sets. In particular, our results indicate that key pathways involved in the control of immune and inflammatory functions were upregulated during DPN, including NF-κB and JAK/STAT pathways. In fact, these pathways are activated in the DRGs of diabetic rats and have been associated with nerve injury in diabetes[188,209,210]. Our findings support targeting these pathways in murine models of diabetes to understand their pathophysiological roles in DPN[189,211]. We found that both pro- and anti-inflammatory cytokine pathways were dysregulated across data sets: IL-2, IL-6, and IL-10 as well as chemokines were all altered in DPN. Studies have shown that cytokines and chemokines not only promote existing inflammatory and immune responses, but also induce oxidative and nitrosative stress, further exacerbating cellular injury in experimental models of DPN[212]. In fact, during inflammation, both pro- and anti-inflammatory pathways are often simultaneously engaged as a disease process such as DPN transitions from active to chronic inflammation. For instance, neuronal repair is initiated by neutrophils[213] and driven by macrophages[214] under specific environmental conditions that are anti-inflammatory; however, as the disease process progresses, the introduction of pro-inflammatory signals overrides the anti-inflammatory response, resulting in tissue destruction. This concept is established in neurodegenerative disorders

such as amyotrophic lateral sclerosis[215], and our data strongly suggest a similar process is occurring in DPN.

The importance of the immune system is further highlighted by the fact that many of the pathways we observed dysregulated across all murine models and human samples, including those involved with transcription, cellular development, and lipid metabolism are also involved in the immune response. We show that HMGB1 signaling, which is centrally involved in the regulation of gene transcription, is one of the most highly dysregulated canonical pathways. However, HMGB1 is also secreted by macrophages and damaged cells and mediates systemic inflammation[216] by signaling through receptors such as the Receptor for Advanced Glycation End-products (RAGE) and Toll-Like receptors (TLRs), both of which have been implicated in obesity-driven inflammation and DPN[217–220]. This signaling cascade may drive NF-κB pathway that further exacerbates the inflammatory response and increases tissue damage.

Moreover, disrupted lipid metabolism is associated with inflammation. PPAR-γ, a major regulator of lipid and glucose metabolism, is altered in murine models as well as in human and has been previously implicated as a common factor in both DPN and diabetic nephropathy[176,180]. Yet, PPAR-γ can also control inflammation in macrophages and dendritic cells[221,222]. Besides its established role in inflammation, the LXR/RXR system has emerged as a key regulator of cholesterol, fatty acid and glucose homeostasis, and neuroprotection[223–225]. Additionally, LXR/RXR has been increasingly shown to play an important role in diabetic complications[225–228]. Interestingly, LXR/RXR is observed as a shared

pathway across murine models[222,229]. To a further extent, our results show an initial downregulation of the LXR/RXR pathway in the *db*/*db* mouse model after 8 weeks of diabetes and an upregulation at late stages of the disease. In contrast, LXR/RXR expression was upregulated in the *ob*/*ob* mouse model throughout the duration of diabetes and after 34 weeks of diabetes in STZ-induced T1DM mice, while no data were reported at earlier time points for T1DM mice. Collectively, our findings point toward a potential involvement of the LXR/RXR pathway in DPN. Taken together, our data further support a pivotal role of the immune system in DPN, though it is unclear from the current data to what extent this involvement is a cause or consequence of neuronal damage. We are currently addressing this question in both experimental[198] and clinical settings (https://clinicaltrials.gov/show/NCT02936843).

On a different note, while numerous pathways were dysregulated across data sets, the direction of transcriptional change was rarely universal. For many pathways, we found that mouse models of DPN and human tissue transcription were differentially expressed in opposite directions; whereas pathways in mice were upregulated, they were frequently downregulated in human patients. Similar cross-species discrepancy in gene expression direction was also observed in diabetic nephropathy between human and murine models[189]. There are several potential explanations for these discrepancies. The first is that the kinetics of murine and human DPN progression are different; we observed transcriptomic changes in mouse models of DPN up to 24 weeks (T2DM) and 34 weeks (T1DM), but it is unlikely these mice completely represent the advanced stages

of DPN encountered in human after decades of disease. Tissue sources may also account for these differences, as human data sets were obtained from sural nerves while mouse data were collected from sciatic nerves. We are currently exploring discordant transcriptomic dysregulation in the sciatic and sural nerves of mouse models, as a similar effect may be occurring here.

Alternatively, the nature of the controls in each species may have influenced the results. Whereas changes observed in the murine models are a result of a diabetic versus non-diabetic comparison, human transcriptomic data are a result of comparisons between progressive and non-progressive DPN. We recently conducted a transcriptional network analysis of DPN progression using the same *db/db* microarray data at 8, 16, and 24 weeks[183] used in the current study. This study identified various DPN progression-associated genes and pathways, which were overlapping with those identified in the present study, such as TLR signaling, dendritic cell maturation, LXR/RXR activation, and various cytokine pathways. Furthermore, O'Brien *et al.*'s original publication on the *ob/ob* mouse model data at 5 and 13 weeks[177] included a similar comparative analysis result. In this study, inflammatory mechanisms were found to have a critical role in early development and progression of DPN, and genes related to inflammation, immune response, and chemotaxis were highly enriched at 5 weeks rather than 13 weeks. Both studies identified MMP12 as the most significantly up-regulated gene across different time points, which was also found to be shared between human and murine DPN in the current study, suggesting its potentially critical role in the progression of DPN in both the experimental and

clinical settings. Finally, in order to compare changes between species, an orthologue conversion was also used to convert murine gene identifiers to their human equivalent genes; as such it is possible that some murine genes were not captured in the current analyses.

We also found that many pathways that were downregulated or a mix of up/down regulation in T2DM-driven DPN were strongly upregulated in the data set from the T1DM STZ mouse model. To validate these data, we re-examined the outlier parameters in the data set as well as the background levels of each microarray; in both cases the exclusion criteria remained unmet (data not shown). The STZ dataset was held to the same criteria as all other murine models which allows for a unified comparison across models and species, yet we still found that most of the detected pathways were highly upregulated in T1DM. These data suggest that while similar molecular pathways are involved in DPN progression, the utilization of these pathways may be very different in T1DM and T2DM. This is supported by our previous study examining transcriptional changes in diabetic peripheral neuropathy and nephropathy in both T1DM and T2DM mouse models; we found that while there was a high transcriptional concordance in diabetic nephropathy, DPN-associated pathways were often highly discordant[188]. Together these data suggest that key molecular pathways are commonly involved in DPN but that they may be differentially regulated in T1DM and T2DM. This concept is further supported by our reports in man, where a systemic review of clinical trials strongly suggest different pathogenic mechanisms underlying DPN in T1DM versus T2DM[230].

In summary, our transcriptional network-based approach, integrating multiple bioinformatics analyses, identified DPN-associated pathways that are highly conserved across multiple murine models and human. Many of the pathways identified highlight the importance of the immune system through cytokine and chemokine signaling as well as the observed dysregulated pathways associated with transcription, cellular development, and lipid metabolism are all involved in the immune response. The observed conserved pathways are likely the key responses in DPN and provide new therapeutic targets for the potential treatment of DPN, a disorder that remains without a drug intervention to date.

CHAPTER III

CONSERVED GENE EXPRESSION CHANGES AND DYSREGULATED
PATHWAYS IN COMPLICATION-PRONE TISSUES OF STREPTOZOTOCIN-
INDUCED DIABETIC MICE

Abstract

Diabetic peripheral neuropathy (DPN) and diabetic nephropathy (DN) are
two common complications of diabetes that are associated with a high degree of
morbidity. Currently, treatments only manage the symptoms of these
complications rather than targeting cause of the disease. There is therefore a
critical need to identify treatment strategies that impact the underlying disease
pathogenesis. In this study, diabetes was induced in Male C57BLKS *db/+* mice
with a single high-dose 150 mg/kg (i.p.) streptozotocin (STZ) injection at 6 weeks
of age. STZ-treated mice developed type 1 diabetes mellitus (T1DM)
phenotypes: significantly lowered body-weight and insulin level, and highly
elevated levels of fasting glucose, triglyceride and cholesterol. Sciatic nerves,
dorsal root ganglia, kidney renal cortex, and glomeruli tissues were harvested at
16 weeks of age and examined for differential expression between control and
STZ-diabetic mice using an RNA-Sequencing (RNA-seq) approach. We identified
differentially expressed genes (DEGs) ranging from 76 to 4130 in four tissues.
242 DEGs were common in three or more tissues, with three quarters of genes
displaying concordance in the directions of expression change across tissues.
We also identified 309 significantly enriched pathways, 38 of which were shared

across at least three tissues. Network analysis revealed clusters of pathways involving oxidative stress, cell cycle regulation, and inflammation as being important enriched pathways from the list of concordant genes. These findings provide transcriptomic profiles of complication-prone tissue in the STZ model of T1DM and describe factors influencing both DPN and DN.

Introduction

T1DM accounts for approximately 5% of the diabetic population and typically describes the autoimmune destruction of pancreatic β cells leading to insulinopenia and systemic hyperglycemia[231]. This condition is managed through rigorous insulin therapy but even under strict glycemic control patients can experience the microvascular complications associated with T1DM. DPN and DN are two of the most common complications associated with diabetes occurring in 20% of patients with T1DM[232–234].

DPN is characterized by the chronic, symmetrical, and distal degeneration of peripheral nerves in a progressive manner leading to symptoms including pain, hypersensitivity, and burning or tingling sensations[235]. Progression of this condition can lead to the loss of sensory input and is often associated with the diabetic foot condition which is the leading cause of non-traumatic lower limb amputations[236]. DN involves the loss of kidney function and is the leading cause of end stage renal disease (ESRD) accounting for around 50% of cases[237]. DN is often identified by proteinuria due to glomeruli damage, such as basement membrane thickening, which can lead to low serum albumin levels. DN is usually a slowly progressive condition but due to current treatments limitations, ultimately

many patients reach ESRD. These complications are in dire need of mechanism-based therapies and to better examine these diseases many animal models have proven invaluable to the support of basic and translational studies aiming to uncover novel therapeutic strategies[192,238].

The most common model used to study T1DM is the STZ-induced model. STZ is a glucosamine-nitrosourea compound isolated from *Streptomyces achromgenes* as a broad spectrum antibiotic and antineoplastic agent[239]. Single high dose (SHD) or consecutive multiple low dose (MLD) of STZ can induce a T1DM like condition in murine models by ablating pancreatic β cells through the glucose transporter 2[240,241]. These dosing paradigms have been shown to have critical differences with SHD having a robust and early complication phenotype as well as high mortality while the MLD regiment exhibits a low to moderate complication phenotype[242–244].

This study utilized the SHD paradigm to examine the transcriptomic changes occurring in DPN (sciatic nerve and dorsal root ganglia) and DN (glomeruli and renal cortex) prone tissues. Many transcriptomic studies have been conducted using microarray data in an attempt to investigate underlying causes of diabetic complications which have indicated mechanisms involving inflammation, oxidative stress, as well as various metabolic processes[176,180,245]. Comparisons between DPN and DN have been previously conducted in an effort to identify a possible unified approach to treating these microvascular complications associated with T1DM and type 2 diabetes mellitus (T2DM)[246,247]. However, the significance of this study is that it examines and compares the

transcriptomic profiles in the STZ-model of T1DM in an effort to identify possible shared mechanisms.

Methods

Sample Collection and Processing

Male C57BLKS (BKS) *db/+* were fed a standard diet (AIN76A; 11.5% kcal fat; Research Diets, New Brunswick, NJ, USA) and cared for in a pathogen-free environment by the University of Michigan Unit for Laboratory Animal Medicine. Diabetes was induced in BKS *db/+* mice with a single high-dose 150 mg/kg (i.p.) STZ injection at 6 weeks of age. STZ-treated mice developed T1DM phenotypes according to Diabetic Complications Consortium guidelines[248,249] including significantly lowered body-weight and insulin level, and highly elevated levels of fasting glucose, triglyceride and cholesterol (Figures 6,7,8).

Total RNA was isolated from sciatic nerves (SCN, n=6), dorsal root ganglia (DRG, n=6), kidney renal cortex (Cortex, n=6), and glomeruli (Glom, n=6) tissues harvested at 16 weeks of age from both untreated and STZ-treated BKS *db/+* mice. RNA quality was evaluated using TapeStation (Agilent, Santa Clara, CA) with an RNA integrity number of ≥8 as the cutoff for further sample processing with the Illumina TruSeq mRNA Sample Prep v2 kit (Catalog #s RS122-2001, RS-122-2002; Illumina, San Diego, CA, USA). Resulting cDNA was sequenced with a paired-end read length of 100 bases using an Illumina HiSeq 2000 (Illumina, Inc., San Diego, CA, USA) by the University of Michigan DNA Sequencing Core (http://seqcore.brcf.med.umich.edu/).
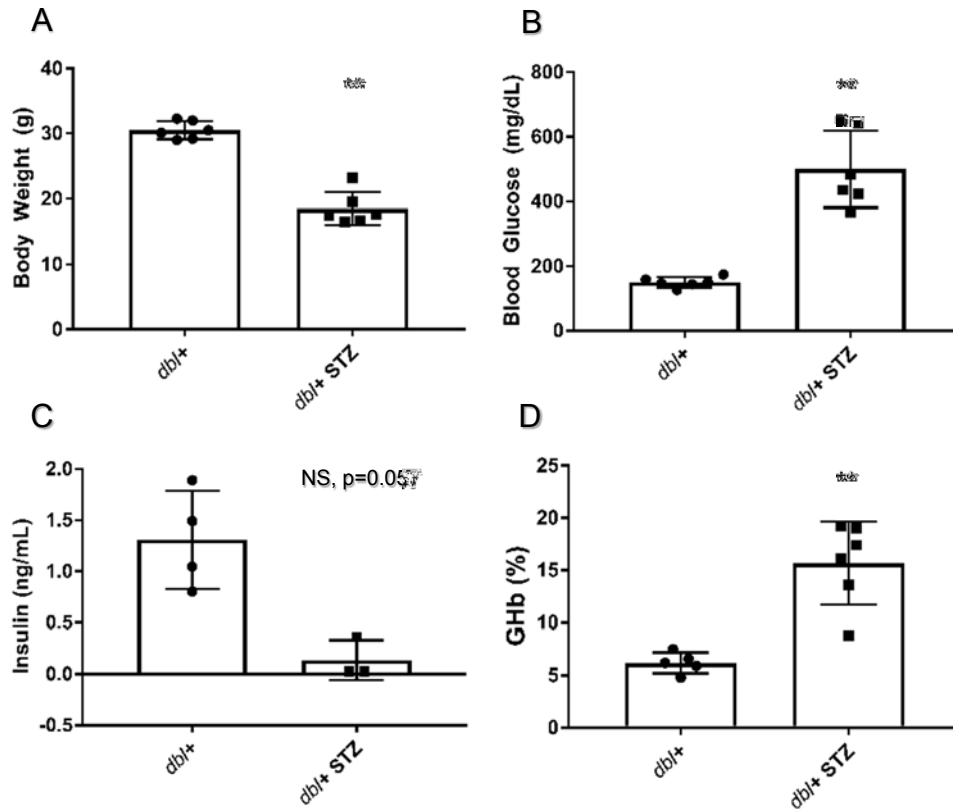
Figure 6. Metabolic Phenotype *db/+* mice testing following STZ treatments.
Metabolic phenotyping including body weight (A), fasting blood glucose (B),
fasting plasma insulin (C), and glycated hemoglobin (D).
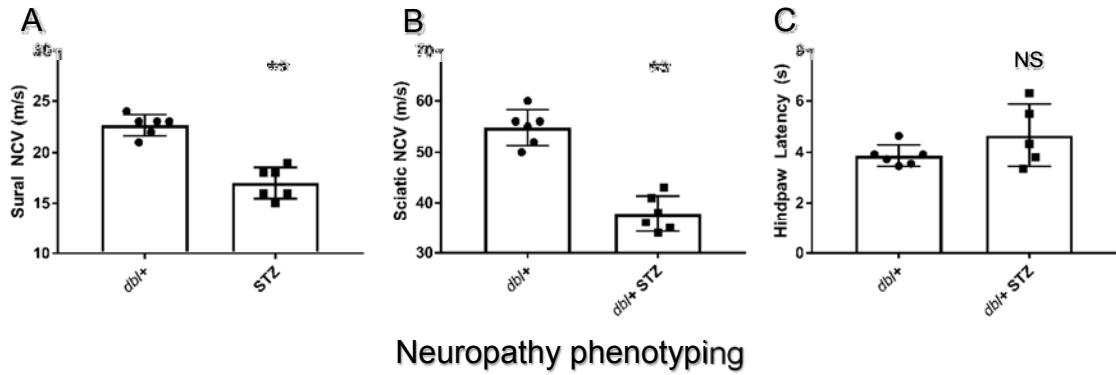
Figure 7. Neuropathy Phenotype *db*/+ mice testing following STZ treatments. Neuropathy phenotyping included sural nerve conduction velocity (NCV) (A), sciatic NCV (B), and hindpaw withdrawal latency (C).
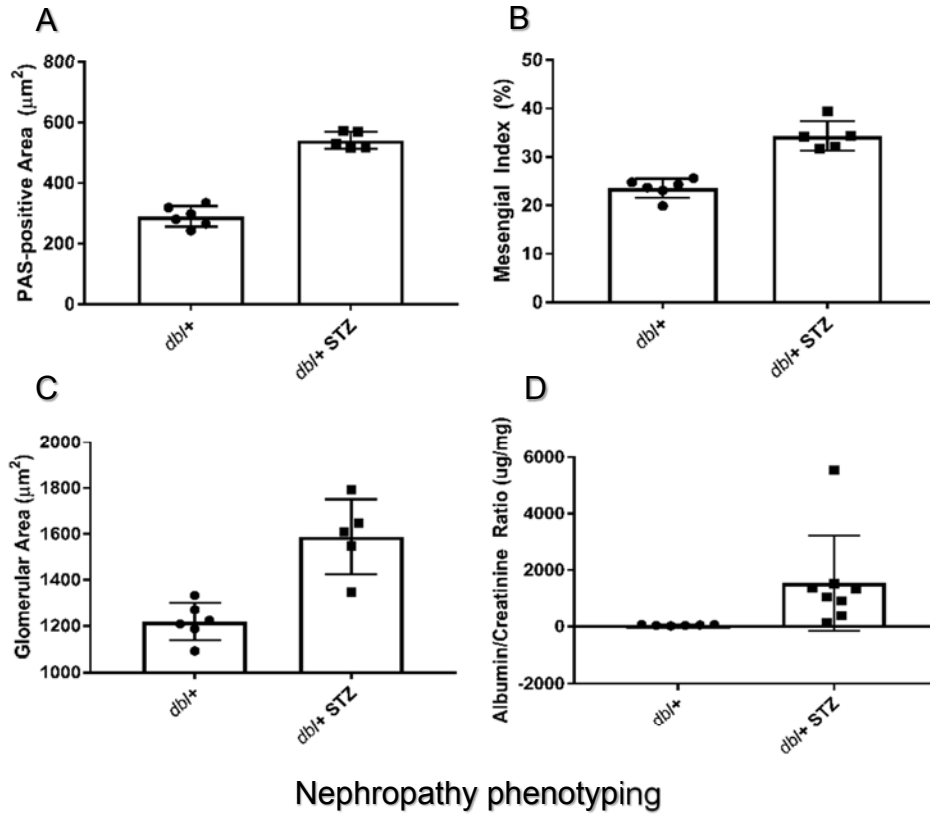
Figure 8. Nephropathy Phenotype *db*/+ mice testing following STZ treatments. (C) Nephropathy phenotyping included glomerular periodic-acid schiff (PAS)-positive area (A), Mesangial Index (B), glomerular area (C), and albumin/creatinine ratio (D). All measurements were taken at 16 weeks of age in all mice. *, p<0.05, **, p<0.01, ***, p<0.001, NS, not significant.

Raw sequencing reads were cleaned using Trimmomatic to remove reads with adapter or Poly-N sequences as well as reads with a quality score <30[250]. Quality control assessment of RNA-Seq data was completed using the FastQC version 0.10.1[251]. Cleaned reads were mapped to the mouse reference genome m38.p6 Refseq using HISAT2[252]. FeatureCounts[253] was used to count uniquely mapped reads while genes with zero expression across samples were omitted from differential expression analysis. Fragments per kilobase of exon per million mapped reads (FPKM) as a measurement of transcript expression were calculated using an in-house script.

Differential Expression and Pathway Enrichment

Differentially expressed genes (DEGs) were identified using the DESeq2 R package[254]. All genes with a Benjamini-Hochberg adjusted p-value less than 0.05 were determined to be differentially expressed between untreated and STZ-treated groups for each tissue type. These DEG lists were used as input for Ingenuity Pathway Analysis (IPA, QIAGEN Inc., https://www.qiagenbioinformatics.com/products/ingenuitypathway-analysis) to determine significantly enriched canonical pathways based on a negative log p-value greater than 1.3[255]. All four tissue types were analyzed for unique and overlapping DEGs and pathways.

Network Clustering

DEGs with shared directional changes across tissues were used as input gene sets for canonical pathway enrichment analysis through IPA. Pathways were determined to be significantly enriched based on a negative log p-value

greater than 1.3 and were then examined for their similarity of gene content. Gene overlap within each pathway were used to determine network edges, while pathways are represented as nodes. The R package InfoMap was used to identify clusters of highly interconnected pathways[256].

Results

Changes in Gene Expression

Global gene expressions were profiled in Cortex, Glom, DRG, and SCN isolated from the STZ-induced murine model of T1DM. DEGs were determined based on a comparison between STZ-treated animals and untreated control animals with a sample size of 6 for each group although one SCN sample from the STZ-treated group failed our quality control assessment. Each tissue had a varying number of DEGs identified with cortex having the most (4,130 DEGs) and DRG holding the least (76 DEGs) while the remaining tissues were much closer in terms of total DEGs with Glom (2,719 DEGs) and SCN (2,621 DEGs).

Figure 9A illustrates the overlap among the four DEG sets identified from each tissue. Of the DEGs only 242 were shared across three or more tissues. While there is a low amount of conserved expression changes across tissues, the overlapping DEGs show a high degree of similarity in regard to direction with 188 concordant and 54 discordant genes across tissue types (Figure 9B). Five genes were differentially expressed across all 4 tissues and down-regulated in all cases except for *Galnt16* in the renal cortex (Table 9). Approximately, half of the DEGs, were found to be unique to the specific tissue except for DRG. The DRG samples had a low number of unique genes with only 32% (24 genes) most likely

due to the low total DEGs identified. The other tissue samples had 52% (SCN, 1368), 55% (Glom, 1496), and 63% (Cortex, 2597) unique gene expression.

Enriched Canonical Pathways

Complete DEG lists were analyzed using IPA to determine enriched canonical pathways. Pathways were determined to be significantly enriched with a –log p-value greater than 1.3. Cortex had the most enriched pathways represented by the DEG list with 182 while DRG had the least with 36. The other tissues, SCN and Glom, had 104 and 162 pathways, respectively. The pathways identified totaled 309 with 6 enriched in all four tissue types and another 32 in at least three tissues (Figure 10). Pathway directionality was not always able to be determined based on Z-score. However, among the top six enriched pathways, acute phase response signaling and colorectal cancer metastasis signaling appear to be up-regulated in nephropathy and down-regulated in neuropathy (Table 10). Within the top six enriched pathways, PI3K/AKT signaling according to the Z-score was down-regulated in all tissues besides DRG. The discrepancy with DRG in this case is likely due to the low gene input being inadequate to calculate the Z-score. Within the larger list of pathways shared across at least three tissue types for which a Z-score was calculated, there are some interesting patterns. Signaling pathways such as p53, protein kinase A, and ILK all showed similar directional changes across tissues.
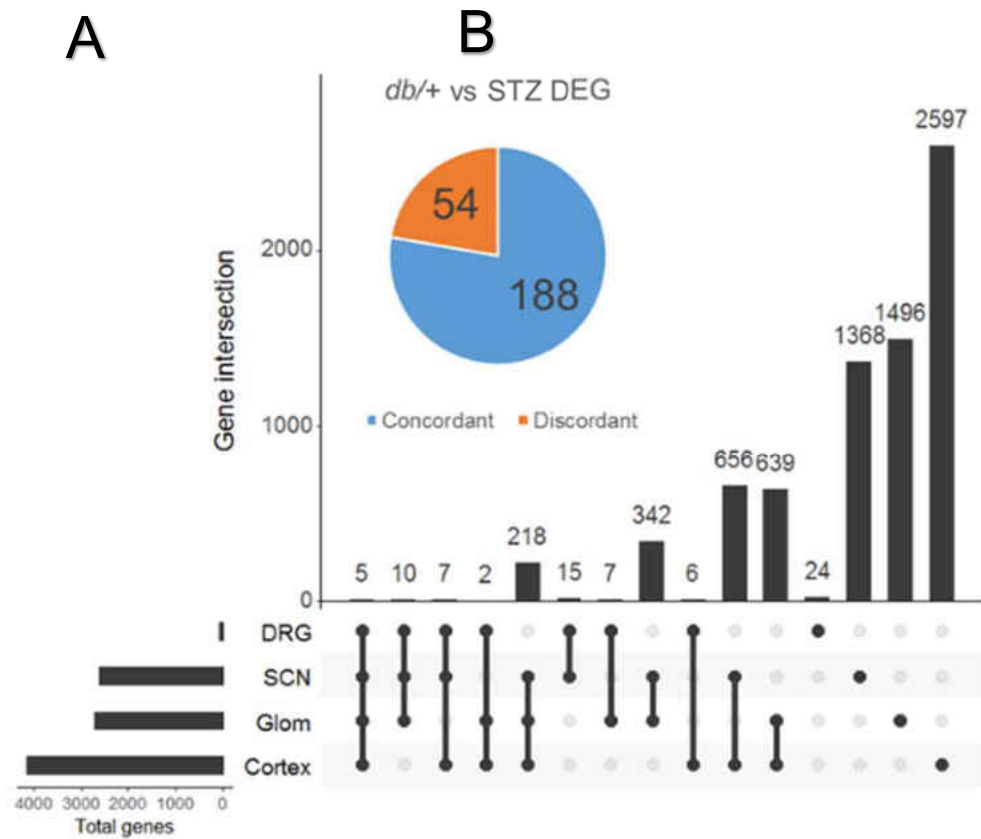
Figure 9. Gene Overlap Common between Complication-Prone Tissue. (A)
The bar graph represent the overlapping differentially expressed (DEG) genes
common among tissue types. **(B)** The venn diagram shows the proportion of
DEGs common across at least three tissue types with either concordant or
discordant expression changes.

Gene Symbol	Description	Cortex	DRG	Glom	SCN
Gm10639	predicted gene 10639	-6.42	-1.95	-2.41	-1.90
Galnt16	Polypeptide N-Acetylgalactosaminyltransferase 16	1.20	-0.96	-0.82	-1.05
Txnip	thioredoxin interacting protein	-1.40	-1.56	-0.87	-0.80
Mt2	metallothionein 2	-2.48	-1.97	-4.13	-2.26
Mt1	metallothionein 1	-2.06	-1.42	-2.81	-1.74
Slc25a16	solute carrier family 25 (mitochondrial carrier, Graves disease autoantigen), member 16	-0.34		-0.45	-0.47
Exoc5	exocyst complex component 5	-0.39		-0.40	-0.37
Mgea5	meningioma expressed antigen 5 (hyaluronidase)	-0.37	-0.54	-0.39	
Agfg2	ArfGAP with FG repeats 2	-0.77		-1.04	-0.81
Brap	BRCA1 associated protein	-0.34		-0.31	-0.38
Agt	angiotensinogen (serpin peptidase inhibitor, clade A, member 8)	-2.19		-1.62	-1.51
Shank3	SH3/ankyrin domain gene 3	0.53		-0.76	-0.66
Tc2n	tandem C2 domains, nuclear	1.30		-1.44	-1.61
Prss23	protease, serine, 23	-0.74		-0.80	-0.84
Pnpla2	patatin-like phospholipase domain containing 2	-1.43		-0.78	-1.13

Table 9. Gene Overlap Common between Complication-Prone Tissue. Each tissue was analyzed for differential expression using the DESeq2 package in R with an adjusted P value<0.05 as the significance cutoff. The color gradient and values within the table are log2 fold change for each gene within the tissue columns.
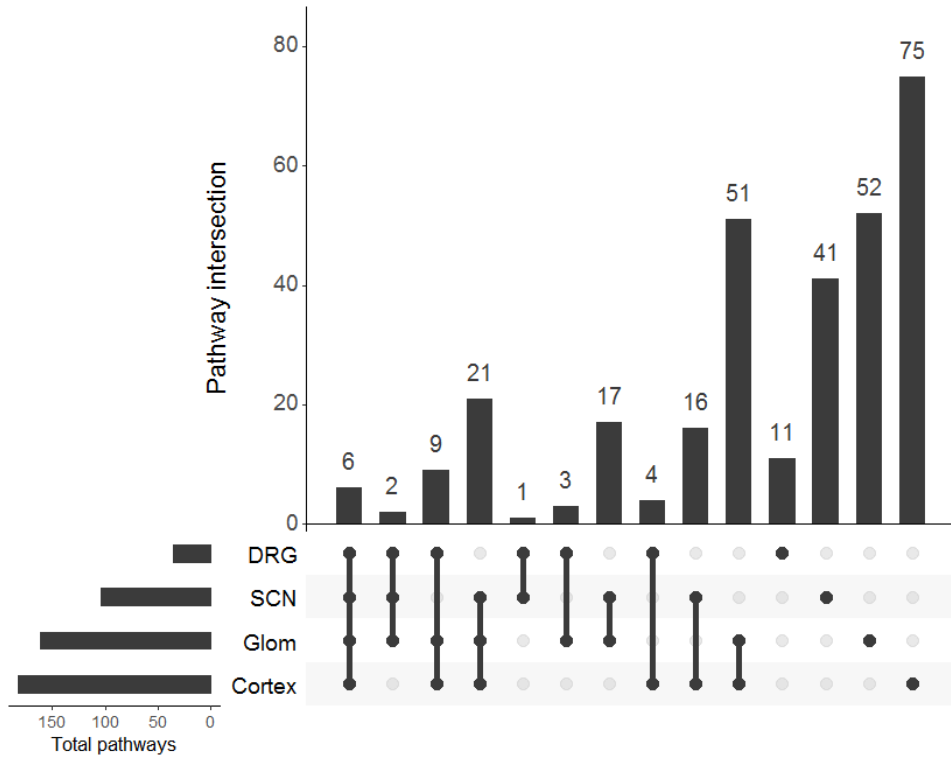
Figure 10. Enriched Pathways Common Between Complication-Prone Tissue. The bar graph represents the overlapping canonical pathways identified by IPA common among tissue types.

Ingenuity Pathway Analysis Enrichment	Cortex	DRG	Glom	SCN
Acute Phase Response Signaling	4.51	2.10	1.76	1.50
Adipogenesis pathway	2.34	1.38	3.47	2.22
Colorectal Cancer Metastasis Signaling	2.81	1.66	1.95	2.28
Role of Macrophages, Fibroblasts and Endothelial Cells in Rheumatoid Arthritis	2.56	1.41	2.58	2.02
PI3K/AKT Signaling	1.78	1.44	2.19	1.77
PTEN Signaling	1.77	1.47	2.40	1.43
Molecular Mechanisms of Cancer	6.99		4.97	4.87
Axonal Guidance Signaling	2.77		6.26	6.29
p53 Signaling	6.41		4.00	3.41
Hepatic Fibrosis / Hepatic Stellate Cell Activation		3.00	2.95	7.65
Aryl Hydrocarbon Receptor Signaling	5.30		3.93	2.87
Glioblastoma Multiforme Signaling	3.86		2.67	3.93
Aldosterone Signaling in Epithelial Cells	4.05		2.70	1.82
Germ Cell-Sertoli Cell Junction Signaling	2.02		2.73	3.54

Table 10. Enriched Pathways Common Between Complication-Prone Tissue. Each DEG set was analyzed for pathway enrichment using IPA then compared to identify common canonical pathways across tissues. The numbers within the table are -log (p values) representing significant enrichment while colors represent Z-scores indicating pathway directionality. Colorless boxes represent no directional change or a Z-score which could not be calculated.

Conversely, glioblastoma multiforme signaling, glioma invasiveness signaling, and integrin signaling was up-regulation in DN and down-regulated in DPN, suggesting different roles between complications. Insulin receptor signaling was down-regulated in DN related tissues while no Z-score was able to be calculated for DPN associated tissues.

Network Analysis of Concordant Gene Pathways

To further investigate possible shared characteristics influencing multiple complications, we isolated the 188 concordant genes out of the 242 genes shared across at least three tissues and used this list as input for IPA. The resulting list of enriched pathways was subjected to network analysis by evaluating for gene overlap to form the edges while pathways served as nodes (Figure 11). InfoMap was then used for community structure analysis which identified five different clusters within the network. This network level analysis explores the interconnections shared across our tissue datasets based on gene-gene associations in order to find related/associated pathways.

The main green cluster involving 17 out of 29 total pathways is a dense group involving pathways related to DNA damage stress responses, oxidative stress, immune response, and cell cycle. The blue cluster of five pathways is related to reactions in response to oxidative stress and maintaining a reducing environment[257,258]. The red cluster of four pathways includes metabolic pathways involved in both salvage and biosynthesis. The smallest clusters of one and two nodes also involve immune response with antigen presentation and histamine biosynthesis.

67
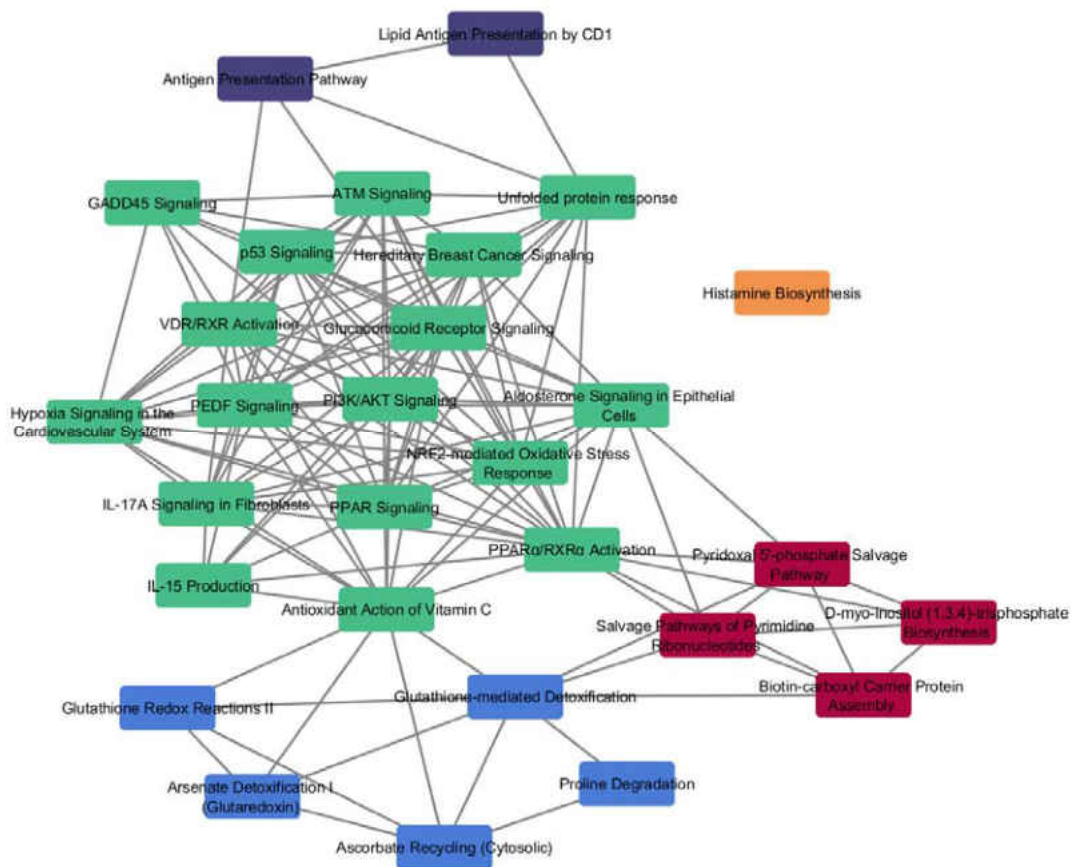
Figure 11. Clustering of Enriched Concordant Pathways. IPA identified 29 significantly enriched canonical pathways based on the list of 188 concordant genes shared across at least three tissue types. Pathways were then examined for their similarity of gene content to determine edges. InfoMap[256], a network clustering package in R, was used to determine clusters as represented by the differently colored nodes.

This small cluster has roles in multiple systems but its immune response is most evident in the context of the other network elements[259,260]. These network-level data of concordant shared genes indicate that both DPN and DN complications involve immune system response, oxidative stress, and cell cycle regulation in T1DM.

As expected, some pathways involved in our concordant DEG network were also enriched across 3 or more including glucocorticoid receptor signaling, aldosterone signaling in epithelial cells, p53 signaling, d-myo-inositol (1,4,5)-triphosphate biosynthesis, and PI3K/AKT signaling. Most other pathways involved in our network were also enriched in one or two individual tissues such as the NRF2-mediated oxidative stress response being upregulated in both DN associated tissues (Table 11).

Ingenuity Canonical Pathways	-log(p-value)	Ratio	z-score	Molecules
NRF2-mediated Oxidative Stress Response	2.96	0.04	NaN	GSTA5,JUNB,DNAJB2,FKBP5,MAFF,ENC1,GSTO1
Glucocorticoid Receptor Signaling	2.58	0.03	NaN	BCL2L1,NFKBIA,HSP90AB1,SGK1,FKBP4,CEBPB,FKBP5,AGT
IL-17A Signaling in Fibroblasts	2.54	0.09	NaN	NFKBIA,LCN2,CEBPB
Salvage Pathways of Pyrimidine Ribonucleotides	2.11	0.04	NaN	NME3,PIM1,SGK1,HIPK1
Histamine Biosynthesis	2.09	1.00	NaN	HDC
Unfolded protein response	1.98	0.05	NaN	CALR,PDIA6,CEBPB
GADD45 Signaling	1.98	0.11	NaN	GADD45B,GADD45G
Antioxidant Action of Vitamin C	1.92	0.04	NaN	PLCB4,NFKBIA,PDIA3,GSTO1
Aldosterone Signaling in Epithelial Cells	1.90	0.03	NaN	PLCB4,HSP90AB1,PDIA3,SGK1,DNAJB2
p53 Signaling	1.88	0.04	NaN	HDAC9,BCL2L1,GADD45B,GADD45G
Pyridoxal 5'-phosphate Salvage Pathway	1.79	0.05	NaN	PIM1,SGK1,HIPK1
Proline Degradation	1.79	0.50	NaN	LOC102724788/PRODH
PPARɑ/RXRɑ Activation	1.78	0.03	0	PLCB4,NFKBIA,HSP90AB1,PDIA3,INSR
Lipid Antigen Presentation by CD1	1.72	0.08	NaN	CALR,PDIA3
PI3K/AKT Signaling	1.71	0.03	0	BCL2L1,NFKBIA,HSP90AB1,INPP5K
D-myo-inositol (1,4,5)-Trisphosphate Biosynthesis	1.69	0.07	NaN	PLCB4,PI4K2A
Biotin-carboxyl Carrier Protein Assembly	1.61	0.33	NaN	ACACB
VDR/RXR Activation	1.58	0.04	NaN	CXCL10,CEBPB,KLF4
Glutathione-mediated Detoxification	1.58	0.06	NaN	GSTA5,GSTO1
ATM Signaling	1.55	0.04	NaN	NFKBIA,GADD45B,GADD45G
Hereditary Breast Cancer Signaling	1.51	0.03	NaN	HDAC9,GADD45B,GADD45G,WEE1
Arsenate Detoxification I (Glutaredoxin)	1.49	0.25	NaN	GSTO1
Ascorbate Recycling (Cytosolic)	1.49	0.25	NaN	GSTO1
Glutathione Redox Reactions II	1.49	0.25	NaN	PDIA3
PEDF Signaling	1.46	0.03	NaN	BCL2L1,NFKBIA,PNPLA2
Antigen Presentation Pathway	1.41	0.05	NaN	CALR,PDIA3
PPAR Signaling	1.36	0.03	NaN	NFKBIA,HSP90AB1,INSR

Table 11. Concordant Gene IPA results from Complication-Prone Tissues.
IPA enriched pathway results from our list of concordant DEGs are listed above.
Ratio indicates the number of genes included in our submitted list to their total
annotation list for that canonical pathway. Z-scores are used to determine
directionality. NaN indicates when a Z-score cannot be calculated and 0 indicates
no directionality based on the submitted genes and their fold change.

Discussion

Bioinformatics analysis in previous studies examined the shared factors between DPN and DN. However, no study has specifically examined the STZ-model of T1DM with a RNA-seq transcriptomic approach. While both T1 and T2DM have related phenotypes in terms of their complications, these diseases have quite different incidences of complications. For example, T1DM complications such as DPN and DN have an incidence rate of approximately 20%, while 42-45% of T2DM patients will also experience these complications[261,262]. Differences between T1 and T2DM complications extend beyond the rate of incidence. For instance, development of changes and neurotrophic support also leading to separate outcomes despite similar hyperglycemic conditions[263–266]. Findings such as these indicate a direct need for examination of T1DM complications as unique in order to develop future approaches for treating and preventing these complications.

The DRG dataset clearly showed a lower amount of expression change due to STZ treatment with only 76 DEGs compared to the other tissues which identified from 2,621 to 4,130 DEGs. The separation seen within the PCA plot suggests that this tissue was not heavily affected by the 10 weeks of hyperglycemia following STZ treatment (Figure 12). However, despite the minor gene expression changes induced in DRG tissue, mice involved in this study still demonstrated clear changes in neuropathic phenotyping (Figure 7). Due to the individual treatment of each tissue, the low amount of DEGs influence our conserved analysis by weighting the study more heavily toward tissues affected
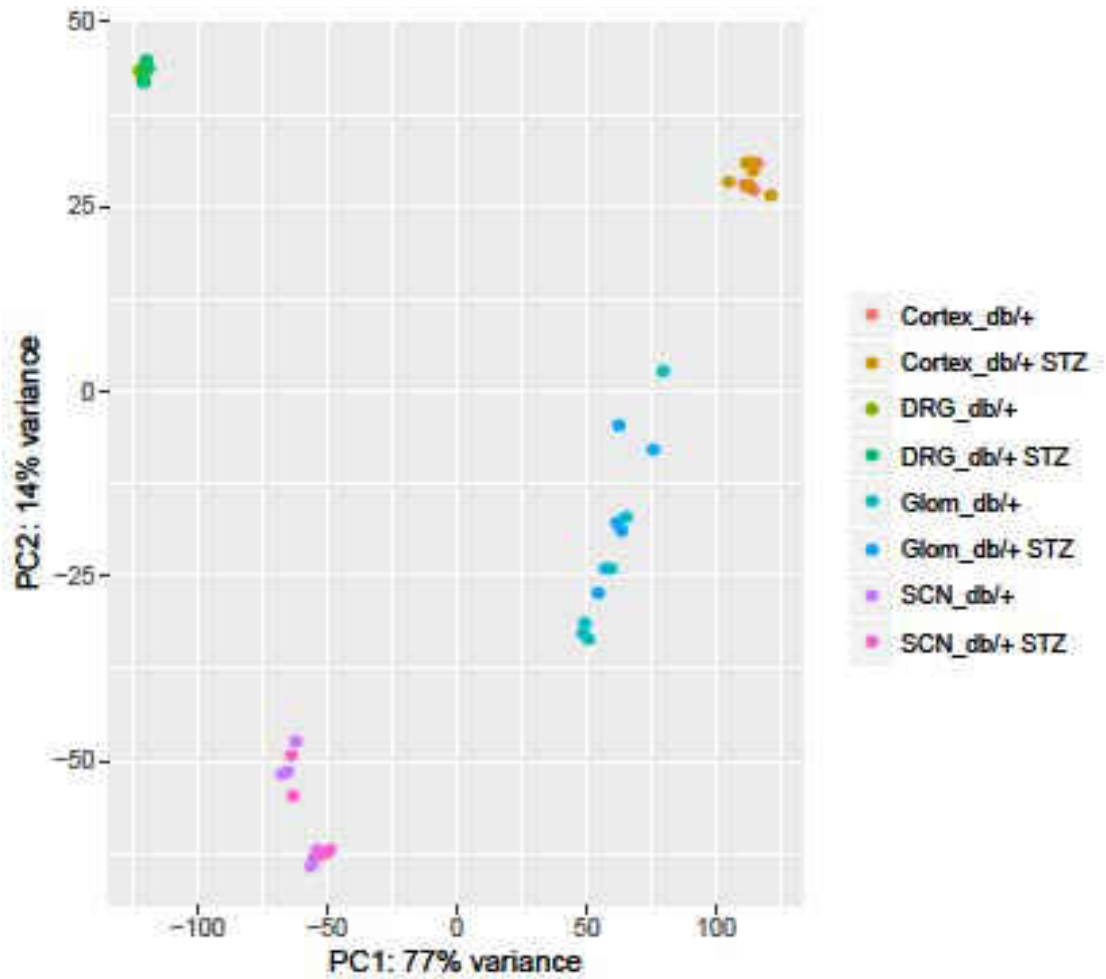
Figure 12. Principal Component Analysis of Four Tissues in STZ Treated Mice and Wild Type Controls. Principal component analysis (PCA) uses an orthogonal transformation to convert correlated variables into linear uncorrelated variables so that variance between samples can be visualized in the dot plot above. Each tissue groups into separate clusters although samples from both STZ treated and wild type mice intermix within those clusters.

by DN complication rather than DPN. While the conserved genes were most often represented in cortex, glomerulus, and sciatic nerve we had very little contribution to the total genes from the DRG tissue. However, despite this caveat, this study has identified potentially critical genes, pathways, and functions that may influence both DPN and DN in T1DM.

The initial examination of genes in the kidney and nerve of the SHD-STZ model after 10 weeks of hyperglycemia in this study revealed that although a low number of genes were disrupted in both DPN and DN, the genes affected in both conditions often showed a similar change when compared to healthy tissue. Over three quarters of shared genes showed a concordant directional change across tissues indicating that these shared genes are most often being influenced in a similar way for both conditions. DRG was the only tissue which did not demonstrate discordant expression directionality within the genes shared across three or more tissues. The other three tissues all had discordant genes with Cortex having the most (22) followed by Glom (16) and then SCN (15). The genes with discordant or opposite directionality between complication tissues need to be carefully considered whenever proposing treatments as these targets may exacerbate one condition while assisting in another. Roughly half of the genes identified as differentially expressed when comparing complication-prone tissue in our STZ-model to the healthy control were unique to the tissue used with the exception of DRG being 32% unique likely due to the low total DEGs. These unique DEGs should also be considered for similar reasons as discordant

73

genes but are most likely unique due to the different gene expression profiles of separate tissues.

In an effort to further elucidate the cellular systems influencing DPN and DN of the STZ T1DM model, pathway analysis of DEGs through IPA was also performed on each tissue as well as on the list of DEGs shared across three or more tissues. Unlike the DEGs shared across tissues which shared a high amount of concordance, the pathways shared across tissues between DPN and DN tissues. Out of 38 shared pathways, 21 were unable to support the Z-score calculation in any tissue (Table 11). However, it is of note that based on the low DEG count of DRGs, no Z-score was able to be calculated for the enriched pathways from DRG tissue. Within the group of pathways enriched in three or more tissues, acute phase response signaling, colorectal cancer metastasis signaling, glioblastoma multiforme signaling, glioma invasiveness signaling, and integrin signaling were all up-regulated in DN and down-regulated in SCN. Shared concordant pathways included ILK signaling and protein kinase A signaling which were up-regulated while PI3K/AKT signaling and p53 signaling were down-regulated. Many of the above pathways revolve around cell proliferation, cell cycle progression, and cell motility in a way that these cellular processes are increased in DN and decreased in DPN. This indicates that progression in both diseases is being observed through proliferation within the kidney tissue and degeneration in the sciatic nerve tissue[267–269].

Pathway analysis was also performed on the list of 188 concordant genes across tissues. To investigate connections and synergies between complications

the pathway results from concordant genes were also subjected to network analysis with overlapping genes as edges while pathways served as nodes. When compared with the list of shared DEGs, the concordant pathway network also showed shared edges (genes) between five pathways enriched within the full DEG data for each tissue as well. These pathways include D-myo-inositol (1,4,5)-trisphosphate biosynthesis, p53 signaling, aldosterone signaling in epithelial cells, glucocorticoid receptor signaling, and PI3k/AKT signaling which share BCL2L1, HSP90AB1, NFKBIA, and PLCB4. These genes were differentially expressed in all tissues, besides DRG, with HSP90AB1 and PLCB4 being upregulated while NFKBIA and BCL2L1 are downregulated. These genes are involved in the cell survival components of these pathways and may be an important influence in the progression of complications via their involvement in multiple pathways affecting three of our complication-prone tissues.

Network analysis also identified clusters of pathways associated with inflammation and oxidative stress as important components involved in the concordant expression profile across tissues (Figure 11). Oxidative stress and the glutathione pathways involved in our network structure specifically, have been shown to be directly linked to the risk of kidney complications in T1DM[258]. Inflammation has also been heavily linked to the progression of diabetic complications[132,270–274]. The pathways involved in our network influencing inflammatory response include glucocorticoid receptor signaling, IL-15 production, histamine biosynthesis, and the antigen presentation pathways. These pathways have been previously linked to diabetic complications with

elevated histamine levels observed in diabetic patients and linked to peripheral vascular diseases[275]. Glucocorticoids have been shown to induce a similar neurochemical pattern to a diabetic state in DPN[276]. PPAR signaling is also involved in our network structure and has been a therapeutic target of T2DM. Pioglitazone, a PPAR agonist, has been shown to have a therapeutic benefit in DN and for reducing neuropathic pain and nervous system inflammation in DPN[247,277–280]. Based on links within the literature, these pathways are also likely involved in the progression of diabetic complications in peripheral nerve and kidney tissues as observed in this study.

In a previous manuscript from our lab examining both DN and DPN in T1DM and T2DM using microarray data we observed both similar results[188]. The previous study examined common dysregulation between T1DM and T2DM. Gene expression in DPN tissue differed between T1DM and T2DM and DN tissue had similar expression patterns between T1DM and T2DM. The data presented here investigated multiple tissues for DN (Glom and Cortex) and DPN (SCN and DRG) while the previous study only examined Glom and SCN. Our previous study saw 62% concordance between DN and DPN in STZ-treated mice while we saw slightly higher with 77.7% of shared genes also sharing a directional change. Similar pathway enrichment reflecting oxidative stress and inflammation were also identified by both studies.

In summary, our comparison of the transcriptomic profiles of nephropathy and neuropathy prone tissues using the STZ-model of T1DM indicate that oxidative stress, cell cycle regulation, and immune response are important

factors conserved between conditions. These findings support previously identified factors influencing microvascular complications in T1DM and provide transcriptomic profiles of multiple tissues within the SHD STZ-model of the disease.

CHAPTER IV

ALPHA-SYNUCLEIN-INDUCED METHYLATION AND GENE EXPRESSION CHANGES IN MICROGLIA

Abstract

Parkinson's disease (PD) is the second most common neurodegenerative condition characterized by loss of dopaminergic neurons, α-synuclein accumulation, and neuroinflammation. Alpha synuclein (α-syn) has been implicated as a contributing factor in PD and can induce an innate immune response in the brain[281,282]. This protein is tightly regulated by methylation, however, the influence α-syn can have on methylation and expression patterns has not been examined[281–286]. Here we used reduced representation bisulfite sequencing (RRBS) to determine DNA methylation changes and RNA-sequencing to examine gene expression changes induced in microglia, the innate immune cell of the brain, by α-syn. The mThy1-Asyn mouse, which overexpresses human α-syn as a model of PD, has been used to study the influence α-syn has on microglia activation. Microglia DNA and RNA were isolated at 3 and 13 months of age from these mice and used for RRBS and RNA-sequencing to capture genomic methylation changes at CpGs and changes in gene expression. These transgenic mice have been shown to present markers of neuroinflammation as early as 1 month and begin to show motor and non-motor symptoms at 3 months similar to a pre-parkinsonian phenotype.

Reduction in dopamine levels and a more severe phenotype are observed at 14 months indicating an early stage Parkinson's phenotype. At 3 months, 27,175 differentially methylated CpGs (DMCs) were identified between healthy and transgenic mice representing 5,315 unique genes and 119 differentially expressed genes (DEGs). Identified genes represented by our DMCs (differentially methylated genes, DMGs) and DEGs from RNA-seq were subject to enrichment analysis using Gene Ontology (GO), Kyoto Encyclopedia of Genes and Genomes (KEGG), and Reactome pathways annotation databases. Biological functions related to adhesion, cellular movement, synaptic transmission, and immune functions were over-represented within our lists of DMGs and DEGs at 3 months, suggesting a possible shift to an activated microglia phenotype at an early stage of PD. The more phenotypically advanced mice at 13 months had 15,226 DMCs representing 3,742 DMGs and 3,766 DEGs. Enriched biological functions and pathways related to migration, adhesion, proliferation, and cellular metabolism/mitochondrial dysfunction were identified from our DEG and DMG lists at 13 months. Network analysis was also used on each dataset to further elucidate possible connections within the data. Networks produced from 3-month DMGs and DEGs were heavily influenced by immune and migration terms. While 13-month networks involved terms related to metabolism and proliferation linked to neurodegenerative functions. Migration and adhesion functions with an emphasis on cell surface interaction were also prominent. Possible correlations between changes in methylation and gene expression were investigated, but the only significant correlation was a negative

correlation with increased methylation in intronic DMCs associated with a decrease in gene expression. Overall, α-syn-induced changes in methylation and gene expression observed in microglia were related to immune response, synaptic transmission, and cellular movement in early stages. Then shifted to cell cycle, immune response, and metabolism in later stages. These pathways are associated with an active immune response from microglia, which influence synaptic transmission as well as induce apoptosis and phagocytose dead cells[287–290].

Introduction

Parkinson's disease (PD) is a common neurodegenerative condition associated with the loss of dopaminergic neurons in the substantia nigra. The loss of dopamine signaling accounts for motor symptoms of PD, including tremors, rigidity, slowness of movement, and postural instability[28]. Patients often experience nonmotor symptoms such as depression, anxiety, sleep disorders, constipation, and cognitive impairment[291]. A hallmark of this disease is protein aggregates called Lewy bodies, which are primarily composed of α synuclein[292].

Alpha synuclein (α-syn) is a protein whose oligomerization and aggregation have been implicated as a contributing factor to a variety of neurodegenerative diseases such as dementia with Lewy bodies, multiple system atrophy, and PD[281]. The function of α-syn is still a subject of debate, but it has been shown to be involved in regulating synaptic transmission and transcription[293–297]. α-syn is highly enriched at the synapse co-localizing with reserve pools of synaptic vesicles and involved with synaptic vesicle cycling,

80

vesicle pool size, mobilization, and endocytosis[298,299]. Both histone and direct DNA interactions have been shown with α-syn in the nucleus through binding to gene promoters and regulation of acetylation-deacetylation cycles of histones[300–303]. Due to the diverse function of α-syn, it is tightly regulated at multiple levels. Transcriptional regulation involving epigenetics such as micro RNAs (miRNA) and particularly DNA methylation have been shown to play a key role in gene expression of α-syn[283–286]. Reduced DNA methylation has been reported to lead to increased α-syn levels in the brain of PD and patients experiencing dementia with Lewy bodies[303,304]. While α-syn has been shown to influence histone acetylation, its influence on genomic methylation patterns has yet to be investigated[302]. Methylation plays a critical role in the regulation of α-syn and the ability to influence changes in methylation may create a positive feedback loop contributing to disease progression[283]. However, the influence α-synuclein has on DNA methylation and gene expression patterns have not been thoroughly explored. Transcriptional and post-translational mechanisms regulating expression levels may play a critical role in PD development[305].

A common challenge to studying α-syn is the heterogeneity of structures it can be found in[281]. Various *in vitro* studies suggest that α-syn is predominantly a monomer in its native state, but conformational changes can be induced by a wide variety of processes[306–313]. In disease conditions, α-syn oligomers are found in axons and presynaptic terminals where they may damage axons and presynaptic terminals[314–319]. To overcome the challenge of structural diversity, *in vivo* models have been designed, which overexpress the SNCA gene[313,320,321].

81

While some models overexpress mutant forms of SNCA, such models only represent the familial form of the disease, which accounts for around 27% of cases[322]. Models expressing unmutated forms of α-syn may better recapitulate the progression of PD in idiopathic cases[323–325].

. The murine model used in this study drives overexpression of full-length human wild-type α-syn under the murine Thy-1 promoter (mThy1-Asyn). This model demonstrates progressive motor and nonmotor symptoms, loss of striatal dopamine, α-syn associated pathology, and similar neuroinflammatory markers typically found in PD patients[96]. These mice present with 1.5-3.4-fold higher α-syn expression than littermate controls. These levels are close to that observed in patients with a familial form of PD with a gene triplication of α-syn[96]. The symptoms these mice experience are progressive; however, no loss in the amount of dopaminergic neurons have been recorded[96,97]. As such, they are often considered as an early-stage progressive model of PD. As early as one month of age, an active immune response was observed through elevated mRNA of cytokines and activated microglia[103,326]. Motor and non-motor symptoms become evident at 3 month, which has been observed using various motor and behavioral tests[98,99]. Dopamine levels rapidly decrease at 14 months along with increase mortality[96]. The time points selected for our study revolve around these observed phenotypic changes. The three-month time point is after initiation of inflammation and once a phenotype begins to develop, representing a pre-parkinsonian time point. The 13-month time point demonstrates an early stage of PD directly before the decline in dopamine levels that occurs at 14

months. These critical time points of initiation of neuroinflammation and progression of PD symptoms provide the opportunity to identify potential biomarkers and therapeutic targets associated with α-synuclein-induced inflammation.

The increase inflammation and activated microglia in this model are consistent with the neuroinflammation measured in patients[99–101]. Microglia are a particular cell of interest in the initiation and progression of PD based on their involvement in the immune response which can be engaged via aggregated α-syn[282]. The M1 activated status is associated with a proinflammatory phenotype and expression of various cytokines and neurotoxic compounds[327–331]. Alternatively, an M2 state related to resting microglia, is associated with the healing and maintenance of neural environment[332–334]. Clinical trials involving inhibition of the immune system using NSAIDs and ibuprofen have yielded mixed results and shown that a non-specific inflammatory blockade will most likely not be a beneficial treatment for patients[335–342]. However, some evidence from these studies does support the prevention and delay of symptoms associated with PD. Therapeutic intervention targeting the phenotype shift between M1 and M2 microglia might be a more effective approach to treatment. Regulatory changes in microglia induced by α-syn would be a novel and unique mechanism involved in PD progression that could uncover new therapeutic targets and strategies. This investigation focused on changes in DNA methylation and gene expression induced by α-syn in microglia involved in shifting microglia to an M1 state.

Materials and Methods

Study Design

This study is an *ex vivo* investigation of the effect of α-syn on transcriptional regulation via methylation and gene expression levels in microglia. Figure 13 outlines and describes the workflow of our study. Briefly, microglia were isolated from 3- and 13-month-old mThy1-Asyn mice and wild type littermate controls for DNA and RNA extraction. Reduced representation bisulfite sequencing (RRBS) was used to identify methylation changes induced by α-syn overexpression. RNA-sequencing was used to measure gene transcription levels to assess the effect of methylation changes on transcription and expression changes in response to α-syn stimulation.

Animals

Mice overexpressing full-length human wild-type α-syn under the murine Thy-1 promoter on the X chromosome were procured from the Chesselet laboratory at the University of California, Los Angeles. The corresponding background of these mice are the B6D2F1/J mice (stock# 100006) from The Jackson laboratory (Bar Harbor, ME). In all performed studies, male animals were used in order to avoid adverse effects produced by females' ability to inactivate the X chromosome, which may contain the inserted human α-syn gene under the m-Thy1 promoter. The genotype of all mice was verified with PCR analysis of tail snip DNA via general endpoint PCR.
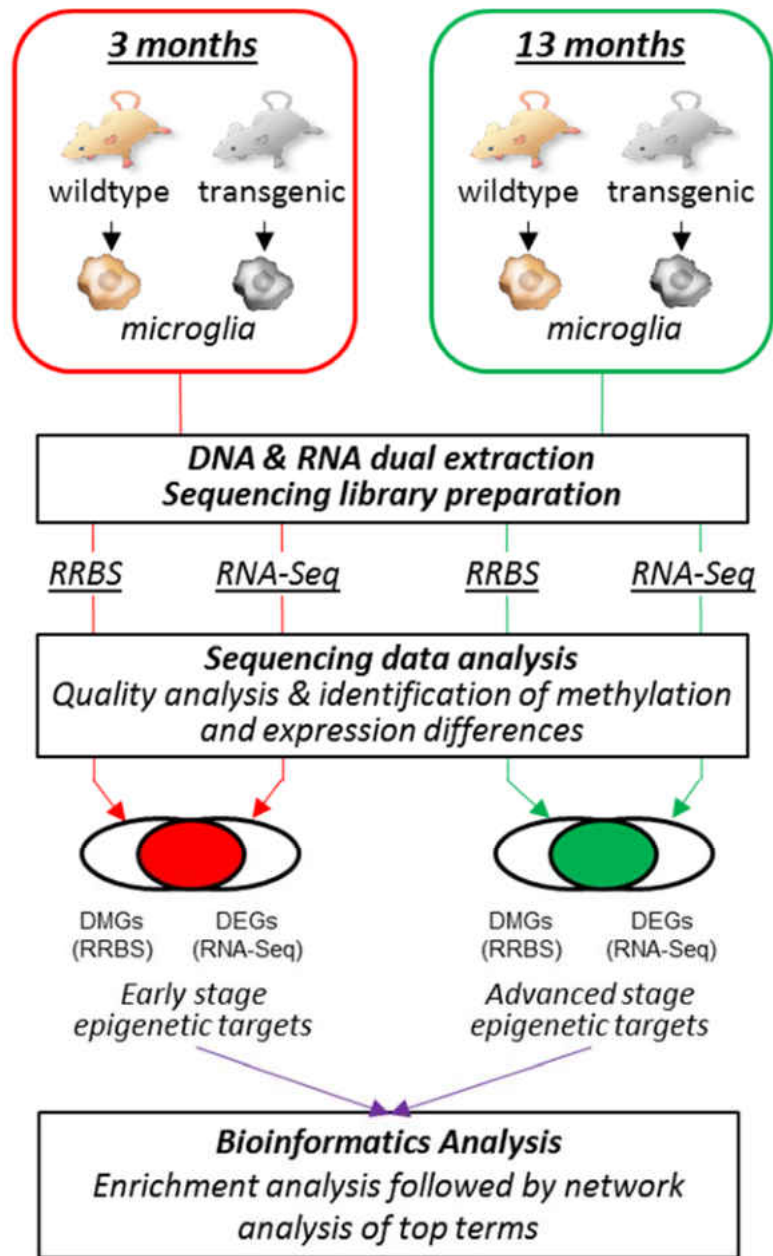
Figure 13. Study 3 Workflow and Description. mThy1-Asyn mice along with littermate controls were aged to 3 and 13 months then euthanized for tissue collection. Microglia were isolated from homogenized whole brains using a percoll gradient. Both RNA and DNA were dually extracted, while the RNA was used transcription sequencing and DNA underwent bisulfite conversion for RRBS. Data were analyzed for DEGs and DMGs in order to identify possible biomarkers. Gene lists were also analyzed for function enrichment using GO, KEGG, and Reactome databases.

The hypoxanthine guanine phosphoribosyl transferase (HPRT) gene was used as the internal control with a forward primer of GAAGAGCTACTGTAATGATCAGTCAACGG and a reverse primer of GAGAGGTCCTTTTCACCAGCAAGC. The forward primer used for the human SNCA gene was GCTACTGCTGTCACACCCGTC and the reverse primer was GATGATGGCATGCAGCACTGG.

Animal Use

All procedures were approved by the University of North Dakota Institutional Animal Care and Use Committee (UND IACUC) protocol 1506-2 ID 47. Mice were provided food and water ad libitum and housed in a 12-hour light/dark cycle. The investigation conforms to the National Research Council of the National Academies Guide for the Care and Use of Laboratory Animals (8th edition)[343].

Microglia Isolation

The protocol used for the isolation of adult mouse microglia was adapted from Lee and Tansey 2013 in *Methods Molecular Biology*[344]. Briefly, freshly perfused brains from euthanized mice were minced using a razor blade and dissociated in medium containing 1mg/mL papin, DMEM, Dispase II (1.2 units/mL) and DNAse I (20 units/mL). After removing the dissociation medium, the tissue was homogenized using various sized serological pipettes and then filtered using a 40µm cell strainer. A percoll gradient of 30%, 37%, and 70% percoll diluted with hank's balanced salt solution (HBSS) was established with homogenized tissue diluted into the 37% solution. The percoll gradient was

centrifuged at 300xg for 40 minutes at 18C to separate microglia cells from other

tissue. The interphase containing the microglia was collected and washed three

times with HBSS to remove the remaining percoll. RLT plus buffer (Qiagen,

ID:80204) was added to the isolated microglia and this lysed solution was added

to QIAshredder homogenizer tubes (Qiagen ID:79654) and spun for 2 minutes at

maximum speed. The collection tube below the QIAshredder was then flash

frozen with liquid nitrogen and stored at -80C to preserve the solution for later

isolation of DNA and RNA.

Dual DNA/RNA Extraction and Isolation

The flash-frozen cells prepared during the microglia isolation protocol

were used with the Qiagen AllPrep DNA/RNA Mini Kit (Qiagen: 80204) to collect

the DNA and RNA from the microglia isolated from our wild type and mThy1-

Asyn mice. Our procedure followed the described Qiagen AllPrep protocol[345].

Briefly, homogenized lysates were thawed and DNA was isolated from RNA via

spin column. RNA and DNA were purified using silica-membrane RNeasy and

AllPrep DNA spin columns. All RNA and DNA isolations from this preparation

were then frozen at -80C to be later used for a global methylation ELISA and

library preparations for sequencing.

Global Methylation Assay

Genomic DNA isolated from microglia preparations was quantified using

the Epoch microplate spectrophotometer (BioTek). The global DNA methylation

status of the microglial DNA from mThy1-Asyn and wild-type mice were

determined using the MethylFlash Global DNA Methylation (5-mC) ELISA Easy

Kit (Epigentek: P-1030) according to Epigentek instructions. Briefly, 100ng of genomic DNA was bound to each well. After washing, 5-methylcytosine detection complex solution was added to each well and incubated for 50 minutes. Wells were washed again, developer solution was added, and optical absorbance was measured at 450nm. The percentage of methylated DNA was calculated based on linear regression analysis.

Methylation Processing using Reduced Representation Bisulfite Sequencing (RRBS)

This procedure for RRBS was adapted from Garrett-Bakelman et al[346]. Briefly, Genomic DNA was extracted from our microglia isolation preparations as per the methods described above. DNA quantity was a measured using a Qubit fluorometer and quality was assessed using TapeStation (Agilent). Due to sample limitations, a DNA integrity number (DIN) could not be used as a defined cut off and sample selection for RRBS processing was based on quantity of DNA where DINs were not measurable. Genomic DNA was digested with the *Msp1* restriction enzyme and purified using phenol:chloroform extraction and ethanol precipitation. Following *Msp1* digestion, genomic DNA underwent blunt-end digestion, phosphorylation, and ligation of adapters with methylated cytosines. Ligated fragments were cleaned and processed for size selection on an agarose gel. Selected fragments were bisulfite converted, amplified by PCR, and cleaned using AMPure XP beads. The libraries were quantified using the Qubit assay and Agilent's High Sensitivity D1000 assay and sequenced on the Illumina Hi-Seq 4000 platform to generate raw sequence RRBS reads.

Quality control assessment of RRBS data was completed using FastQC version 0.11.5[251]. Raw Sequencing reads were cleaned using Trim Galore! (version 0.5.0 Babraham Bioinformatics, UK) to remove reads with adapter contamination and reads with a Phred quality score <30[347]. Trim Galore also has a special setting for RRBS data that was utilized (--rrbs). Cleaned reads were mapped to an *in silico* bisulfite converted mouse reference genome m38.p6-Refseq using Bismark v0.20.0[348] and Bowtie2 v2.3.4.2[349]. The R package MethylKit v1.8.1[350] was used to count uniquely mapped reads and assess changes in methylation between wild-type and mThy1-Asyn mice at both our 3 month and 13 month time points. Differentially methylated CpGs (DMCs) were defined as a 10% or greater difference in cytosine methylation levels between wild-type and mThy1-Asyn mice with an adjusted p-value <0.01. Differentially methylated genes (DMGs) were based on the total unique gene identifiers within the list of DMCs. DMCs were annotated based on genes and CpG island features using gene bodies and 2,5, and 10 kb regions upstream from transcription start sites (TSSs) using the genomation[351] R package. Annotation of murine CpG islands were obtained from the University of California, Santa Cruz (http://genome.ucsc.edu/ :GRCm38/mm10), and annotation of the murine genes were obtained from Ensembl[352] (http://www.ensembl.org) and Entrez[353] (http://www.ncbi.nlm.nih.gov/Entrez/).

RNA-Sequencing Processing

Total RNA was obtained from isolated microglia preparations as per the methods described in dual DNA/RNA extraction and isolation section above.

RNA quality was evaluated using TapeStation (Agilent, Santa Clara, CA). Due to sample limitations, a RNA integrity number of 5 was used as a cutoff for further processing. These samples were processed using the NEBNext Ultra II RNA Library Prep Kit (Catalog #E7770L/#E7775L) for Illumina. Resultant cDNA was sequenced with a paired-end read length of 150 bases using and Illumina HiSeq 2000 by Novogene (https://en.novogene.com/).

Raw sequencing reads were cleaned using Trimmomatic to remove reads with adapter or Poly-N sequences as well as reads with a quality score <30[250]. Quality control assessment of RNA-Seq data was completed using the FastQC version 0.11.5[251]. Cleaned reads were mapped to the mouse reference genome m38.p6 Refseq using HISAT2[252]. FeatureCounts[253] was used to count uniquely mapped reads while genes with zero expression across samples were omitted from differential expression analysis. Fragments per kilobase of exon per million mapped reads (FPKM) as a measurement of transcript expression were calculated using an in-house script. Differentially expressed genes (DEGs) were identified using the DESeq2[254] R package using a significance cut off of a <0.05 adjusted p-value (adj. p-value).

Enrichment and Network Analysis

Enrichment analysis of both DEGs and DMGs was conducted using our in-house enrichment analysis R package RichR (http://github.com/hurlab/RichR). Gene Ontology[354] (GO), Kyoto Encyclopedia of Genes and Genomes[354–356] (KEGG) and Reactome Pathway Database[357,358] were used to identify enriched

90

biological functions and pathways represented within our gene lists. An adjusted p-value <0.05 was used as a significance cutoff.

The enrichment results using three different annotation databases were combined and visualized in a network by RichR with enrichment terms as nodes and shared gene contents of nodes indicated by edges. The top 20 (or less) terms selected based on adjusted p-value from each annotation set were used in network visualization. Cytoscape[359] was used to visualize the network and colorize nodes based on adjusted p-value. Within the network, node shape indicates the annotation data each term is from. All networks were organized using the inverted self-organizing map layout with minimal manual node rearrangement for visibility.

Results

Microglia were isolated from the brains of mThy1-Asyn mice and their littermate wild type controls to profile the DNA methylation patterns and gene expression changes induced by the overexpression of α-synuclein. This model of PD experiences changes in striatal dopamine levels, progressive motor and non-motor symptoms, α-synuclein associated pathology, and inflammation similar to what is observed in PD patients[95,96]. The time points (3 and 13 months) of tissue collection were selected based on phenotypic changes observed in this model associated with progressive symptoms and microglia associated inflammation. Inflammatory markers can be observed as early as 1 month indicating early stage neuroinflammation before mice become symptomatic[360]. Dopamine levels rapidly decrease between 12 and 14 months and motor symptoms of PD become

evident representing an early stage of PD similar to when patients become symptomatic[97,100,361]. Methylation and gene expression profiles at these time points offer unique insight into the initiation of neuroinflammation and progression of PD symptoms associated with α-synuclein induces inflammation.

α-synuclein-Induced Methylation Changes in Microglia

Changes in methylation induced by α-synuclein overexpression were first examined by quantifying global DNA methylation using the MethylFlash ELISA which indicated an increase in methylation in the microglia from our transgenic animals (Figure 14). These changes were further investigated using global methylation patterns from RRBS of DNA isolated from microglia within the mThy1-Asyn mouse. Quality assessment using FASTQC did not identify any samples of low quality to be omitted from the study. Trim Galore was used for quality and adapter trimming of reads to be passed to Bismarck and Bowtie2 for alignment. The summary of prepared samples including number of reads obtained (M seqs), duplicate sequences (% Dups), GC content (%GC), percentage of reads trimmed (% Trimmed), and percentage of reads successfully aligned (Bismarck Alignment %) can be found in Table 12. The R package MethylKit assessed changes in methylation between transgenic and control mice to determine DMCs based on a change in methylation (delta beta) and an adjusted p-value<0.01. DMCs were annotated to CpG island features and genetic regions in relation to the transcription start site of genes using the genomation R package.
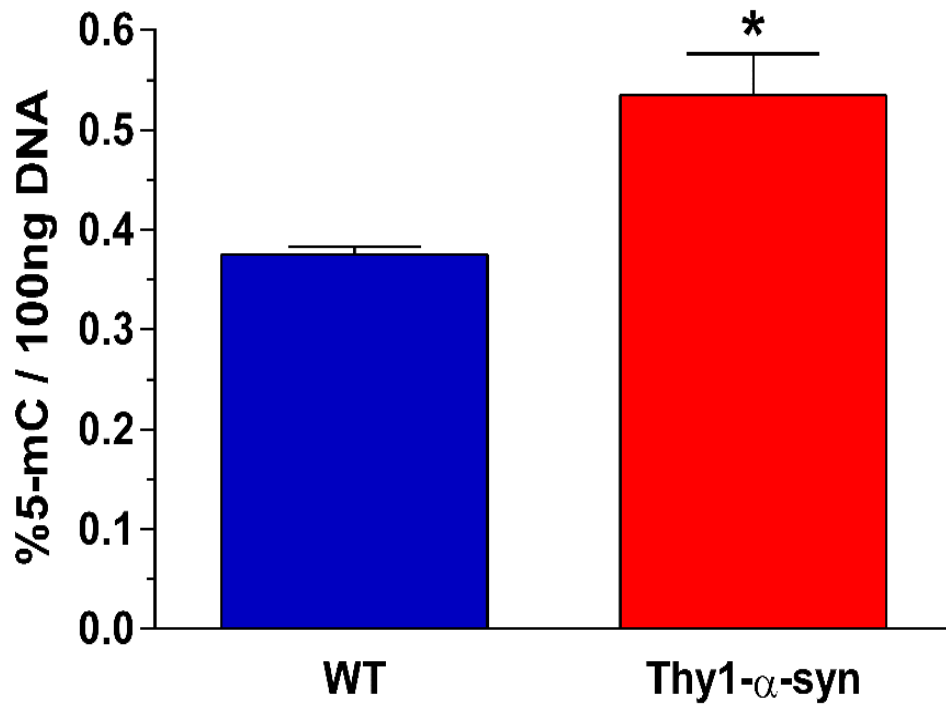
Figure 14. Global DNA Methylation ELISA Results. Isolated DNA from 13-month-old wild-type (n=3) and mThy1-Asyn (n=6) mice were also used in a Global DNA methylation ELISA Easy kit from Epigentek. The results demonstrate a significant increase in global 5-methylcytosine in the transgenic model's DNA.

Sample Name	DNA	RNA	Bismarck Alignment %	% Trimmed	% Dups	% GC	Total Reads (millions)	RNA Total Reads (millions)	Reads after trimming	HISAT2 Alignment %
13H01			67.70%	1.00%	89.50%	32%	125.2	44.2	43.0 (97.25%)	93.26%
13H02			64.90%	1.00%	89.00%	33%	113.9	48.2	46.9 (97.31%)	93.20%
13H03			65.00%	1.00%	87.40%	32%	104.9	46.1	43.8(95.17%)	91.99%
13H04			64.10%	1.10%	88.30%	32%	143.1	NA	NA	NA
13H05			66.60%	1.00%	87.20%	33%	125.2	49.9	48.7 (97.67%)	93.07%
13H06			65.30%	1.20%	87.60%	32%	103.6	46.4	45.3 (97.42%)	93.29%
13H07			61.30%	1.00%	90.40%	32%	176.6	NA	NA	NA
13H08			64.20%	1.00%	86.80%	32%	110.2	55.9	54.6 (97.64%)	92.77%
13H09			NA	NA	NA	NA	NA	70.0	68.4 (97.71%)	91.88%
13H10			65.00%	1.10%	86.80%	32%	104.7	68.8	67.4 (97.91%)	93.01%
13W01			59.60%	1.10%	87.40%	32%	81.1	NA	NA	NA
13W02			40.60%	1.10%	88.40%	33%	111.7	NA	NA	NA
13W03			42.10%	1.00%	89.80%	33%	93	62.9	61.4 (97.63%)	94.32%
13W04			39.60%	0.90%	89.10%	32%	93.7	82.0	80.3 (97.88%)	94.50%
13W05			NA	NA	NA	NA	NA	70.3	68.6 (97.65%)	94.34%
13W06			NA	NA	NA	NA	NA	86.9	85.0(97.88%)	94.05%
3H01			59.60%	1.10%	89.90%	32%	123.2	57.2	55.9 (97.73%)	94.78%
3H02			58.50%	1.00%	90.00%	32%	110.1	NA	NA	NA
3H03			55.10%	1.00%	88.70%	33%	98.5	75.8	74.2 (97.91%)	95.01%
3H04			NA	NA	NA	NA	NA	57.8	56.2 (97.07%)	83.39%
3H05			45.90%	1.00%	89.50%	33%	127.1	66.7	65.1 (97.48%)	93.59%
3W01			63.40%	1.00%	90.30%	31%	146.4	71.6	69.7 (97.37%)	94.83%
3W02			54.00%	1.00%	87.30%	32%	84	61.0	59.2 (96.97%)	93.84%
3W03			56.30%	1.00%	90.00%	31%	187.9	NA	NA	NA
3W04			49.80%	1.10%	86.70%	32%	95.3	57.2	55.3 (96.72%)	93.64%

Table 12. Sample Alignment Summary. Each mouse in both the 13- and 3-month groups are listed on the left. Their inclusion in either RRBS (DNA) or RNA-seq (RNA) is indicated by the blue and green coloring, respectively. The assessment of each sample in terms of DNA included the millions of sequences provided, percentage trimmed, and percentage of alignment using Bismarck along with the percent of duplicated sequences and GC content. The RNA assessment of each included sample includes the total reads, reads after trimming, and the percentage of reads aligned using HISAT2.

Microglial DNA harvested from our 3-month-old mice (4 wild type, 4 mThy1-Asyn) had 27,175 DMCs between transgenic and wild type mice based on a minimum delta beta of 10% and an adjusted p-value<0.01. Across our samples from 3-month animals, 1,234,490 total sites were measured with 11,441 significant CpGs showing an increase in methylation (hypermethylation) and 15,734 showing a decrease in methylation (hypomethylation). The delta beta for the identified CpGs range from a 65% increase to a 72% decrease in methylation. The top and bottom 20 DMCs, based on delta beta, and their associated genes can be found in Tables 13 and 14. Based on the murine annotation from University of California, Santa Cruz (UCSC), 6% of identified CpGs can be found in CpG island regions and 8% in CpG shore regions (Figure 15A). These areas in relation to transcription start sights have been shown to influence gene expression[362,363]. Annotation for promoter, exon, intron, and intergenic gene regions were also used to evaluate and classify the DMCs identified (Figure 15B). While 10% of DMCs were in promoter regions and 15% located in exon regions of genes, the vast majority were found in intron (38%) or intergenic regions (37%).

Multiple CpGs are assigned to the same genes in various locations on the genome, which prevents any gene level determinations from this data without further information. However, identifying all unique genes associated with the DMCs provides a list of genes that could be influenced by methylation changes in our model, or DMGs.

EntrezID	Gene Symbol	Description	Δβ	Adj. Pvalue	Gene Location
84704	Snurf	SNRPN upstream reading frame	65.35	3.76E-69	chr7 , 60005200
84704	Snurf	SNRPN upstream reading frame	64.27	3.41E-64	chr7 , 60005229
84704	Snurf	SNRPN upstream reading frame	61.71	1.30E-59	chr7 , 60005187
27412	Peg12	paternally expressed 12	54.90	3.96E-10	chr7 , 62464177
20280	Scp2	sterol carrier protein 2, liver	48.33	7.94E-54	chr4 , 108136742
74387	4932438H23Rik	RIKEN cDNA 4932438H23 gene	45.79	7.32E-47	chr16 , 91104256
17880	Myh11	myosin, heavy polypeptide 11, smooth muscle	45.28	2.28E-34	chr16 , 14271833
57440	Ehd3	EH-domain containing 3	44.59	4.15E-59	chr17 , 73823939
545677	Gm12888	predicted gene 12888	42.79	1.67E-55	chr4 , 121355852
56429	Dpt	dermatopontin	41.64	7.64E-07	chr1 , 164823213
56280	Mrpl37	mitochondrial ribosomal protein L37	41.01	1.29E-18	chr4 , 107013861
57440	Ehd3	EH-domain containing 3	40.17	1.82E-33	chr17 , 73820506
329015	Atg2a	autophagy related 2A	39.02	1.81E-43	chr19 , 6248005
20680	Sox7	SRY (sex determining region Y)-box 7	38.63	2.41E-07	chr14 , 63942190
63913	Fam129a	family with sequence similarity 129, member A	38.22	5.55E-15	chr1 , 151621799
76422	Mroh3	maestro heat-like repeat family member 3	38.02	1.22E-16	chr1 , 136162561
14538	Gcnt2	glucosaminyl (N-acetyl) transferase 2, I-branching enzyme	37.92	1.41E-04	chr13 , 40888061
252974	Tspear	thrombospondin type laminin G domain and EAR repeats	37.23	1.01E-03	chr10 , 77664526
320772	Mdga2	MAM domain containing glycosylphosphatidylinositol anchor 2	36.97	8.13E-14	chr12 , 66932444
12145	Cxcr5	chemokine (C-X-C motif) receptor 5	36.44	7.10E-27	chr9 , 44514115

Table 13. Top 20 DMCs at 3 Months. Differentially methylated CpGs were determined between wild type and mThy1-Asyn mice at 3 months of age and paired with their gene annotation. The 20 CpGs with the greatest increase in methylation (Δβ) along with their associated gene annotation.

EntrezID	Gene Symbol	Description	Δβ	Adj. Pvalue	Gene Location
26381	Esrrg	estrogen-related receptor gamma	-72.17	2.98E-38	chr1 , 187630622
329540	Nol4l	nucleolar protein 4-like	-61.77	1.27E-51	chr2 , 153422452
16558	Kif16b	kinesin family member 16B	-53.81	7.96E-61	chr2 , 142788388
21873	Tjp2	tight junction protein 2	-48.50	4.79E-17	chr19 , 24216202
66230	Mrps28	mitochondrial ribosomal protein S28	-46.97	1.12E-09	chr3 , 8894548
215303	Camk1g	calcium/calmodulin-dependent protein kinase I gamma	-46.30	1.93E-50	chr1 , 193384944
17463	Psmd7	proteasome (prosome, macropain) 26S subunit, non-ATPase, 7	-43.77	3.17E-32	chr8 , 108009687
57278	Bcam	basal cell adhesion molecule	-43.56	7.56E-12	chr7 , 19767561
18109	Mycn	v-myc avian myelocytomatosis viral related oncogene, neuroblastoma derived	-41.28	7.48E-28	chr12 , 12694576
70881	Nt5c1b	5'-nucleotidase, cytosolic IB	-40.61	7.38E-18	chr12 , 10242598
68498	Tspan11	tetraspanin 11	-40.46	2.17E-70	chr6 , 127866059
56748	Nfu1	NFU1 iron-sulfur cluster scaffold	-39.54	1.19E-15	chr6 , 86949756
26381	Esrrg	estrogen-related receptor gamma	-39.52	2.01E-39	chr1 , 187630781
67755	Ddx47	DEAD (Asp-Glu-Ala-Asp) box polypeptide 47	-39.21	4.23E-26	chr6 , 135035635
13195	Ddc	dopa decarboxylase	-38.89	6.88E-08	chr11 , 11822370
233081	Ffar1	free fatty acid receptor 1	-37.80	2.03E-07	chr7 , 30866410
20927	Abcc8	ATP-binding cassette, sub-family C (CFTR/MRP), member 8	-37.62	1.80E-09	chr7 , 46178186
71517	9030624J02Rik	RIKEN cDNA 9030624J02 gene	-37.44	1.68E-47	chr7 , 118773890
217364	Engase	endo-beta-N-acetylglucosaminidase	-37.38	1.71E-07	chr11 , 118487128
18314	Olfr17	olfactory receptor 17	-37.21	5.91E-08	chr7 , 107085773

Table 14. Bottom 20 DMCs at 3 Months. Differentially methylated CpGs were determined between wild type and mThy1-Asyn mice at 3 months of age and paired with their gene annotation. The 20 genes that demonstrate the greatest decrease in methylation (Δβ) along with their associated gene annotation.
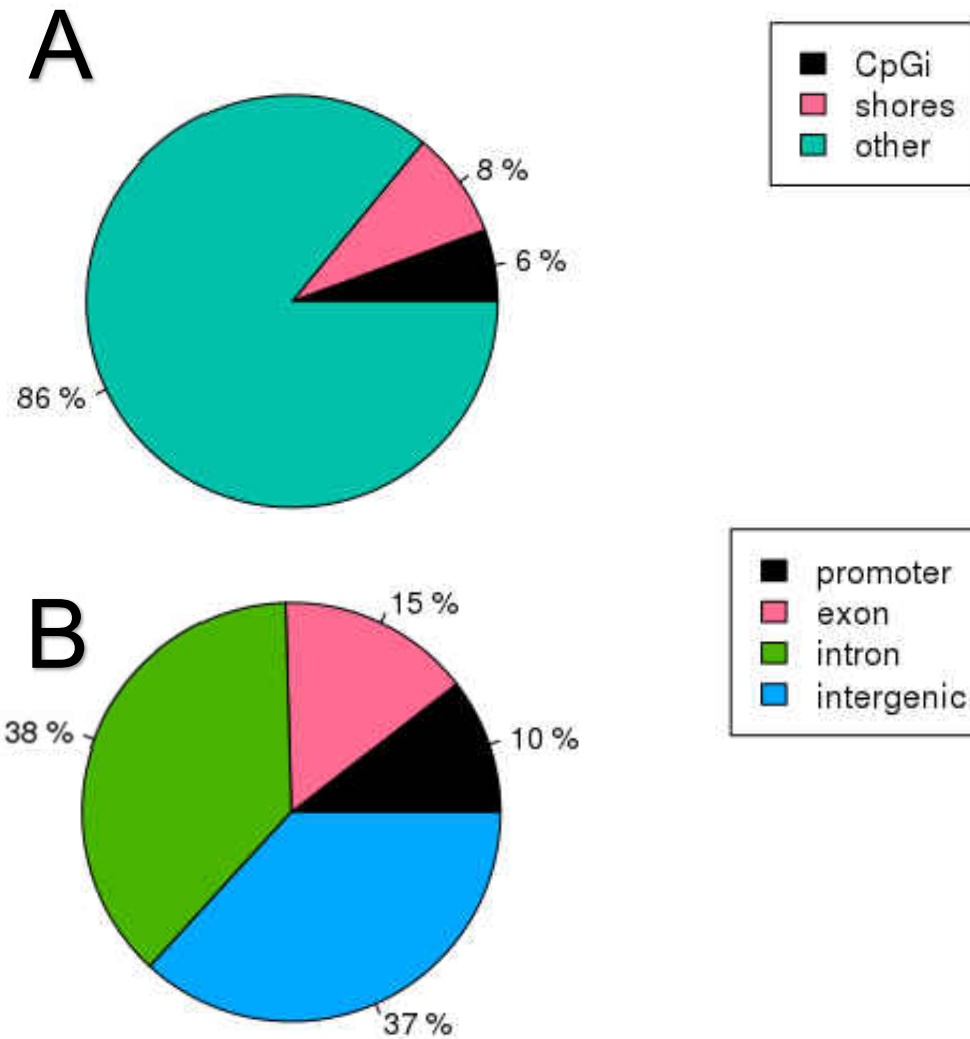
Figure 15. Genomic Regions of 3 Month DMCs. DMCs were identified from our 3-month animals through RRBS. **(A)** The DMCs identified composed of 6 % island and 8% shore CpG regions. **(B)** The majority of DMCs are intergenic or located in the intron of genes with only 10% found in the promoter regions.

These DMCs are located in genomic locations associated with 5,315 unique DMGs. The list of DMGs from our 3-month-old mice were used for functional analysis with an in-house R package RichR. Enriched biological functions and pathways represented within our gene list were identified which consisted of 1904 GO terms, 115 Reactome Pathways, and 26 KEGG functions based on a significance cutoff of adjusted p-value <0.05. The top 20 enriched terms from each database based on adjusted p-value were merged together for network analysis. The network of associated terms was created using RichR with enriched terms serving as nodes and shared DEGs forming edges between nodes (Figure 16). Visualization of the network was executed using Cytoscape to color nodes based on an adjusted p-value scale and to change node shape based on their annotation database. All GO terms are circular nodes, KEGG terms are represented by triangle nodes, and Reactome pathways have diamond nodes. Network layout was minimally adjusted for visibility from the inverted self-organized map layout from Cytoscape. Subnetworks of nodes related to neuronal development, synaptic transmission, intracellular signaling, and adhesion/migration can all be identified within the network.

Similarly, microglial DNA was harvested from 13-month-old mice (4 wild type, 9 mThy1-Asyn) for methylation profiling. Although our later 13-month animals exhibit a more severe phenotype, there were less DMCs identified in 13-month than in the previous 3-month group. Across our samples from 13-month animals, 1,151,250 total sites were measured, with 10,436 DMCs being hypermethylated and 4,790 DMCs hypomethylated. The older mice had 15,226

99
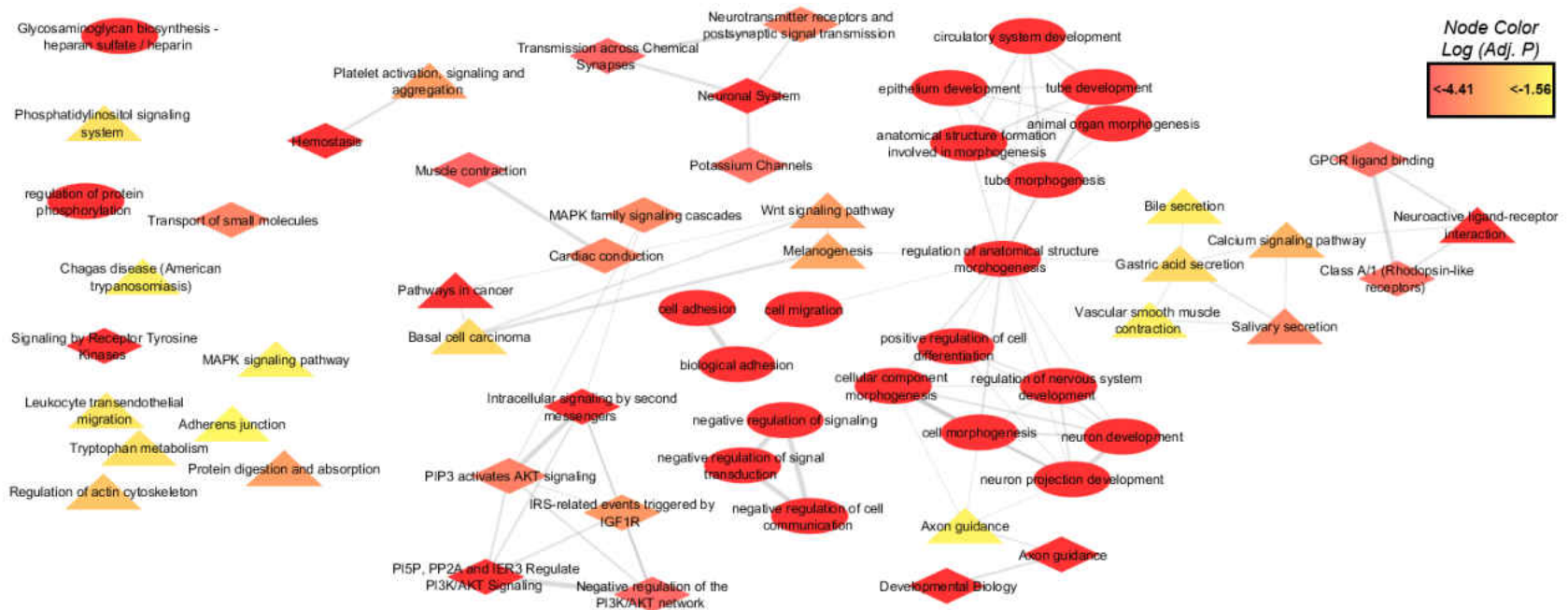
Figure 16. Enrichment Network from 3 Month DMCs. DMCs were focused to a gene level and used for enrichment analysis through GO (circle), KEGG (triangle), and Reactome (diamond). Top 20 adjusted p-value enrichment terms from each list make up the nodes of the network while shared genes between terms are represented by the edges. Node color correlates to adjusted p-value. Network layout is from the Cytoscape inverted self-organized map layout.

DMCs, which were annotated to 3,742 genes (DMGs) using a 10% change in methylation as a minimum and a cutoff of an adjusted p value <0.01. The DMCs identified had a delta beta range from a 43% increase to a 55% decrease in methylation. The top and bottom 20 DMCs, based on delta beta, and their associated genes can be found in Tables 15 and 16. From the DMCs identified, 5% are found in CpG islands with another 9% in CpG shores (Figure 17A). Similar to our 3-month group, the majority of DMCs are located in intron (41%) and intergenic regions (35%) while 10% were located in promoters and 15% in exons (Figure 17B).

The DMG list from our 13-month mice were also assessed for enrichment of biological functions and pathways from GO (1782 terms), Reactome Pathway (106 pathways), and KEGG (54 functions) databases. An adjusted p-value<0.05 was used as a cutoff in determining if a term was significantly enriched. The top 20 enriched terms based on adjusted p-value were selected to be used for network analysis to further identify thematic clusters within the data (Figure 18). Network files were generated with RichR files while Cytoscape was used to visualize the network with node shapes corresponding to a terms database and color indicating the adjusted p-value. Cytoscape's inverted self-organized map layout was used to organize the network with slight manual adjustments for visibility. Terms related to adhesion and locomotion are the most common within the network. The largest cluster of highly connected terms is largely related to proliferation and development, such as neurogenesis, generation of neurons, regulation of cell process, and neuronal differentiation.

| EntrezID	Gene Symbol	Description	Δβ	Adj. Pvalue	Gene Location
14873	Gsto1	glutathione S-transferase omega 1	43.06	1.26E-47	chr19 , 47856960
71972	Dnmbp	dynamin binding protein	39.50	2.26E-30	chr19 , 43901230
74287	Kcmf1	potassium channel modulatory factor 1	39.01	1.03E-17	chr6 , 72869748
12306	Anxa2	annexin A2	38.21	4.99E-11	chr9 , 69517991
93685	Entpd7	ectonucleoside triphosphate diphosphohydrolase 7	37.45	1.91E-10	chr19 , 43706608
217837	Itpk1	inositol 1,3,4-triphosphate 5/6 kinase	36.85	4.88E-11	chr12 , 102706751
243308	A430033K04Rik	RIKEN cDNA A430033K04 gene	36.12	4.62E-22	chr5 , 138647371
171167	Fut10	fucosyltransferase 10	35.43	1.58E-30	chr8 , 31262370
13819	Epas1	endothelial PAS domain protein 1	34.85	1.17E-08	chr17 , 86786799
226251	Ablim1	actin-binding LIM protein 1	34.34	1.47E-12	chr19 , 57238326
240667	Sec31b	Sec31 homolog B (S. cerevisiae)	33.51	5.97E-49	chr19 , 44531201
20361	Sema7a	sema domain, immunoglobulin domain (Ig), and GPI membrane anchor, (semaphorin) 7A	33.39	1.19E-06	chr9 , 57954086
105782	Scrib	scribbled planar cell polarity	33.35	1.21E-07	chr15 , 76059286
56280	Mrpl37	mitochondrial ribosomal protein L37	33.26	7.34E-10	chr4 , 107056075
53626	Insm1	insulinoma-associated 1	32.91	8.51E-04	chr2 , 146184015
15445	Hpd	4-hydroxyphenylpyruvic acid dioxygenase	32.88	5.22E-18	chr5 , 123197372
140703	Emid1	EMI domain containing 1	32.69	1.33E-06	chr11 , 5139618
101434	Ceacam15	carcinoembryonic antigen-related cell adhesion molecule 15	32.65	5.68E-04	chr7 , 16670321
12306	Anxa2	annexin A2	32.47	6.57E-08	chr9 , 69518031
14683	Gnas	GNAS (guanine nucleotide binding protein, alpha stimulating) complex locus	32.34	4.07E-04	chr2 , 174326956

Table 15. Top 20 DMCs at 13 Months. Differentially methylated CpGs were determined between wild type and mThy1-Asyn mice at 13 months of age and paired with their gene annotation. The 20 CpGs with the greatest increase in methylation (Δβ) along with their associated gene annotation.

EntrezID	Gene Symbol	Description	Δβ	Adj. Pvalue	Gene Location
68243	A930018 P22Rik	RIKEN cDNA A930018P22 gene	-55.44	2.36E-28	chr2 , 104167970
17076	Ly75	lymphocyte antigen 75	-54.50	4.25E-70	chr2 , 60396648
68243	A930018 P22Rik	RIKEN cDNA A930018P22 gene	-47.07	3.18E-32	chr2 , 104167969
75051	Ccdc173	coiled-coil domain containing 173	-45.94	3.79E-47	chr2 , 69766312
68243	A930018 P22Rik	RIKEN cDNA A930018P22 gene	-44.71	4.26E-82	chr2 , 104168099
68243	A930018 P22Rik	RIKEN cDNA A930018P22 gene	-44.48	7.73E-83	chr2 , 104168129
21838	Thy1	thymus cell antigen 1, theta	-44.12	1.85E-30	chr9 , 44049625
68243	A930018 P22Rik	RIKEN cDNA A930018P22 gene	-42.83	6.73E-56	chr2 , 104168158
329421	Myo3b	myosin IIIB	-40.23	1.54E-16	chr2 , 70149298
241556	Tspan18	tetraspanin 18	-39.35	1.96E-64	chr2 , 93351814
22174	Tyro3	TYRO3 protein tyrosine kinase 3	-39.26	7.53E-23	chr2 , 119805409
21838	Thy1	thymus cell antigen 1, theta	-37.36	8.57E-16	chr9 , 44049669
19089	Prkcsh	protein kinase C substrate 80K-H	-37.29	4.20E-06	chr9 , 22015846
21838	Thy1	thymus cell antigen 1, theta	-36.96	9.69E-20	chr9 , 44049598
21938	Tnfrsf1b	tumor necrosis factor receptor superfamily, member 1b	-36.15	1.56E-10	chr4 , 145222523
56369	Apip	APAF1 interacting protein	-36.03	7.26E-26	chr2 , 103112082
74194	Rnd3	Rho family GTPase 3	-35.64	4.17E-22	chr2 , 51076402
387511	Tas2r134	taste receptor, type 2, member 134	-35.58	7.20E-58	chr2 , 51667495
71918	Zcchc24	zinc finger, CCHC domain containing 24	-35.13	3.10E-06	chr14 , 25780948
54120	Gipc2	GIPC PDZ domain containing family, member 2	-35.08	3.81E-06	chr3 , 152092787

Table 16. Bottom 20 DMCs at 13 Months. Differentially methylated CpGs were determined between wild type and mThy1-Asyn mice at 13 months of age and paired with their gene annotation. The 20 genes that demonstrate the greatest decrease in methylation (Δβ) along with their associated gene annotation.
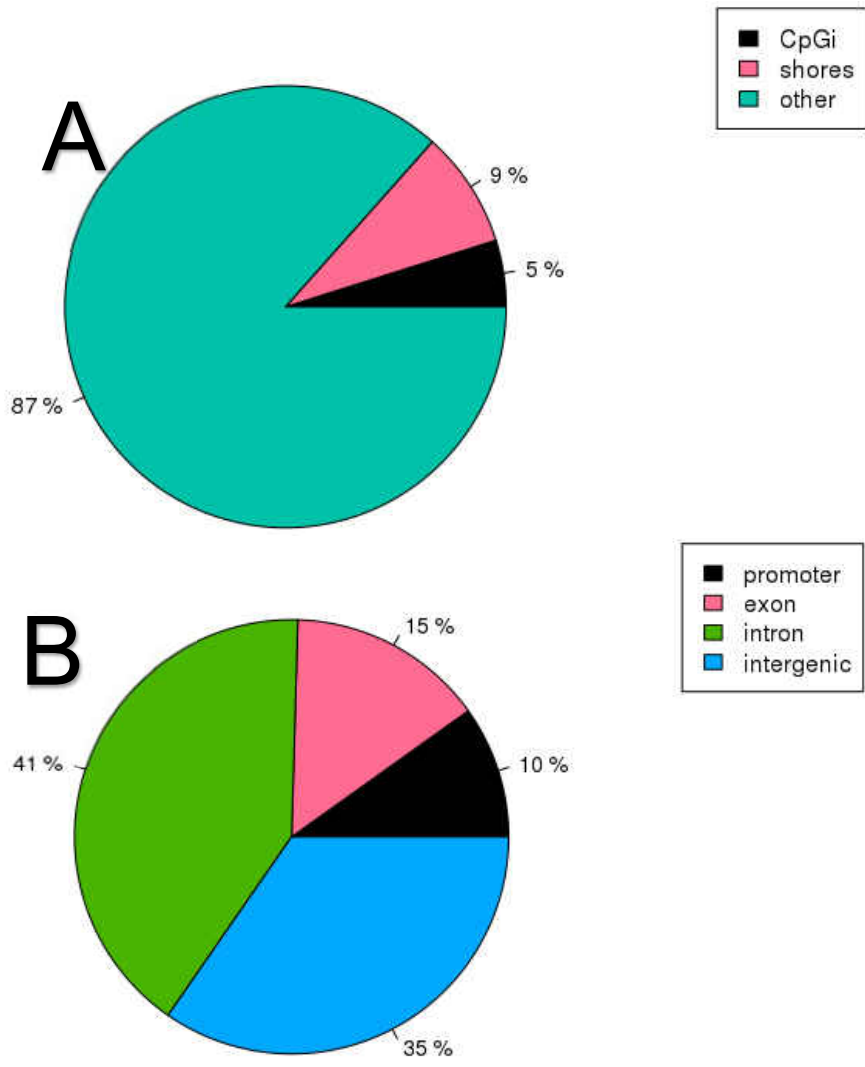
Figure 17. Genomic Regions of 13-Month DMCs. DMCs were identified from our 13-month animals through RRBS. **(A)** The DMCs identified in the 13-month comparison were composed of 5% CpG islands. **(B)** The majority of DMCs were in intron or intergenic regions but 10% were from promoter regions of genes. The list of DMCs were focused down to gene level and used for enrichment analysis.
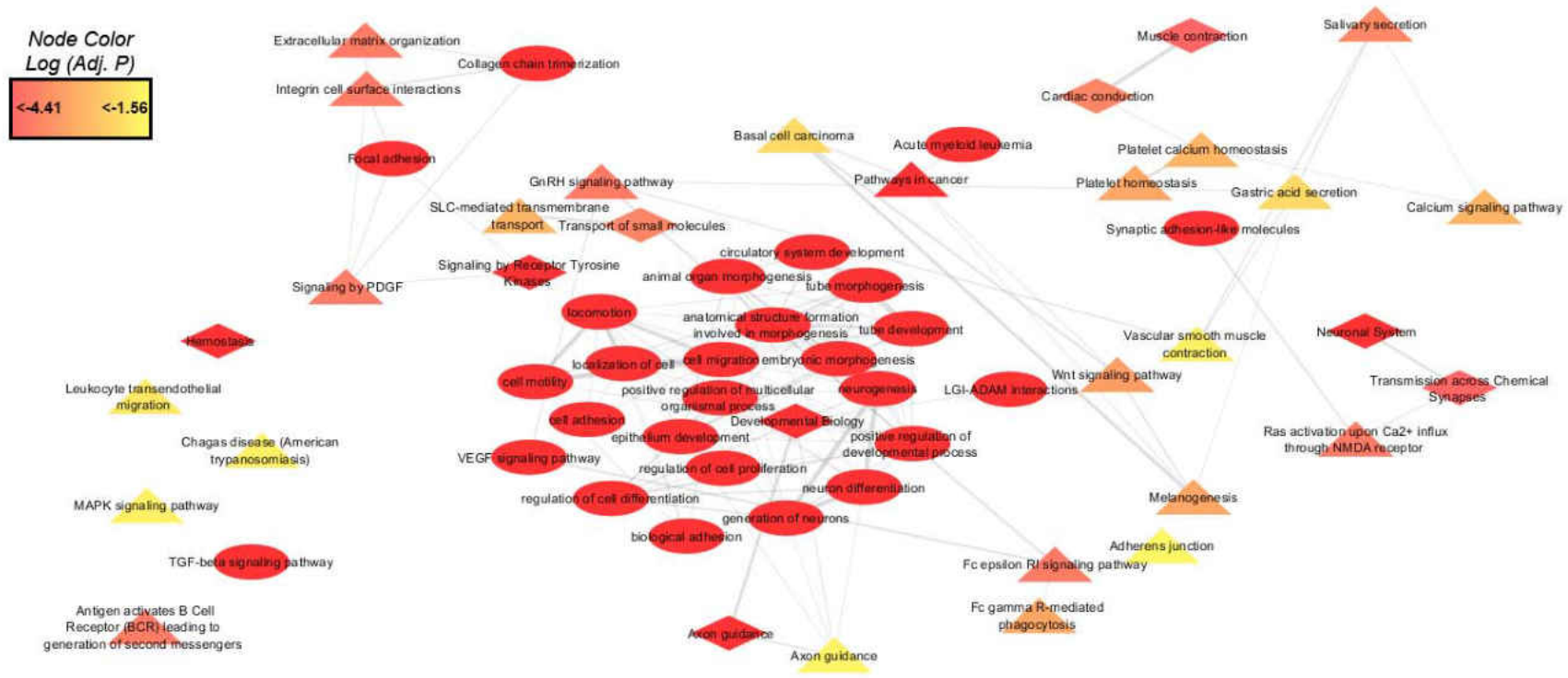
Figure 18. Enrichment Network from 13-Month DMCs. The top 20 adjusted p-value terms from GO (circle), KEGG (triangle), and Reactome (diamond) represent the nodes and shared genes between term annotations form the edges. Node color is based on adjusted p-value and the network layout is adjusted from the Cytocape inverted self-organized map for visibility.

The subnetwork related to cell surface interactions with terms such as focal adhesion, integrin cell surface interactions, extracellular matrix, and collagen chain trimerization is connected to platelet-derived growth factor (PDGF) and receptor tyrosine kinase signaling (RTK). PDGF and RTK have been shown to induce proliferation in glial cells[364–366].

α-synuclein-induced Gene Expression Changes in Microglia

Gene expression changes induced by α-synuclein overexpression were measured in microglia isolated from wild type and mThy1-Asyn mice using RNA-sequencing. Adapter and low-quality reads were trimmed before alignment using Trimmomatic. The quality of data obtained from sequencing was assessed using FastQC, which did not identify any samples for exclusion based on read quality. HISAT2 aligned cleaned reads to the mouse reference genome and DESeq2 determined DEGs based on read counts using an adjusted p-value <0.05 as a cutoff. The summary, including reads obtained, reads after trimming, and percentage of reads aligned for each sample, can be found in Table 12.

Microglial RNA harvested from 3-month-old wild-type (n=3) and mThy1-Asyn (n=4) mice had 119 DEGs based on an adjusted p-value cutoff of <0.05. The top and bottom 20 DEGs based on log2 fold change (log2FC) are available in Tables 17 and 18. Some of the most upregulated genes include chemokines such as Ccl1 and Ccl17. The complete DEG list was investigated for functional terms and pathways represent in our gene lists based on annotation from GO (38 terms), Reactome pathways (3 pathways), and KEGG (3 functions) databases and an

EntrezID	Gene Symbol	Description	Adj. Pvalue	log2FC
76237	6430628N08Rik	RIKEN cDNA 6430628N08 gene	0.01	6.31
105349	Akr1c18	aldo-keto reductase family 1, member C18	0.03	6.04
235379	Gldn	gliomedin	0.00	3.38
20290	Ccl1	chemokine (C-C motif) ligand 1	0.03	3.02
12919	Crhbp	corticotropin releasing hormone binding protein	0.00	2.66
12823	Col19a1	collagen, type XIX, alpha 1	0.05	2.26
66673	Sorcs3	sortilin-related VPS10 domain containing receptor 3	0.03	2.00
21838	Thy1	thymus cell antigen 1, theta	0.01	1.89
16161	Il12rb1	interleukin 12 receptor, beta 1	0.01	1.87
15561	Htr3a	5-hydroxytryptamine (serotonin) receptor 3A	0.04	1.80
320429	Trank1	tetratricopeptide repeat and ankyrin repeat containing 1	0.03	1.78
20303	Ccl4	chemokine (C-C motif) ligand 4	0.01	1.74
15563	Htr5a	5-hydroxytryptamine (serotonin) receptor 5A	0.03	1.72
14810	Grin1	glutamate receptor, ionotropic, NMDA1 (zeta 1)	0.03	1.70
20295	Ccl17	chemokine (C-C motif) ligand 17	0.02	1.69
319942	A530016L24Rik	RIKEN cDNA A530016L24 gene	0.02	1.63
14417	Gad2	glutamic acid decarboxylase 2	0.02	1.62
242773	Slc45a1	solute carrier family 45, member 1	0.04	1.60
67331	Atp8b3	ATPase, class I, type 8B, member 3	0.03	1.59
72978	Cnih3	cornichon family AMPA receptor auxiliary protein 3	0.04	1.55

Table 17. 20 most up-regulated DEGs at 3 Months. Differentially expressed genes were determined between wild type and mThy1-Asyn mice at 3 months of age. The 20 genes with the greatest increase in expression are presented in this table.

EntrezID	Gene Symbol	Description	Adj. Pvalue	log2FC
13861	Epx	eosinophil peroxidase	0.00	-2.51
16521	Kcnj5	potassium inwardly-rectifying channel, subfamily J, member 5	0.01	-2.47
76615	Got1l1	glutamic-oxaloacetic transaminase 1-like 1	0.00	-2.20
53856	Prg3	proteoglycan 3	0.05	-2.17
68509	Ptx4	pentraxin 4	0.01	-2.16
22262	Uox	urate oxidase	0.02	-2.12
229277	Stoml3	stomatin (Epb7.2)-like 3	0.02	-2.05
403180	Ccdc121	coiled-coil domain containing 121	0.02	-2.04
67747	Ribc2	RIB43A domain with coiled-coils 2	0.00	-2.03
75573	Prr29	proline rich 29	0.02	-2.00
381522	Ccdc180	coiled-coil domain containing 180	0.00	-1.97
53873	Ear6	eosinophil-associated, ribonuclease A family, member 6	0.02	-1.76
66758	Zfp474	zinc finger protein 474	0.02	-1.75
213248	Wdr49	WD repeat domain 49	0.05	-1.75
434756	Akap14	A kinase (PRKA) anchor protein 14	0.03	-1.74
320159	Fam179a	family with sequence similarity 179, member A	0.02	-1.69
74338	Slc6a19	solute carrier family 6 (neurotransmitter transporter), member 19	0.02	-1.66
381284	Crocc2	ciliary rootlet coiled-coil, rootletin family member 2	0.02	-1.63
56087	Dnah10	dynein, axonemal, heavy chain 10	0.01	-1.63
110082	Dnah5	dynein, axonemal, heavy chain 5	0.02	-1.63

Table 18. 20 most down regulated DEGs at 3 Months. Differentially expressed genes were determined between wild type and mThy1-Asyn mice at 3 months of age. The 20 genes that demonstrate the greatest decrease in expression are presented in this table.

adj. p-value <0.05. RichR performed enrichment analysis and constructed a network using the top 20 terms from GO (adj. p-value) and the full lists of enrichment terms from KEGG and Reactome (Figure 19). The network file was visualized using Cytoscape with an inverted self-organized map layout which was manually adjusted for visibility.

The more severe phenotype associated with the older (13 month) mice used in our study was reflected by the higher number of DEGs identified between wild type (n=5) and mThy1-Asyn (n=8) mice. RNA harvested from isolated microglia in these older animals identified 3,766 DEGs using an adjusted p-value cutoff of <0.05. The top and bottom 20 DEGs based on log2 fold change (FC) are shown in Tables 19 and 20. RichR was used to determine functional enrichment terms and pathways represented within the DEG list. Overall 1,509 GO terms, 230 Reactome pathways, and 35 KEGG functions were determined to be enriched within our dataset. The top 50 enriched terms from GO enrichment based on adjusted p-value can be found in Figure 20. Many of the GO terms are related to development, migration, and adhesion.
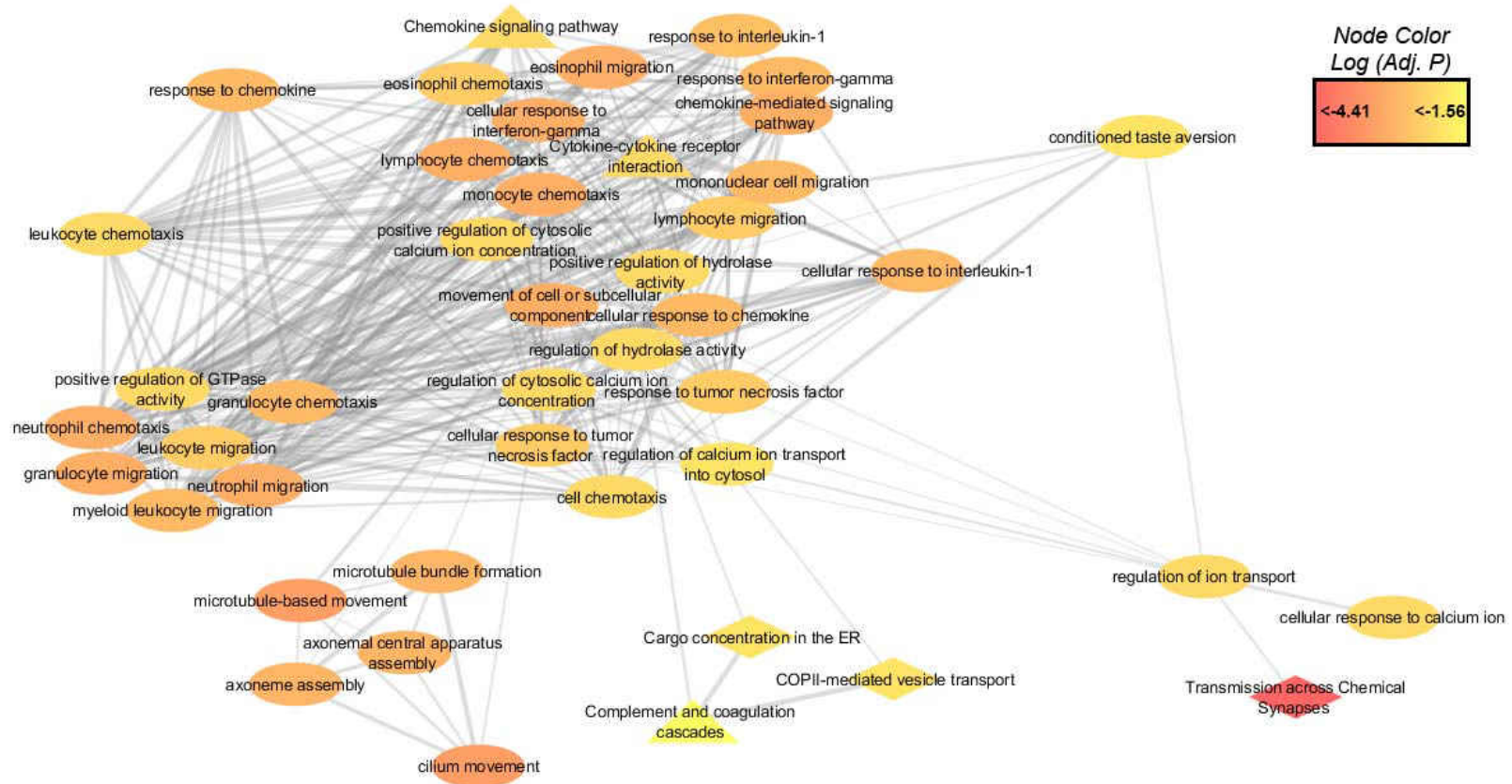
Figure 19. Enrichment Network from 3-Month DEGs. The differentially expressed genes from the 3-month analysis were assessed for enrichment of biological functions and pathways using the GO (circle), KEGG (triangle), and Reactome (diamond) databases. The top 20 (adj. p-value) enrichment terms from each database serve as the network nodes and the shared genes between term annotations serve as the edges connecting them. Node shape is based on the terms database (see above), while color represents the adjusted p-value score of each term. The network layout is adjusted from Cytoscape's inverted self-organized map for visibility.

| EntrezID	Gene Symbol	Description	Adj. Pvalue	log2FC
NA	Igkv8-34	immunoglobulin kappa variable 8-34	0.0329	6.76
15891	Ibsp	integrin binding sialoprotein	0.0004	5.75
NA	Ighg1	immunoglobulin heavy constant gamma 1 (G1m marker)	0.0007	5.69
380683	Sec14l3	SEC14-like lipid binding 3	0.0020	5.07
24108	Ubd	ubiquitin D	0.0419	4.68
22431	Wt1	Wilms tumor 1 homolog	0.0075	4.34
192188	Stab2	stabilin 2	0.0002	4.28
15378	Hnf4a	hepatic nuclear factor 4, alpha	0.0411	4.23
NA	Trav12-3	T cell receptor alpha variable 12-3	0.0077	4.19
50701	Elane	elastase, neutrophil expressed	0.0000	4.02
53873	Ear6	eosinophil-associated, ribonuclease A family, member 6	0.0000	3.81
16833	Ldhc	lactate dehydrogenase C	0.0010	3.80
442829	Ccin	calicin	0.0396	3.80
619288	Fam71a	family with sequence similarity 71, member A	0.0304	3.78
170813	Ms4a3	membrane-spanning 4-domains, subfamily A, member 3	0.0000	3.67
19074	Prg2	proteoglycan 2, bone marrow	0.0005	3.66
13861	Epx	eosinophil peroxidase	0.0002	3.66
17523	Mpo	myeloperoxidase	0.0000	3.64
13035	Ctsg	cathepsin G	0.0000	3.39
19152	Prtn3	proteinase 3	0.0001	3.36

Table 19. 20 most up regulated DEGs at 13 Months. Differentially expressed genes were determined between wild type and mThy1-Asyn mice at 13 months of age. The 20 genes with the greatest increase in expression are presented in this table.

EntrezID	Gene Symbol	Description	Adj. Pvalue	log2FC
75512	Gpx6	glutathione peroxidase 6	0.0015	-4.21
56184	Msgn1	mesogenin 1	0.0303	-2.05
74556	Themis3	thymocyte selection associated family member 3	0.0199	-2.01
380780	Serpina11	serine (or cysteine) peptidase inhibitor, clade A (alpha-1 antiproteinase, antitrypsin), member 11	0.0049	-1.97
332396	Kcnk18	potassium channel, subfamily K, member 18	0.0000	-1.84
NA	Gm10570	predicted gene 10570	0.0065	-1.76
259114	Olfr570	olfactory receptor 570	0.0180	-1.75
234724	Tat	tyrosine aminotransferase	0.0038	-1.51
14539	Opn1mw	opsin 1 (cone pigments), medium-wave-sensitive (color blindness, deutan)	0.0484	-1.50
14765	Gpr50	G-protein-coupled receptor 50	0.0486	-1.49
26380	Esrrb	estrogen related receptor, beta	0.0000	-1.48
75600	Calml4	calmodulin-like 4	0.0000	-1.38
69083	Sult1c2	sulfotransferase family, cytosolic, 1C, member 2	0.0197	-1.37
68800	Prr32	proline rich 32	0.0003	-1.35
13393	Dlx3	distal-less homeobox 3	0.0162	-1.34
14836	Gsc	goosecoid homeobox	0.0023	-1.32
12869	Cox8b	cytochrome c oxidase subunit VIIIb	0.0005	-1.32
230824	Grhl3	grainyhead-like 3	0.0000	-1.31
18256	Oc90	otoconin 90	0.0029	-1.30
72789	Veph1	ventricular zone expressed PH domain-containing 1	0.0182	-1.30

Table 20. 20 most down regulated DEGs at 13 Months. Differentially expressed genes were determined between wild type and mThy1-Asyn mice at 13 months of age. The 20 genes that demonstrate the greatest decrease in expression are presented in this table.
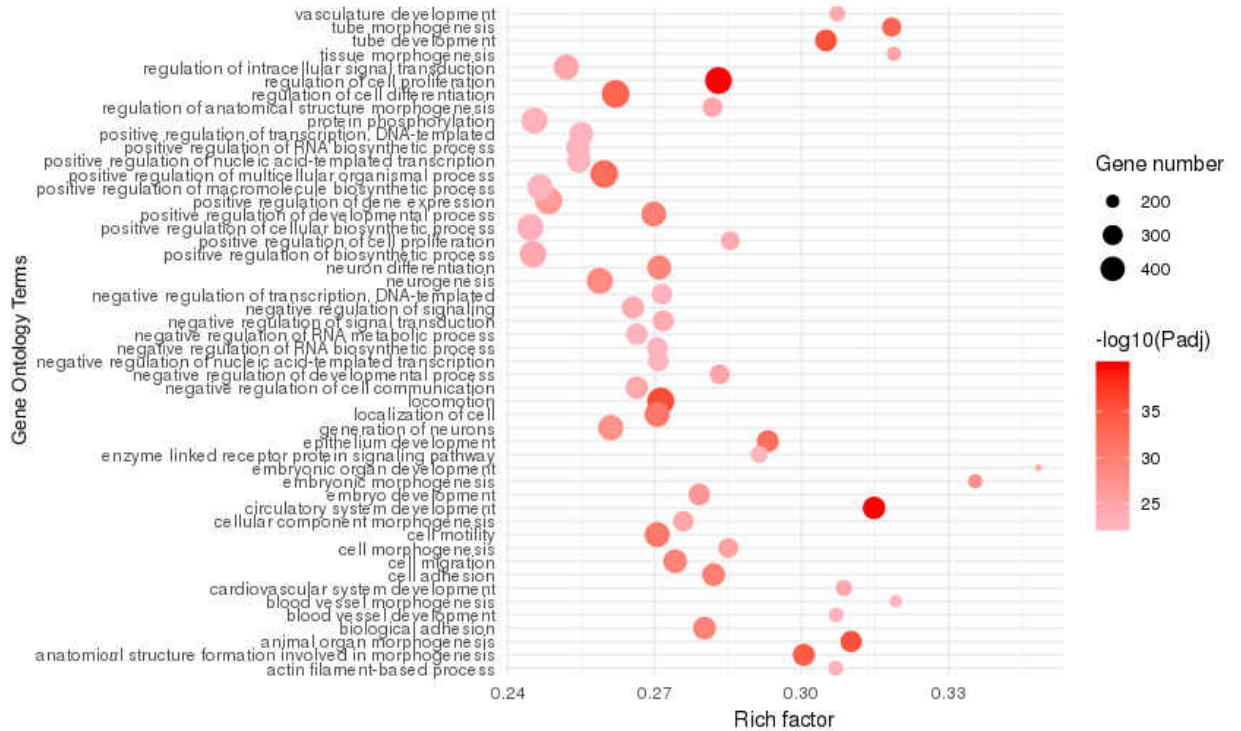
Figure 20. GO Enrichment in 13-Month DEGs. DEGs identified from the 13-month comparison were analyzed for enrichment in terms of GO annotation. The top 50 most significantly enriched terms are listed. Dot size corresponds to the number of genes in each group, while color represent the significance level of enrichment. Rich factor indicates the ratio of genes submitted to the number of genes annotated to a function or pathway as an addition measure of enrichment.

113

The top 50 most enriched KEGG pathways (Figure 21) includes terms involved with various cancer pathways along with immune and adhesion related functions. While Reactome pathways identified enriched pathways related to cell cycle, immune system, and mitochondrial dysfunction (Figure 22). Network analysis through RichR and Cytoscape were used to visualize associations between terms based on common genes (Figure 23). A clear subnetwork associated with cell cycle and mitosis can be seen and a smaller subnetwork related to immune system function is also present. The largest subnetwork includes many terms involved in cellular metabolism, which share edges with neuroinflammatory conditions such as Parkinson's, Alzheimer's, and Huntington's disease.

Potential DEGs related to the progression of the mTHy1-Asyn phenotype were investigated by examining both 3- and 13-month DEG lists for shared genes. Table 21 shows the 9 shared genes between the two groups. Out of the 9 shared genes, 4 appear to be directionally discordant while the other 5 are concordant between groups. The genes demonstrating a decrease in expression at 3 months but increased expression at 13 include Epx, Prg3, and Ear6. The only other discordant gene is Stra6, which has increased expression at 3 months and decreased at 13 months. All other genes display an increase in expression levels at both time points. These genes, including Zfp683, Il12rb1, Ccl4, Ccl3, and Ccrl2, are related to a proinflammatory status involving macrophage inflammatory proteins.
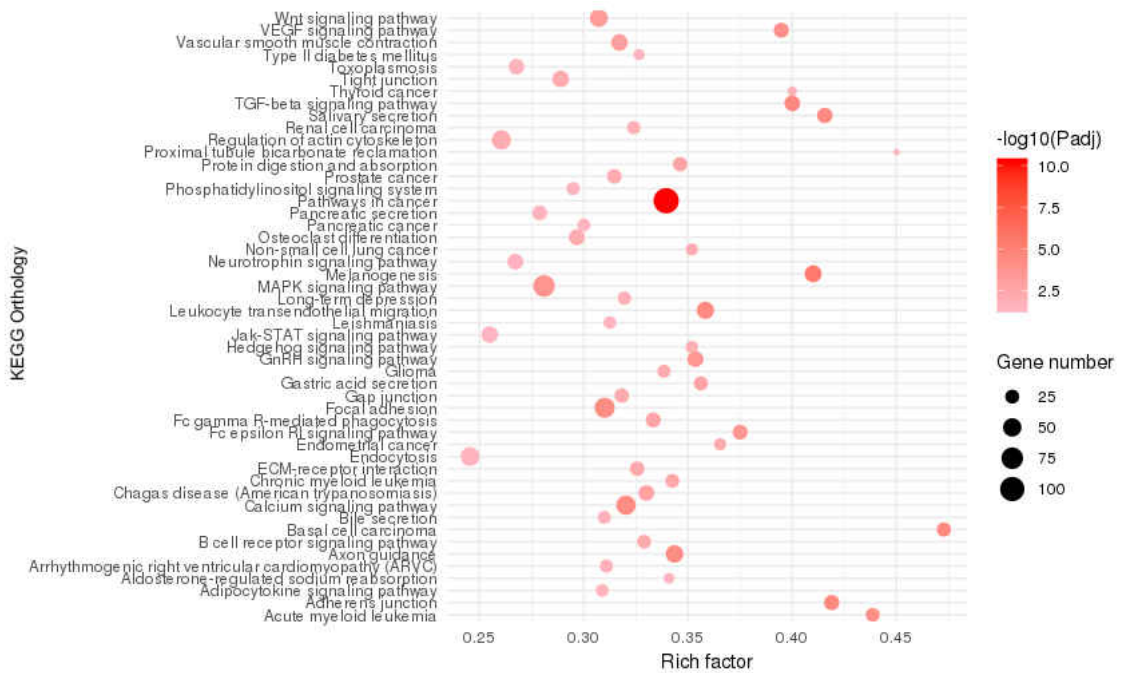
Figure 21. KEGG Enrichment in 13 Month DEGs. DEGs identified from the 13-month comparison were analyzed for enrichment in terms of KEGG annotation. The top 50 most significant terms are listed. Dot size corresponds to the number of genes in each group, while color represent the significance level of enrichment. Rich factor indicates the ratio of genes submitted to the number of genes annotated to a function or pathway as an addition measure of enrichment.
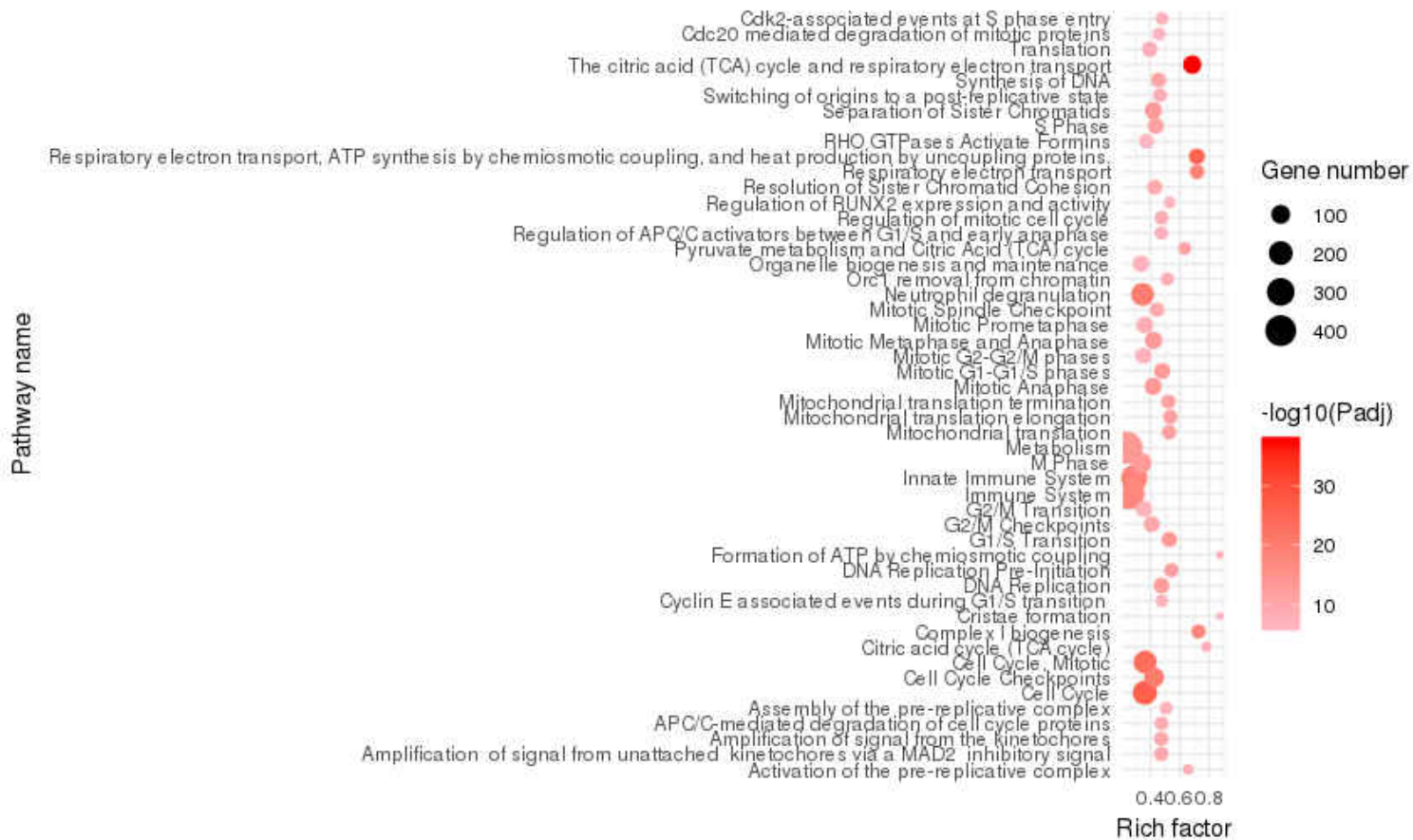
Figure 22. Reactome Pathway Enrichment in 13 Month DEGs. DEGs identified from the 13-month comparison were analyzed in terms of Reactome annotation. The top 50 most significant pathways are listed. Dot size corresponds to the number of genes in each group, while color represent the significance level of enrichment. Rich factor indicates the ratio of genes submitted to the number of genes annotated to a function or pathway as an addition measure of enrichment.
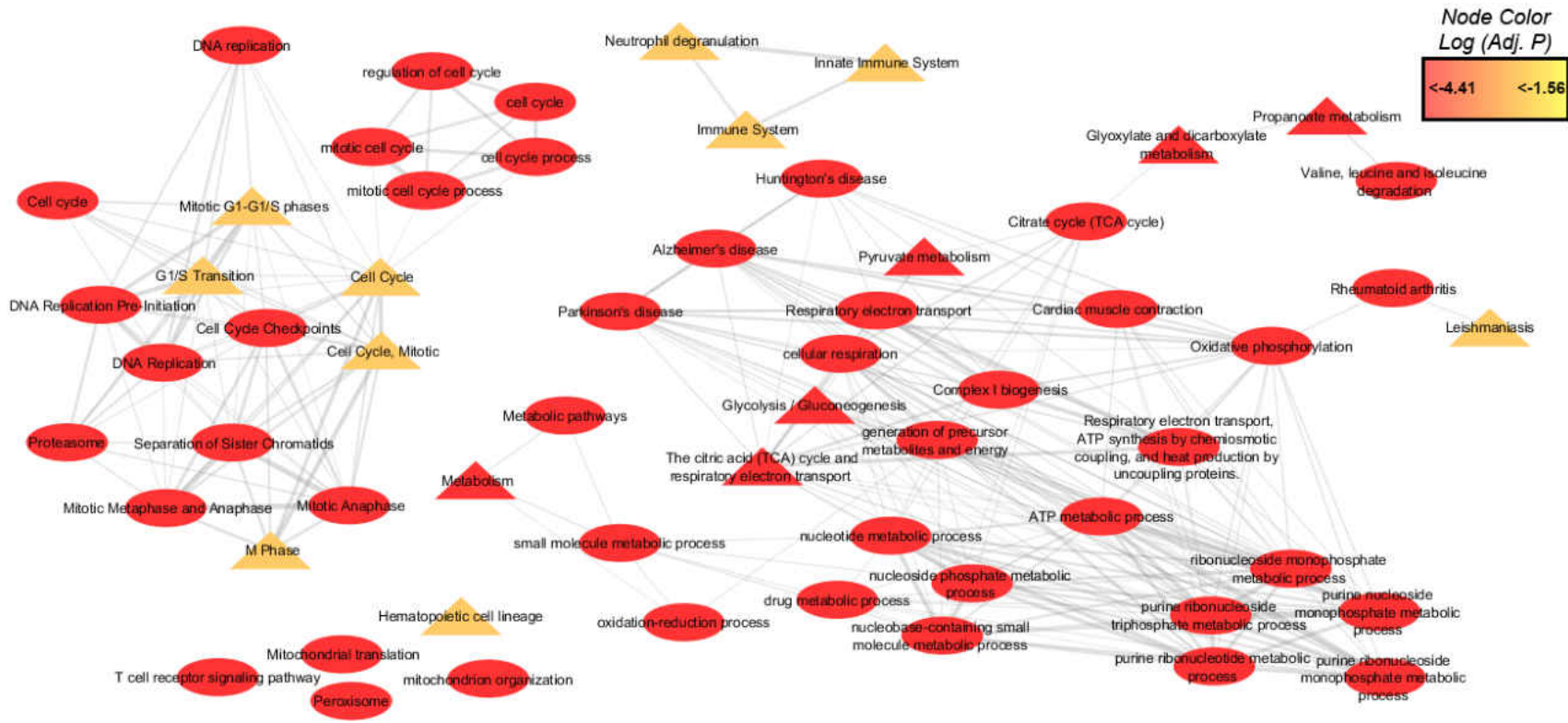
Figure 23. Enrichment Network from 13 Month DEGs. The differentially expressed genes from the 13-month analysis were assessed for enrichment of biological functions and pathways using the GO (circle), KEGG (triangle), and Reactome (diamond) databases. The top 20 (adj. p-value) enrichment terms from each database serve as the network nodes and the shared genes between term annotations serve as the edges connecting them. Node shape is based on the terms database (see above) while color represents the adjusted p-value score of each term. The network layout is adjusted from Cytoscape's inverted self-organized map for visibility.

Gene Symbol	Description	13 Month Log2FC	3 Month Log2FC
Zfp683	zinc finger protein 683	1.53	1.62
Stra6	stimulated by retinoic acid gene 6	-0.50	0.62
Il12rb1	interleukin 12 receptor, beta 1	1.05	1.87
Ccl4	chemokine (C-C motif) ligand 4	2.39	1.74
Ccrl2	chemokine (C-C motif) receptor-like 2	1.91	1.44
Epx	eosinophil peroxidase	3.66	-2.51
Ccl3	chemokine (C-C motif) ligand 3	1.91	1.29
Prg3	proteoglycan 3	3.20	-2.17
Ear6	eosinophil-associated, ribonuclease A family, member 6	3.81	-1.76

Table 21. DEGs shared between 3- and 13-Month Groups. Nine genes were found to be differentially expressed at both time points within this study. The gene symbols are on the left, followed by a description and the log2FC values in 13- and 3-month comparisons. The color gradient indicates an increase (red) or decrease (blue) in log2FC. Out of the 9 common DEGs, 5 are concordant while 4 are discordant between groups.

Correlation between Identified DMGs and DEGs

Changes in DNA methylation are often thought to influence gene expression levels based on CpG location in relation to the gene and transcription start sight. Possible correlations between changes in methylation and changes in expression between identified DMGs and DEGs were investigated and the results are summarized in Figure 24A. DMCs were separated into their annotated regions such as CpG islands and shores as well as gene promoter, intron, exon, and intergenic regions. Gene names for each DMC belonging to these groups were obtained from the UCSC annotation and matched to their corresponding DEGs. The overlap between DMCs related genes and DEGs ranged from 1 to 320 shared genes. Pearson correlation tests were used to determine correlation coefficients. Each DMC with gene annotation matching identified DEGs were used in the Pearson correlation calculation. When one gene had multiple DMCs, the expression value obtained during DEG analysis was counted multiple times for each DMC. All five genomic regions of interest were examined for correlation but only intronic DMCs in 13-month-old animals had a significant slightly negative correlation (r=-0.15, p=0.008) between delta beta and fold change (Figure 24B).

A

DataSet		Annotation	CpGs	Genes	Shared RNA	Pearson	Pearson P
13 Month		Island	310	121	1	NA	NA
DEGs	3766	Shore	536	358	66	-0.05	0.7
DMCs	15226	Promoter	590	373	65	-0.2	0.11
DMGs	3742	Exon	1157	673	120	-0.002	0.98
		Intron	2817	1442	320	-0.15	0.008
3 Month		Island	888	329	2	-1	NA
DEGs	119	Shore	1283	834	3	0.56	0.67
DMCs	27175	Promoter	1602	961	8	-0.33	0.42
DMGs	5315	Exon	3046	1607	10	-0.144	0.69
		Intron	6789	3033	28	0.07	0.74

B
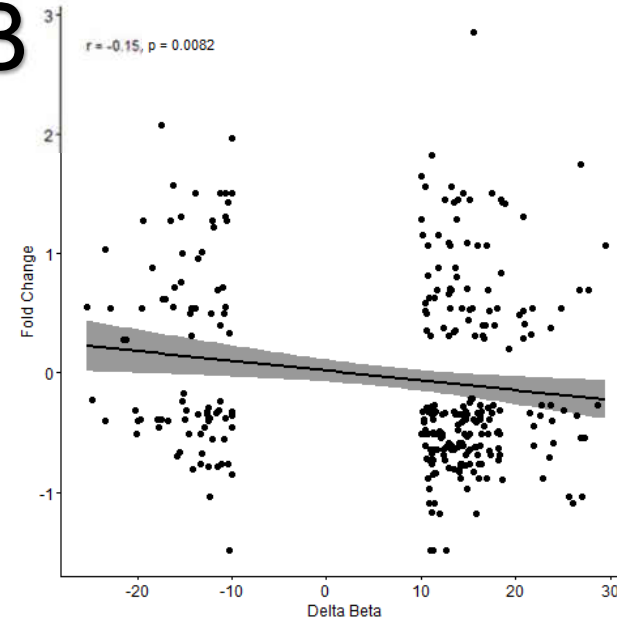
Figure 24. Correlation Summary of Genes Both Differentially Methylated and Expressed. Genomic and CpG associated regions for the identified DMCs from both comparisons were assessed for their correlation with measured gene expression from RNA-sequencing. **(A)** The summary table of DMC annotation shows the total amount of DMCs identified and how many DMGs are represented in that list along with the associated DEGs identified. DMCs that belong to genomic promoter, exon, or intronic regions or from CpG associated island or shore regions were used to assess the correlation between methylation and gene expression changes. **(B)** The only region which showed a significant correlation was the intronic region in the 13-month dataset.

Discussion

This study examined regulation of the immune response in the central nervous system by examining changes related to genomic methylation and gene expression in microglia from the mThy1-Asyn mouse model of PD. This model overexpresses human wild-type α-syn and exhibits a neuroinflammatory phenotype with progressive PD like symptoms[96]. RRBS and RNA-seq were used to measure methylation and gene expression changes at 3 and 13 months of age. These time points were selected based on phenotypic changes associated with a pre-parkinsonian phenotype at 3 months and an early stage symptomatic phenotype with a decrease of striatal dopamine occurring at 14 months[96–98,361]. This study provides a unique opportunity to identify changes induced by aggregate and oligomerized α-syn on microglia, which are largely responsible for the neuroinflammation associated with PD[367].

The examination of changes induced in our early stage mice at 3 months identified a wide variety of changes in methylation and relatively few in gene expression. Overall, 11,441 DMCs were identified from the microglia of our transgenic mice at 3 months with 6% positioned within CpG islands and 10% in promoter regions. The genes which were annotated to the DMCs identified were associated with neuronal development, synaptic transmission, intracellular signaling, adhesion, and migration functions based on enrichment analysis using GO, Reactome pathways, and KEGG databases. Microglia are highly involved in the regulation of synaptic activity and have been shown to be the major players in synaptic pruning[368]. The enrichment of these pathways may suggest a shift

121

from a resting phenotype, involved in maintaining neuronal homeostasis, to an active inflammatory state requiring mobility. Gene expression data from these mice also reflect this possible shift in phenotype. We identified 119 DEGs when comparing transgenic to wild-type controls. Some of the most upregulated genes include Ccl1 which is a chemokine that attracts immune cells and Ccl17 which induces chemotaxis, both are indicative of a proinflammatory response. Enrichment analysis of the complete list of 119 DEGs using GO, Reactome, and KEGG, identified biological functions involved in immune function and cellular movement represented by our gene list. Both methylation and expression changes were annotated to similar functional terms; however, no significant correlations between DMC locations and gene expression were identified within our 3-month animals.

Changes induced in methylation and gene expression in 13-month-old animals reflect a more severe phenotype representing the early stages of Parkinson's symptoms. Examination of global genome methylation patterns identified 10,436 DMCs of which 5% were located within CpG islands and 10% in promoter regions. When focused to a gene level based on gene annotation for each CpG, these DMCs represent 3,742 DMGs. Enrichment analysis on this list of DMGs revealed function terms involving cell locomotion, adhesion, and development. Network analysis of these terms identified a subnetwork of interconnected terms involving cell surface interactions, adhesion, and extracellular matrix with platelet derived growth factor signaling (PDGF) and receptor tyrosine kinases (RTK). Both PDGF and RTK signaling have been

122

shown to be strong inducers of proliferation[364,366] and our DMG enrichment

network exhibits a wide variety of terms indicative of proliferation (Figure 18).

Increased mobility and proliferation of microglia has been linked to

neurodegeneration[369]. Gene expression changes in these animals represent

similar functions to that identified in the methylation analysis.

Overall, 3,766 DEGs were identified and examined for functional

enrichment as well. Gene ontology identified adhesion and migration functions

that were enriched, KEGG results indicate involvement of the immune system,

and Reactome pathways represented in the data are highly related to

metabolism and the immune system. However, all three annotation databases

represented an abundance of terms reflecting proliferation. Network analysis

examining the top 20 enriched terms from each annotation database also

provided insight into how these systems interact. While proliferation and cell

cycle terms were present throughout this analysis, in the network they form an

isolated cluster. This may not mean that these functions are not related to other

themes observed in the data such as metabolism and immune function since our

network analysis is limited to gene overlap and is non-directional. Another small

cluster of terms related to immune involvement is also isolated from the main

body of the generated network. The main subnetwork is composed of terms

related to metabolism that have shared edges with neurodegenerative conditions

such as Parkinson's disease, Alzheimer's disease, and Huntington's disease.

Terms relating to mitochondrial dysfunction, which is often proposed as a

causative factor in neurodegenerative diseases[24,57,370–372], were also identified in

this data. In our network analysis, while some mitochondria terms are disconnected islands, others involved in cellular respiration were directly linked to disease terms. The data representing our early stage PD animals indicate that activated microglia are subjected to the mitochondrial stress associated with exposure to aberrant α-syn[371,373,374].

Correlations between identified methylation changes and gene expression changes were investigated for DMCs located in CpG Islands, CpG shores, promoters, exons, and introns. The only significant correlation between the data was identified from DMCs in intronic regions which had a negative correlation with gene expression (r=-0.15, p=0.008). Furthermore, overlap between 3- and 13-month animals were also evaluated for genes related to progression of the disease. Comparing DEG lists resulted in 9 genes that were represented in both datasets from the comparison between wild type and transgenic mice. Of those 9 genes, 5 showed an increase in expression in both datasets while the other 4 genes were directionally discordant going up in one group and down in the other. Three of the concordant genes are immune related (Ccl4, Ccrl2, and Il12rb1) and involved in immune recruitment and chemotaxis[375]. All but one of the genes that change during the progression of the disease from 3 to 13 months have a lowered expression level at 3 months and are over expressed at 13 months. These genes include eosinophil peroxidase (Epx), proteoglycan3 (Prg3) and eosinophil-associated, ribonuclease A family member 6 (Ear6).

Epx has been linked to the serpine superfamily of proteins which commonly serve as protease inhibitors controlling proteolytic cascades[376–379].

Serpineb9 which is a cysteine protease is slightly upregulated at 13 months in our data (data not shown) and not significantly different at 3 months. Cysteine proteases are important for microglia as they are critical for accelerated collagen and elastin degradation at sites of inflammation and play a role in MHC class II immune response, apoptosis, and extracellular matrix remodelling[370,380]. One of the enriched functions in the 13-month DMCs was collagen chain trimerization which was connected to cell surface interactions, extracellular matrix organization, focal adhesion, signaling by RTK and PDGF signaling. The evidence for this cascade from Epx expressions levels and interactions are not direct and require further investigation. However, this potential interaction may warrant further investigation. In our data, little overlap between 3 and 13-month-old mice is observed. This is most likely due to a low sample size in the 3-month group which resulted in a low amount of DEGs being identified.

When considering these findings and their biological meaning it is important to keep in mind certain limitations of this study. One such limitation likely affecting the correlation between RNA and DNA is that we were not able to use both DNA and RNA samples from each mouse due to sample quality concerns. Samples with the highest quantity and quality of RNA/DNA were selected, while attempting to limit the number of non-overlapping animals between DNA and RNA analysis to 2 or less. Another challenge to analyse the data regarding the samples used is that no validation experiments certifying that the isolated cells from the brain were in fact microglia. Due to low cell counts from isolations and limited number of animals, all possible sources of DNA and

RNA from each cell isolation had to be preserved with the intent of validating representative isolations experiments at a later date. One caveat to the data presented is that interpreting immune function such as cytokine expression from RNA levels has proven to be inconsistent with protein levels[381]. The model used also presents some limitations to our study, since we are studying immune function and the murine immune system differs from humans in some significant ways such as toll receptors, nitric oxide synthase, cytokines, and cytokine receptors[382]. These difference between human and mouse may influence the translatability of results observed in this study. All data presented in this study are *in silico* results from high-throughput sequencing and as such will require wet lab validation likely through pyrosequencing to measure methylation sites and reverse transcription polymerase chain reaction (RT-PCR) to measure gene transcription levels.

Despite its limitations, this investigation has identified interesting candidates for further evaluation in regard to α-syn-induced microglial activation and associated progression of PD. The possible influence α-syn has on genomic methylation patterns may act as a feedback loop based on the regulatory role methylation plays in the genes expression and this possibility warrants further investigation. Investigation into the Epx genes involvement in collagen degradation via serpine may be important insight into microglia's role of synaptic regulation in the progression of PD. In order to better understand the biological implications of the data presented, similar analysis involving other phenotypic time points for in this model system would be necessary.

In summary, from the data presented we have shown that α-syn overexpression can induce methylation changes in microglia in the mThy1-α-syn model of PD. At 3 months, or pre-parkinsonian, these mice show an increase in cell mobility and inflammatory functions related to activation of microglia early on. While at 13 months, immune and mobility related functions are still present but metabolic functions are more prevalent and linked to neurodegenerative disease annotation as well. Despite observed changes in functional terms being similar between methylation and gene expression, there was a low amount of correlation between these changes. Intronic CpGs at 13 months were the only significant correlation with gene expression with an increase in methylation correlating to a decrease in expression. Few genes were differentially expressed at both 3 and 13 months however, the conserved change in Epx may warrant further investigation.

CHAPTER V

DISCUSSION

The goal of the first study was to identify a possible common underlying cause of DPN across models, species, and time points. This study was executed using a unified analysis pipeline to examine eight publicly available microarray datasets from sciatic nerve tissue and identify highly conserved pathways associated to DPN. DEGs related to DPN were identified between non-diabetic and diabetic samples in murine models, and non-progressive and progressive human samples. DEG lists were constructed into literature association networks, which were graphically compared between human and each murine network to obtain shared subnetworks. Identified subnetworks were merged and subjected to pathway and centrality analysis. The top 50 of multiple measures of centrality identified the 64 most central genes which showed enrichment of 272 canonical pathways. Network and cluster analysis of the most central pathways revealed themes such as apoptosis, inflammatory response, degradation, as well as immune and kinase signaling were the most involved in the network. These conserved pathways are likely the key responses in DPN and provide new therapeutic targets for the potential treatment of DPN, a disorder that remains without a drug intervention to date.

The second study of this dissertation focused on the SHD STZ model of T1DM by examining gene expression changes in tissues associated with DN and DPN at 16 weeks. RNA-sequencing was used to examine expression changes in renal glomerulus and cortex (DN) as well as sciatic nerve and dorsal root ganglia (DPN) following RNA extraction and library preparation. Lists of DEGs were analyzed using IPA to describe enriched pathways represented in each tissue. Overlap of DEGs and Pathways were examined with 244 genes and 38 pathways being conserved across three or more tissues. The conserved pathways included PTEN signaling, PI3K signaling, adipogenesis pathway, acute phase response signaling, and colorectal cancer metastasis signaling. Of the 244 genes, 188 of them were directionally concordant. The 188 concordant genes were analyzed using IPA and subjected to network analysis, which identified clusters relating to oxidative stress, cell cycle, and immune response. These findings provide transcriptomic profiles of complication-prone tissue in the SHD STZ model and support previously identified factors influencing microvascular complications in T1DM.

Our findings regarding DPN in both studies largely agree with the established literature regarding this complication[246,247,383–385]. Various cellular stress mechanisms have been implicated in DPN such as hyperglycemia, dyslipidemia, hypoxia, ischemia, vascular insufficiency, metabolic syndrome, impaired insulin signalling, and inflammation as summarized by this review[386]. The data presented here largely revolve around the role of inflammation. Diabetic patients have been shown to experience chronic inflammation through both

RAGE and TLR activation by circulating high levels of glycation end products[216–220]. Lipid signaling involvement in the immune response has also been established in the literature and diabetic patients have been shown to display dyslipidemia[387]. The first study, which examined multiple models of DPN, observed a possible central role involving LXR/RXR signaling which is responsible for regulating lipid metabolism, inflammation, as well as cholesterol efflux and catabolism[225–228]. While our second study did not observe a similar change in our model of type 1 diabetes, other studies regarding unified complication analysis have observed changes in PPAR-γ signaling which is also a lipid metabolism regulatory pathway[388]. It is possible these changes are unique to the type 2 diabetes form of DPN, since therapeutic strategies such as a PPAR-γ agonist (pioglitazone)[199] did not yield any benefit in STZ-treated mice (data not shown). Strict glycemic control is also less beneficial in slowing the progression of DPN in patients with type 2 diabetes than it is in type 1 patients[230] suggesting some differences between these diseases despite symptom similarity.

Many proposed stress mechanisms can be linked to the chronic inflammation in both type 1 and type 2 diabetes. Hyperglycemia and dyslipidemia may induce an inflammatory response[389] and hypoxic or ischemic conditions can drive immune cell dysregulation[390]. One of the main mechanisms of the immune response to eliminate pathogens is via production of reactive oxygen species[391] which have been shown to be neurotoxic[392]. Largely the role of inflammation in the progression of DPN remains unclear despite supporting evidence in the studies presented. However, this is currently being explored both

experimentally[198] as well as in clinical trials involving the use of non-steroidal anti-inflammatory drugs (salsalate) in type 1 diabetic patients (https://clinicaltrials.gov/ct2/show/NCT02936843).

In the third study of this dissertation, an overexpression model of PD was used to investigate the methylation and gene expression changes induced by α-syn in microglia. Microglia were isolated from mThy1-Asyn mice at 3 and 13 months for DNA and RNA extraction. Generated libraries from this procedure were used for RRBS and RNA-sequencing, respectively. These transgenic mice have been shown to present markers of neuroinflammation as early as 1 month and begin to show motor and non-motor symptoms at 3 months similar to a pre-parkinsonian phenotype. Reduction in dopamine levels and a more severe phenotype can be observed at 14 months indicating an early stage Parkinson's phenotype. However, this model of PD has not been shown to have a reduction in total number of dopaminergic neurons as is observed in PD patients[96,104].

The mThy1-Asyn mice at 3 months, or pre-parkinsonian stage, demonstrate an increase in cell mobility and inflammatory functions related to activation of microglia. These results are congruent with the established phenotype of these mice at 3 months with increased levels of neuroinflammation. The early stage PD phenotype observed in mice at 13 months demonstrated enrichment in immune and cell mobility functions as well, but the majority of functional terms are related to metabolism and mitochondria dysfunction. Mitochondrial dysfunction has well established literature support its role in PD and is the target of many chemically induced models and genetic forms of

PD[30,57]. However, it has also been shown to create a feedback loop by promoting inflammation while many pro-inflammatory mediators may disrupt mitochondrial activity[372].

Despite similar functional enrichment in methylation and gene expression changes observed at both time points, there was very little correlation between changes in methylation and observed expression changes. Intronic CpGs in our 13-month dataset held a negative correlation with the associated DEGs. Nine genes were differentially expressed at both 3 and 13 months with 5 concordant and 4 discordantly expressed. The concordant gene list was associated with inflammatory genes related to recruitment and chemotaxis. The discordant genes may indicate progressive changes in the course of disease such as the involvement of Epx which may influence microglia activity through its interaction with serpine.

While these studies examine inherently different systems in DPN and PD, there is evidence supporting systemic inflammatory events influencing the neurocognitive decline in Alzheimer's Disease[393]. By monitoring TNF-α serum levels in Alzheimer's patients Holmes et al. observed a 2- and 4-fold increase in cognitive decline associated with acute and system inflammatory events, respectively. In healthy individuals systemic infections lead to a sickness behavior associated with decreased appetite[394] and lethargy[395] but these responses are often short lived up and not thought to have long-term consequences. It is possible that in the elderly or a diseased state, microglia are influenced by their microenvironment into a prepared state leading to a more

profound inflammatory response that contributes to disease symptoms and progression. Studies examining activated microglia in neurodegenerative models, at the first sign of behavioral changes, have shown chemokine ligand 2 (CCL2) to be one of the early activated inflammatory mediators[396]. Investigation into CCL2 null mice have shown that microglia have a less dramatic inflammatory response than wild type mice[397]. This evidence may implicate CCL2 signaling in the prepared microglia status proposed. Further investigation into the communication between the peripheral and central immune system and the influence it may have on the nervous system would provide valuable insight into the progression of neurodegenerative conditions.

Future Directions

In order to further investigate the role of inflammation in DPN it would be useful to further characterize DPN progression in the non-obese diabetic (NOD) mouse which is an immunodeficient mouse strain. The NOD mouse displays hyperalgesia at 8 weeks and hypoalgesia at 12 weeks suggesting development of neuropathic pain and may represent DPN progression[133,152]. A possible DPN comparison between the NOD mouse, SHD STZ-treated model of T1DM, a healthy wild-type control, and mice treated with a non-steroidal anti-inflammatory drug (NSAID) as well as STZ would yield valuable information on the involvement of inflammation. These models, assuming they had the same background, would provide similar systems with varying levels of inflammation or immune response. The NOD mouse is considered immune deficient, STZ treatment along with a NSAID would knockdown immune activity to a lesser degree than the NOD

mutation, and STZ treatment alone would provide a T1DM model with a fully functioning immune system. Measurements of disease progression and severity of symptoms would offer insight into the physiologic contribution that inflammation may or may not have on DPN. Transcriptomic analysis may provide insight into molecular mechanistic difference within the disease system in the absence or presence of an immune response. This would also open avenues for addition research into potential immune specific therapeutic targets by investigating DEGs only present when immunodeficient models (NOD and NSAID-treated) are compared with a healthy immune system in the STZ model. If the NOD mouse does not demonstrate symptomatic DPN naturally then an alternative approach is to use STZ to induce a more severe T1DM phenotype associated with DPN.

Insight into the role inflammation has on the progression of T2DM associated DPN could also be obtained by exacerbating the already low grade inflammation that is experienced with diabetes using a treatment regimen with an inflammatory stimulus[143,398,399]. Ideally, RAGE[135] would be targeted rather than engaging another aspect of the immune system; however, pharmacological agents that currently target this receptor consist of only antagonists[400]. A study examining the progression of DPN in a model of T2DM, such as the *db/db* mouse, compared to a healthy wild-type control, LPS-treated *db/db*, NSAID-treated *db/db*, and RAGE antagonists-treated *db/db* would provide a scale of differing levels of immune response. This could allow a way to determine the level of contribution inflammation has to DPN progression.

Further insight into the role that neuroinflammation plays in the mThy1-Asyn phenotype and the methylation and expression changes induced by α-syn in microglia can be approached in multiple ways. The current approach has indicated some promising results and is worthy of being applied in another study examining further time points in these animals such as at one month before appearance of symptoms, after 14 months following the loss of 40% of striatal dopamine, and a midway time point around 7 months would all yield interesting results. Studies involving a higher number of animals and biological validation of sampling would likely yield more insight than the current study provides into the methylation and expression changes that α-syn can induce. Another interesting option is the use of a CSF1R inhibitor such as PLX3397 to deplete the brain of the mThy1-Asyn mouse of microglia[401]. The use of CSF1R inhibitors to reduce microglia proliferation has been shown to improve recovery after CNS injury[402,403]. In our system, it would provide a way to examine the rate of progression of symptoms in the absence of microglia to evaluate the influence inflammation has disease progression. This may also uncover underlying causes and new therapeutic targets by eliminating a confounding factor in examination of the condition.

There has been shown to be an increased prevalence of peripheral neuropathy in PD compared to age matched controls[404]. It may be worth investigating if the mThy1-Asyn mouse also experiences peripheral neuropathy. A simple ELISA on blood samples from the mThy1-Asyn would establish if this model experiences peripheral inflammation similar to what is observed in PD patients[405]. The

aggregate α-syn pathology has been observed in the peripheral nervous system of the mThy1-Asyn mouse which is likely to engage the peripheral immune system similar to what is observed in the CNS. If these mice experience peripheral inflammation and neuropathy, then a possible unified analysis of the above described studies could provide thorough insight into the interaction between the nervous and the immune system. A similar approach could be investigating the cognitive and neurodegenerative status of a chronic inflammation model such as the interleukin 10 (IL-10) knockout mouse.

Limitations of the Work Presented in this Dissertation

The research presented in this dissertation supports the involvement and contribution of inflammation and the immune response in progression of neurodegeneration. The limitations of the work discussed in this dissertation are presented as follows.

In the first study, the murine models of DPN that were used were on varied backgrounds. The genetic background of mice has been shown to affect the progression of neuropathy and presentation of symptoms in murine model systems[158]. All data used in this study was publicly available after being used in other publications and were not originally designed to be compared but were processed through a unified pipeline to allow comparison between datasets. However, generation of these model animals on a unified background strain for the purposes of this study were not feasible so this is a caveat of any information gathered from these results. Another limitation in both studies related to DPN is that the sciatic nerve biopsy process taken from the animals includes Schwann

cells during the RNA isolation. Much of the signal captured from both RNA expression analysis performed originated from Schwann cells surrounding the sciatic nerve.

The use of a murine model when examining inflammatory changes should always be considered a caveat since the murine immune system differs from humans in some significant ways such as toll receptors, nitric oxide synthase, cytokines, and cytokine receptors just to name a few which may influence the results observed in this study[382]. All data presented in these studies are *in silico* results from high throughput sequencing and as such will require technical validation and would be strongly supported by biological validation experiments.

Summary Conclusions

The work presented in this dissertation strongly implicates inflammation as a contributing factor to neurodegenerative conditions of both the peripheral and central nervous system (Figure 25). Analysis of transcriptomic data from multiple models of DPN to human patients identified clusters of terms related to inflammation, degradation, apoptosis, as well as kinase and immune signaling as conserved changes across multiple time points, models, and species of DPN. Further analysis into the STZ model of T1DM across multiple complication-prone tissues identified clusters related to DNA-damage response, oxidative stress, and immune response between diabetic nephropathy and DPN. These results suggest that peripheral inflammation may be an underlying cause of DPN. α-syn overexpression-induced methylation and gene expression changes are indicative of an M1 microglia phenotype in concert with symptomatic progression of PD.

These results warrant further investigation into the role inflammation plays on the

progression of neurodegenerative disease and the neuro-microenvironment in

both the central and peripheral nervous systems.
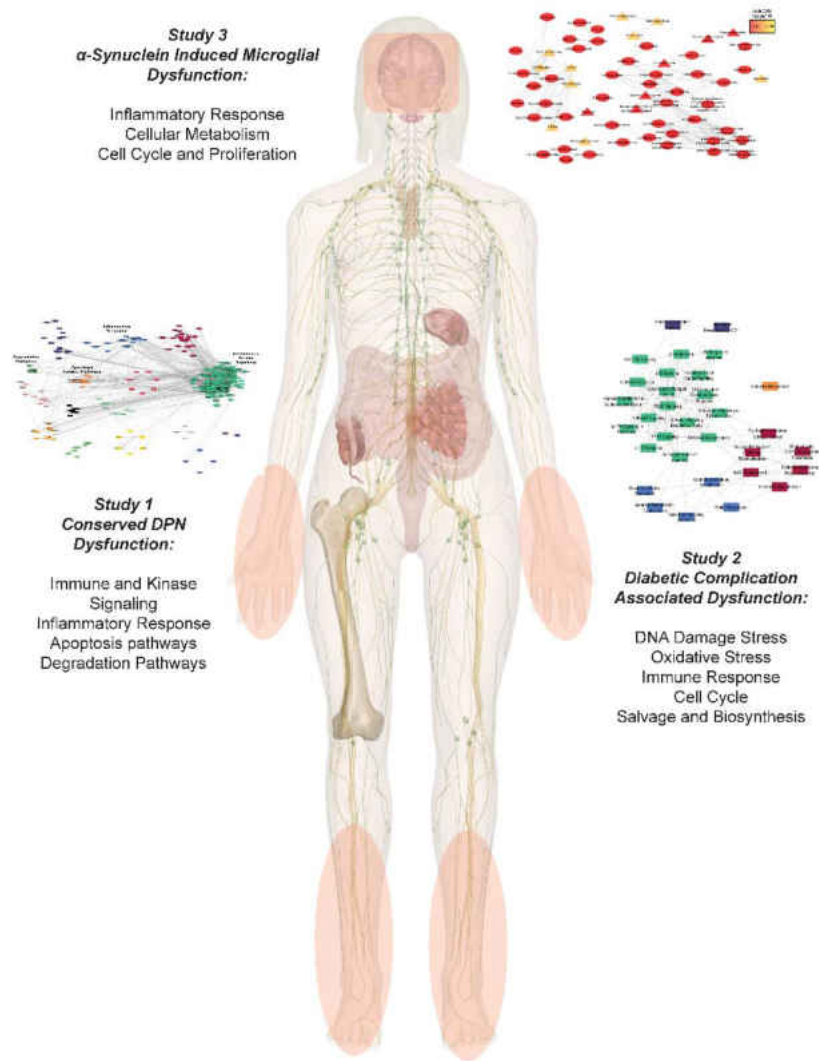
Figure 25. Summary Figure. The biological systems displayed within the human body include the nervous system and immune system (www.innerbody.com). Red areas highlight the nervous tissue of interest for this dissertation. Each study's results are summarized by their final network figures. The first study found immune signaling, inflammation, apoptosis, and degradation as conserved centrally influential pathways in both diabetic patients and mouse models of DPN. The second study examined both nephropathy and neuropathy associated with diabetes in an STZ-induced mouse model to identify DNA damage response, oxidative stress, immune response, cell cycle signaling, as well as salvage and biosynthesis pathways as being influenced in both complications. The third study examined the microglia from an α-synuclein overexpression mouse model of Parkinson's disease. Microglial changes associated with aberrant α-synuclein included an inflammatory response, cellular metabolism dysfunction, as well as cell cycle and proliferation. These results may indicate a vulnerability of nervous tissue to an inflammatory environment.

CHAPTER VI

REFERENCES

1.   Del Rio Hortega, P. Tercera aportación al conocimiento morfológico e interpretación funciónal de la oligodendroglía. *Memorias la Real Soc. Española Hist. Nat.* **40,** 40–122 (1928).
2.   Del Rio Hortega, P. ¿Son homologables la glia de escasas radiaciones y la célula de schwann? *Boletín la Soc. española Biol.* **16,** 1–4 (1922).
3.   del Río-Hortega, P. La glía de escasa radiaciones (Oligodendroglia). *Boletín la Real Soc. Española Hist. Nat.* **21,** 63–92 (1921).
4.   Schäfer, M. K. *et al.* Complement C1q is dramatically up-regulated in brain microglia in response to transient global cerebral ischemia. *J. Immunol.* (2000). doi:10.1016/S0162-3109(00)80038-7
5.   Simi, A., Lerouet, D., Pinteaux, E. & Brough, D. Mechanisms of regulation for interleukin-1β in neurodegenerative disease. *Neuropharmacology* (2007). doi:10.1016/j.neuropharm.2007.02.011
6.   Di Paolo, N. C. & Shayakhmetov, D. M. Interleukin 1α and the inflammatory process. *Nat. Immunol.* (2016). doi:10.1038/ni.3503
7.   McCoy, M. K. & Tansey, M. G. TNF signaling inhibition in the CNS: Implications for normal brain function and neurodegenerative disease. *Journal of Neuroinflammation* (2008). doi:10.1186/1742-2094-5-45
8.   Saijo, K. *et al.* A Nurr1/CoREST Pathway in Microglia and Astrocytes Protects Dopaminergic Neurons from Inflammation-Induced Death. *Cell* (2009). doi:10.1016/j.cell.2009.01.038
9.   Lassmann, H., Brück, W. & Lucchinetti, C. Heterogeneity of multiple sclerosis pathogenesis: Implications for diagnosis and therapy. *Trends in Molecular Medicine* (2001). doi:10.1016/S1471-4914(00)01909-2
10.   McGeer, P. L. & McGeer, E. G. Inflammatory processes in amyotrophic lateral sclerosis. *Muscle and Nerve* (2002). doi:10.1002/mus.10191
11.   Zhang, W. *et al.* Aggregated α-synuclein activates microglia: a process leading to disease progression in Parkinson's disease. *FASEB J.* (2005). doi:10.1096/fj.04-2751com
12.   Wang, P. *et al.* Aggravation of Alzheimer's disease due to the COX-2-mediated reciprocal regulation of IL-1β and Aβ between glial and neuron cells. *Aging Cell* (2014). doi:10.1111/acel.12209
13.   Virchow, R. Gesammelte Abhandlungen zur Wissenschaftlichen Medizen. *Frankfurt am Main Meidinger U Comp* (1856).
14.   Streit, W. J. Microglia as neuroprotective, immunocompetent cells of the CNS. *GLIA* (2002). doi:10.1002/glia.10154

15. Liddelow, S. A. *et al.* Neurotoxic reactive astrocytes are induced by activated microglia. *Nature* (2017). doi:10.1038/nature21029

16. Jacque, C. M. *et al.* Determination of glial fibrillary acidic protein (GFAP) in human brain tumors. *J. Neurol. Sci.* (1978). doi:10.1016/0022-510X(78)90107-7

17. Eric R. Kandel, James H. Schwartz, Thomas M. Jessell, Steven A. Siegelbaum, A. J. H. *Principles of Neural Science*. (McGraw Hill Medical, 1996).

18. Anderson, M. A. *et al.* Astrocyte scar formation AIDS central nervous system axon regeneration. *Nature* (2016). doi:10.1038/nature17623

19. Bradl, M. & Lassmann, H. Oligodendrocytes: Biology and pathology. *Acta Neuropathologica* (2010). doi:10.1007/s00401-009-0601-5

20. Cannella, B. & Raine, C. S. Multiple Sclerosis: Cytokine Receptors on Oligodendrocytes Predict Innate Regulation. *Ann. Neurol.* (2004). doi:10.1002/ana.10764

21. Ramesh, G., Benge, S., Pahar, B. & Philipp, M. T. A possible role for inflammation in mediating apoptosis of oligodendrocytes as induced by the Lyme disease spirochete Borrelia burgdorferi. *J. Neuroinflammation* (2012). doi:10.1186/1742-2094-9-72

22. Stufflebeam, R. *Neurons, Synapses, Action Potentials, and Neurotransmission. The Mind Project* (2008).

23. Hirsch, E. C. & Hunot, S. Neuroinflammation in Parkinson's disease: a target for neuroprotection? *Lancet Neurol.* **8,** 382–397 (2009).

24. Hunter, R. L. *et al.* Inflammation induces mitochondrial dysfunction and dopaminergic neurodegeneration in the nigrostriatal system. *J. Neurochem.* (2007). doi:10.1111/j.1471-4159.2006.04327.x

25. Castaño, A., Herrera, A. J., Cano, J. & Machado, A. Lipopolysaccharide Intranigral Injection Induces Inflammatory Reaction and Damage in Nigrostriatal Dopaminergic System. *J. Neurochem.* (2010). doi:10.1046/j.1471-4159.1998.70041584.x

26. Tysnes, O. B. & Storstein, A. Epidemiology of Parkinson's disease. *J. Neural Transm.* **124,** 901–905 (2017).

27. Parkinson, J. An essay on the shaking palsy. 1817. *J. Neuropsychiatry Clin. Neurosci.* (1817). doi:10.1176/jnp.14.2.223

28. *Parkinson's Disease*. (CRC Press, 2004).

29. Jankovic, J. *Parkinson's disease: Diagnosis, motor symptoms and non-motor features. Journal of neurology, neurosurgery, and psychiatry* (2013). doi:10.2217/9781780843391

30. Dauer, W. & Przedborski, S. Parkinson's disease: Mechanisms and models. *Neuron* **39,** 889–909 (2003).

31. Bernheimer, H., Birkmayer, W., Hornykiewicz, O., Jellinger, K. & Seitelberger, F. Brain dopamine and the syndromes of Parkinson and Huntington Clinical, morphological and neurochemical correlations. *J. Neurol. Sci.* (1973). doi:10.1016/0022-510X(73)90175-5

32. Lees, A. J., Hardy, J. & Revesz, T. Parkinson's disease. *Lancet* **373,** 2055–2066 (2009).

33. Sveinbjornsdottir, S. The clinical symptoms of Parkinson's disease. *Journal of Neurochemistry* (2016). doi:10.1111/jnc.13691

34. Mayo Clinic. Parkinson's disease - Symptoms and causes - Mayo Clinic. *Mayo Clinic: Diseases and Conditions* (2018).

35. Jellinger, K. A. More frequent Lewy bodies but less frequent Alzheimer-type lesions in multiple system atrophy as compared to age-matched control brains. *Acta Neuropathol.* (2007). doi:10.1007/s00401-007-0227-4

36. Engelender, S. Ubiquitination of α-synuclein and autophagy in Parkinson's disease. *Autophagy* (2008). doi:10.4161/auto.5604

37. Hornykiewicz, O. & SJ, K. Biochemical pathophysiology of Parkinson's disease. *Adv. Neurol.* 19–34 (1987).

38. Terry, R. D. in *Advances in Dementia Research* (2011). doi:10.1007/978-3-7091-6781-6_12

39. Lashuel, H. A., Hartley, D., Petre, B. M., Walz, T. & Lansbury, P. T. Amyloid pores from pathogenic mutations. *Nature* (2002). doi:10.1038/418291a

40. Ding, T. T., Lee, S. J., Rochet, J. C. & Lansbury, P. T. Annular α-synuclein protofibrils are produced when spherical protofibrils are incubated in solution or bound to brain-derived membranes. *Biochemistry* (2002). doi:10.1021/bi020139h

41. Lashuel, H. A. *et al.* α-synuclein, especially the parkinson's disease-associated mutants, forms pore-like annular and tubular protofibrils. *J. Mol. Biol.* (2002). doi:10.1016/S0022-2836(02)00735-0

42. Hutton, J. T., Morris, J. L., Román, G. C., Imke, S. C. & Elias, J. W. Treatment of Chronic Parkinson's Disease With Controlled-Release Carbidopa/Levodopa. *Arch. Neurol.* **45,** 861–864 (1988).

43. Voges, J., Koulousakis, A. & Sturm, V. Deep brain stimulation for Parkinson's disease. *Acta Neurochirurgica, Supplementum* (2007). doi:10.1007/978-3-211-33081-4_19

44. Zangaglia, R. *et al.* Macrogol for the treatment of constipation in Parkinson's disease. A randomized placebo-controlled study. *Mov. Disord.* (2007). doi:10.1002/mds.21243

45. Langston, J. W., Tetrud, J. W., Irwin, I. & Ballard, P. Chronic Parkinsonism in Humans Due to a Product of Meperidine-Analog Synthesis. *Science (80-.).* (1983).

46. Brooks, A. I., Chadwick, C. A., Gelbard, H. A., Cory-Slechta, D. A. & Federoff, H. J. Paraquat elicited neurobehavioral syndrome caused by dopaminergic neuron loss. *Brain Res.* (1999).

47. Day, B. J., Patel, M., Calavetta, L., Chang, L. Y. & Stamler, J. S. A mechanism of paraquat toxicity involving nitric oxide synthase. *Proc. Natl. Acad. Sci. U. S. A.* (1999). doi:10.1073/pnas.96.22.12760

48. Tanner, C. M. Epidemiology of Parkinson's disease. *Neurol. Clin.* **10,** 317–329 (1992).

49. Hernán, M. A., Takkouche, B., Caamaño-Isorna, F. & Gestal-Otero, J. J. A meta-analysis of coffee drinking, cigarette smoking, and the risk of Parkinson's disease. *Ann. Neurol.* (2002). doi:10.1002/ana.10277

50. Noyce, A. J. *et al.* Meta-analysis of early nonmotor features and risk factors for Parkinson disease. *Annals of Neurology* (2012). doi:10.1002/ana.23687

51. Polymeropoulos, M. H. *et al.* Mutation in the α-synuclein gene identified in families with Parkinson's disease. *Science (80-.).* (1997). doi:10.1126/science.276.5321.2045

52. Corti, O., Lesage, S. & Brice, A. What Genetics Tells us About the Causes and Mechanisms of Parkinson's Disease. *Physiol. Rev.* (2011). doi:10.1152/physrev.00022.2010

53. Nalls, M. A. *et al.* Large-scale meta-analysis of genome-wide association data identifies six new risk loci for Parkinson's disease. *Nat. Genet.* (2014). doi:10.1038/ng.3043

54. Goldman, S. M. *et al.* Head injury, alpha-synuclein Rep1, and Parkinson's disease. *Ann. Neurol.* (2012). doi:10.1002/ana.22499

55. Olanow, C. W. & McNaught, K. S. P. Ubiquitin-proteasome system and Parkinson's disease. *Movement Disorders* (2006). doi:10.1002/mds.21013

56. Ross, C. A. & Poirier, M. A. Protein aggregation and neurodegenerative disease. *Nat. Med.* (2004). doi:10.1038/nm1066

57. Bose, A. & Beal, M. F. Mitochondrial dysfunction in Parkinson's disease. *Journal of Neurochemistry* (2016). doi:10.1111/jnc.13731

58. Nussbaum, R. L. & Polymeropoulos, M. H. Genetics of Parkinson's disease. *Hum. Mol. Genet.* (1997). doi:10.1093/hmg/6.10.1687

59. Nalls, M. A. *et al.* Imputation of sequence variants for identification of genetic risks for Parkinson's disease: A meta-analysis of genome-wide association studies. *Lancet* (2011). doi:10.1016/S0140-6736(10)62345-8

60. Chang, D. *et al.* A meta-analysis of genome-wide association studies identifies 17 new Parkinson's disease risk loci. *Nat. Genet.* (2017). doi:10.1038/ng.3955

61. Chiueh, C. C. *et al.* Neurochemical and behavioral effects of systematic and intranigral administration of N-methyl-4-phenyl-1,2,3,6-tetrahydropyridine in the rat. *Eur. J. Pharmacol.* (1984). doi:10.1016/0014-2999(84)90221-8

62. Betarbet, R. *et al.* Chronic systemic pesticide exposure reproduces features of Parkinson's disease. *Nat. Neurosci.* (2000). doi:10.1038/81834

63. Kogan, F. J., Nichols, W. K. & Gibb, J. W. Influence of methamphetamine on nigral and striatal tyrosine hydroxylase activity and on striatal dopamine levels. *Eur. J. Pharmacol.* (1976). doi:10.1016/0014-2999(76)90090-X

64. Ungerstedt, U. 6-hydroxy-dopamine induced degeneration of central monoamine neurons. *Eur. J. Pharmacol.* (1968). doi:10.1016/0014-2999(68)90164-7

65. Blesa, J. & Przedborski, S. Parkinson's disease: animal models and dopaminergic cell vulnerability. *Front. Neuroanat.* (2014). doi:10.3389/fnana.2014.00155

66. Shimoji, M., Zhang, L., Mandir, A. S., Dawson, V. L. & Dawson, T. M. Absence of inclusion body formation in the MPTP mouse model of Parkinson's disease. *Mol. Brain Res.* (2005). doi:10.1016/j.molbrainres.2005.01.012

67. Halliday, G. *et al.* No Lewy pathology in monkeys with over 10 years of severe MPTP parkinsonism. *Mov. Disord.* (2009). doi:10.1002/mds.22481

68. Przedbroski, S. *et al.* Dose-dependent lesions of the dopaminergic nigrostriatal pathway induced by instrastriatal injection of 6-hydroxydopamine. *Neuroscience* (1995). doi:10.1016/0306-4522(95)00066-R

69. Cicchetti, F., Drouin-Ouellet, J. & Gross, R. E. Environmental toxins and Parkinson's disease: what have we learned from pesticide-induced animal models? *Trends in Pharmacological Sciences* (2009). doi:10.1016/j.tips.2009.06.005

70. Miller, G. W. Paraquat: The Red Herring of Parkinson's Disease Research. *Toxicol. Sci.* **100,** 1–2 (2007).

71. Thrash, B., Thiruchelvan, K., Ahuja, M., Suppiramaniam, V. & Dhanasekaran, M. Methamphetamine-induced neurotoxicity: The road to Parkinson's disease. *Pharmacological Reports* (2009). doi:10.1016/S1734-1140(09)70158-6

72. Ayadi, A. El & Zigmond, M. J. Low concentrations of methamphetamine can protect dopaminergic cells against a larger oxidative stress injury: Mechanistic study. *PLoS One* (2011). doi:10.1371/journal.pone.0024722

73. Capela, J. P. *et al.* Molecular and cellular mechanisms of ecstasy-induced neurotoxicity: An overview. *Molecular Neurobiology* (2009). doi:10.1007/s12035-009-8064-1

74. Costa, G. *et al.* MPTP-induced dopamine neuron degeneration and glia activation is potentiated in MDMA-pretreated mice. *Mov. Disord.* (2013). doi:10.1002/mds.25646

75. Jensen, K. F. *et al.* Mapping toxicant-induced nervous system damage with a cupric silver stain: a quantitative analysis of neural degeneration induced by 3,4-methylenedioxymethamphetamine. *NIDA Res. Monogr.* **136,** 133–134 (1993).

76. Goldberg, M. S. *et al.* Parkin-deficient Mice Exhibit Nigrostriatal Deficits but not Loss of Dopaminergic Neurons. *J. Biol. Chem.* (2003). doi:10.1074/jbc.M308947200

77. Hinkle, K. M. *et al.* LRRK2 knockout mice have an intact dopaminergic system but display alterations in exploratory and motor co-ordination behaviors. *Mol. Neurodegener.* (2012). doi:10.1186/1750-1326-7-25

78. Sanchez, G. *et al.* Unaltered striatal dopamine release levels in young Parkin knockout, Pink1 knockout, DJ-1 knockout and LRRK2 R1441G transgenic mice. *PLoS One* (2014). doi:10.1371/journal.pone.0094826

79. Andres-Mateos, E. *et al.* DJ-1 gene deletion reveals that DJ-1 is an atypical peroxiredoxin-like peroxidase. *Proc. Natl. Acad. Sci.* (2007). doi:10.1073/pnas.0703219104

80. Kim, R. H. *et al.* Hypersensitivity of DJ-1-deficient mice to 1-methyl-4-phenyl-1,2,3,6-tetrahydropyrindine (MPTP) and oxidative stress. *Proc. Natl. Acad. Sci.* (2005). doi:10.1073/pnas.0501282102

81. Kitada, T. *et al.* Impaired dopamine release and synaptic plasticity in the striatum of Parkin-/- mice. *J. Neurochem.* (2009). doi:10.1111/j.1471-

4159.2009.06152.x

82. Itier, J. M. *et al.* Parkin gene inactivation alters behaviour and dopamine neurotransmission in the mouse. *Human Molecular Genetics* (2003). doi:10.1093/hmg/ddg239

83. Goldberg, M. S. *et al.* Nigrostriatal dopaminergic deficits and hypokinesia caused by inactivation of the familial parkinsonism-linked gene DJ-1. *Neuron* (2005). doi:10.1016/j.neuron.2005.01.041

84. Gispert, S. *et al.* Parkinson phenotype in aged PINK1-deficient mice is accompanied by progressive mitochondrial dysfunction in absence of neurodegeneration. *PLoS One* (2009). doi:10.1371/journal.pone.0005777

85. Gautier, C. A., Kitada, T. & Shen, J. Loss of PINK1 causes mitochondrial functional defects and increased sensitivity to oxidative stress. *Proc. Natl. Acad. Sci.* (2008). doi:10.1073/pnas.0802076105

86. Andres-Mateos, E. *et al.* Unexpected Lack of Hypersensitivity in LRRK2 Knock-Out Mice to MPTP (1-Methyl-4-Phenyl-1,2,3,6-Tetrahydropyridine). *J. Neurosci.* (2009). doi:Doi 10.1523/Jneurosci.4357-09.2009

87. Tong, Y. *et al.* Loss of leucine-rich repeat kinase 2 causes impairment of protein degradation pathways, accumulation of alpha-synuclein, and apoptotic cell death in aged mice. *Proc. Natl. Acad. Sci.* (2010). doi:10.1073/pnas.1004676107

88. Lin, X. *et al.* Leucine-Rich Repeat Kinase 2 Regulates the Progression of Neuropathology Induced by Parkinson's-Disease-Related Mutant α-synuclein. *Neuron* (2009). doi:10.1016/j.neuron.2009.11.006

89. Paumier, K. L. *et al.* Behavioral Characterization of A53T Mice Reveals Early and Late Stage Deficits Related to Parkinson's Disease. *PLoS One* (2013). doi:10.1371/journal.pone.0070274

90. van der Putten, H. *et al.* Neuropathology in mice expressing human alpha-synuclein. *J. Neurosci.* (2000). doi:20/16/6021 [pii]

91. Gomez-Isla, T. *et al.* Motor dysfunction and gliosis with preserved dopaminergic markers in human α-synuclein A30P transgenic mice. *Neurobiol. Aging* (2003). doi:10.1016/S0197-4580(02)00091-X

92. Masliah, E. *et al.* Dopaminergic loss and inclusion body formation in α-synuclein mice: Implications for neurodegenerative disorders. *Science (80-.).* (2000). doi:10.1126/science.287.5456.1265

93. Su, X., Federoff, H. J. & Maguire-Zeiss, K. A. Mutant α-synuclein overexpression mediates early proinflammatory activity. *Neurotox. Res.* (2009). doi:10.1007/s12640-009-9053-x

94. Chen, L., Thiruchelvam, M. J., Madura, K. & Richfield, E. K. Proteasome dysfunction in aged human α-synuclein transgenic mice. *Neurobiol. Dis.* (2006). doi:10.1016/j.nbd.2006.02.004

95. Rockenstein, E. *et al.* Differential neuropathological alterations in transgenic mice expressing α-synuclein from the platelet-derived growth factor and Thy-1 promoters. *J. Neurosci. Res.* (2002). doi:10.1002/jnr.10231

96. Chesselet, M. F. *et al.* A Progressive Mouse Model of Parkinson's Disease: The Thy1-aSyn ('Line 61') Mice. *Neurotherapeutics* **9,** 297–314 (2012).

97. Lam, H. A. *et al.* Elevated tonic extracellular dopamine concentration and altered dopamine modulation of synaptic activity precede dopamine loss in the striatum of mice overexpressing human α-synuclein. *J. Neurosci. Res.* **89,** 1091–1102 (2011).

98. Fleming, S. M. Early and Progressive Sensorimotor Anomalies in Mice Overexpressing Wild-Type Human -Synuclein. *J. Neurosci.* (2004). doi:10.1523/jneurosci.3080-04.2004

99. Fleming, S. M. Behavioral Outcome Measures for the Assessment of Sensorimotor Function in Animal Models of Movement Disorders. *International Review of Neurobiology* (2009). doi:10.1016/S0074-7742(09)89003-X

100. Ouchi, Y., Yagi, S., Yokokura, M. & Sakamoto, M. Neuroinflammation in the living brain of Parkinson's disease. *Park. Relat. Disord.* **15,** 200–204 (2009).

101. Nagatsu, T., Mogi, M., Ichinose, H. & Togari, A. in *Advances in Research on Neurodegeneration* (2012). doi:10.1007/978-3-7091-6301-6_19

102. McGeer, P. L., Itagaki, S., Akiyama, H. & McGeer, E. G. Rate of cell death in parkinsonism indicates active neuropathological process. *Ann. Neurol.* (1988). doi:10.1002/ana.410240415

103. Watson, M. B. *et al.* Regionally-specific microglial activation in young mice over-expressing human wildtype alpha-synuclein. *Exp. Neurol.* (2012). doi:10.1016/j.expneurol.2012.06.025

104. Cheng, H. C., Ulane, C. M. & Burke, R. E. Clinical progression in Parkinson disease and the neurobiology of axons. *Annals of Neurology* (2010). doi:10.1002/ana.21995

105. Galley, H. F. & Webster, N. R. The immuno-inflammatory cascade. *Br. J. Anaesth.* (1996). doi:10.1093/bja/77.1.11

106. Brinkmann, V. *et al.* Neutrophil Extracellular Traps Kill Bacteria. *Science (80-.).* (2004). doi:10.1126/science.1092385

107. Murphy, K. & Weaver, C. *Janeway's Immunbiology. Janeway's Immunbiology* (2016). doi:10.1007/s13398-014-0173-7.2

108. Helmy, K. Y. *et al.* CRIg: A macrophage complement receptor required for phagocytosis of circulating pathogens. *Cell* (2006). doi:10.1016/j.cell.2005.12.039

109. Gasque, P. Complement: A unique innate immune sensor for danger signals. *Molecular Immunology* (2004). doi:10.1016/j.molimm.2004.06.011

110. Awad, A. *et al.* Natural killer cells induce eosinophil activation and apoptosis. *PLoS One* (2014). doi:10.1371/journal.pone.0094492

111. Gordon, S. Phagocytosis: An Immunobiologic Process. *Immunity* (2016). doi:10.1016/j.immuni.2016.02.026

112. Bianchi, M. E. DAMPs, PAMPs and alarmins: all we need to know about danger. *J. Leukoc. Biol.* (2006). doi:10.1189/jlb.0306164

113. Takeuchi, O. & Akira, S. Pattern Recognition Receptors and Inflammation. *Cell* (2010). doi:10.1016/j.cell.2010.01.022

114. Arnit, I. *et al.* Unbiased reconstruction of a mammalian transcriptional network mediating pathogen responses. *Science (80-.).* (2009).

doi:10.1126/science.1179050

115. Mantovani, A., Cassatella, M. A., Costantini, C. & Jaillon, S. Neutrophils in the activation and regulation of innate and adaptive immunity. *Nature Reviews Immunology* (2011). doi:10.1038/nri3024

116. Alberts, B. *et al.* in *Molecular Biology of the Cell* (2002). doi:10.1287/trsc.1050.0142

117. Kuchroo, V. K. *et al.* B7-1 and B7-2 costimulatory molecules activate differentially the Th1/Th2 developmental pathways: Application to autoimmune disease therapy. *Cell* **80,** 707–718 (1995).

118. Samad, T. A. *et al.* Interleukin-1 β-mediated induction of Cox-2 in the CNS contributes to inflammatory pain hypersensitivity. *Nature* (2001). doi:10.1038/35068566

119. Zhang, X. C., Kainz, V., Burstein, R. & Levy, D. Tumor necrosis factor-α induces sensitization of meningeal nociceptors mediated via local COX and p38 MAP kinase actions. *Pain* (2011). doi:10.1016/j.pain.2010.10.002

120. Binshtok, A. M. *et al.* Nociceptors are interleukin-1beta sensors. *J Neurosci* (2008). doi:28/52/14062 [pii]\n10.1523/JNEUROSCI.3795-08.2008

121. Annibaldi, A. & Meier, P. Checkpoints in TNF-Induced Cell Death: Implications in Inflammation and Cancer. *Trends in Molecular Medicine* (2018). doi:10.1016/j.molmed.2017.11.002

122. Kolb, J. P., Oguin, T. H., Oberst, A. & Martinez, J. Programmed Cell Death and Inflammation: Winter Is Coming. *Trends in Immunology* (2017). doi:10.1016/j.it.2017.06.009

123. Choy, J. *et al.* The regulation and consequences of immune-mediated cell death in atheromatous diseases. *Cardiovasc. Toxicol.* **3,** 269–82 (2003).

124. Opal, S. M. & DePalo, V. A. Anti-inflammatory cytokines. *Chest* **117,** 1162–1172 (2000).

125. World Health Organization. WHO | About diabetes. *World Health Organization* (2015).

126. Kitabchi, A.E., Umpierrez, G.E., Miles, J.M., Fisher, J. N. Hyperglycemic Crises in Adult Patients. *Diabetes Care* (2009). doi:10.2337/dc06-9916

127. WHO. Diabetes Programme. *World Heal. Organ.* (2018).

128. Yagihashi, S. & Mizukami, H. in *Diabetes and Aging-related Complications* (2017). doi:10.1007/978-981-10-4376-5_3

129. Simon, A. C. R. & DeVries, J. H. The effect of intensive treatment of diabetes on the development and progression of long-term complications in insulin-dependent diabetes mellitus. The Diabetes Control and Complications Trial Research Group. *N. Engl. J. Med.* (1993). doi:10.1056/NEJM199309303291401

130. Turner, R. Intensive blood-glucose control with sulphonylureas or insulin compared with conventional treatment and risk of complications in patients with type 2 diabetes (UKPDS 33). *Lancet* (1998). doi:10.1016/S0140-6736(98)07019-6

131. Vincent, A. M., Russell, J. W., Low, P. & Feldman, E. L. Oxidative stress in the pathogenesis of diabetic neuropathy. *Endocrine Reviews* (2004). doi:10.1210/er.2003-0019

132. Vincent, A. M., Callaghan, B. C., Smith, A. L. & Feldman, E. L. Diabetic neuropathy: Cellular mechanisms as therapeutic targets. *Nature Reviews Neurology* **7,** 573–583 (2011).

133. Obrosova, I. G. Increased Sorbitol Pathway Activity Generates Oxidative Stress in Tissue Sites for Diabetic Complications. *Antioxid. Redox Signal.* (2005). doi:10.1089/ars.2005.7.1543

134. Bierhaus, A. & Nawroth, P. P. Multiple levels of regulation determine the role of the receptor for AGE (RAGE) as common soil in inflammation, immune responses and diabetes mellitus and its complications. *Diabetologia* (2009). doi:10.1007/s00125-009-1458-9

135. Sugimoto, K., Yasujima, M. & Yagihashi, S. Role of advanced glycation end products in diabetic neuropathy. *Curr. Pharm. Des.* (2008).

136. Vincent, A. M. *et al.* Receptor for advanced glycation end products activation injures primary sensory neurons via oxidative stress. *Endocrinology* (2007). doi:10.1210/en.2006-0073

137. Wiggin, T. D. *et al.* Elevated triglycerides correlate with progression of diabetic neuropathy. *Diabetes* (2009). doi:10.2337/db08-1771

138. Vincent, A. M. *et al.* Dyslipidemia-induced neuropathy in mice: The role of oxLDL/LOX-1. *Diabetes* (2009). doi:10.2337/db09-0047

139. Nowicki, M. *et al.* Oxidized low-density lipoprotein (oxLDL)-induced cell death in dorsal root gangion cell cultures depends not on the lectin-like oxLDL receptor-1 but on the toll-like receptor-4. *J. Neurosci. Res.* (2010). doi:10.1002/jnr.22205

140. Kim, B., McLean, L. L., Philip, S. S. & Feldman, E. L. Hyperinsulinemia induces insulin resistance in dorsal root ganglion neurons. *Endocrinology* (2011). doi:10.1210/en.2011-0029

141. Kim, B. & Feldman, E. L. Insulin resistance in the nervous system. *Trends in Endocrinology and Metabolism* (2012). doi:10.1016/j.tem.2011.12.004

142. Tesch, G. H. Role of macrophages in complications of Type 2 diabetes. in *Clinical and Experimental Pharmacology and Physiology* (2007). doi:10.1111/j.1440-1681.2007.04729.x

143. King, G. L. The Role of Inflammatory Cytokines in Diabetes and Its Complications. *J. Periodontol.* (2008). doi:10.1902/jop.2008.080246

144. Li, F., Drel, V. R., Szabó, C., Stevens, M. J. & Obrosova, I. G. Low-dose poly(ADP-ribose) polymerase inhibitor-containing combination therapies reverse early peripheral diabetic neuropathy. *Diabetes* (2005). doi:10.2337/diabetes.54.5.1514

145. Wright, A. & Nukada, H. Sciatic nerve morphology and morphometry in mature rats with streptozocin-induced diabetes. *Acta Neuropathol.* (1994). doi:10.1007/BF00296495

146. Beiswenger, K. K., Calcutt, N. A. & Mizisin, A. P. Dissociation of thermal hypoalgesia and epidermal denervation in streptozotocin-diabetic mice. *Neurosci. Lett.* (2008). doi:10.1016/j.neulet.2008.06.079

147. Wang, Z. & Gleichmann, H. GLUT2 in pancreatic islets: Crucial target molecule in diabetes induced with multiple low doses of streptozotocin in mice. *Diabetes* (1998). doi:10.2337/diab.47.1.50

148. Bolzán, A. D. & Bianchi, M. S. Genotoxicity of Streptozotocin. *Mutation Research - Reviews in Mutation Research* (2002). doi:10.1016/S1383-5742(02)00044-3

149. Leiter, E. H. in *Current Protocols in Immunology* (2004). doi:10.1002/0471142735.im1509s24

150. Delovitch, T. L. & Singh, B. The nonobese diabetic mouse as a model of autoimmune diabetes: Immune dysregulation gets the NOD. *Immunity* (1997). doi:10.1016/S1074-7613(00)80392-1

151. Ize-Ludlow, D. *et al.* Progressive erosion of β-cell function precedes the onset of hyperglycemia in the NOD mouse model of type 1 diabetes. *Diabetes* (2011). doi:10.2337/db11-0373

152. Gabra, B. H. & Sirois, P. Hyperalgesia in non-obese diabetic (NOD) mice: A role for the inducible bradykinin B1 receptor. *Eur. J. Pharmacol.* (2005). doi:10.1016/j.ejphar.2005.03.018

153. Szabó, C. *et al.* Role for nitrosative stress in diabetic neuropathy: evidence from studies with a peroxynitrite decomposition catalyst. *FASEB J.* (2004). doi:10.1096/fj.04-1913fje

154. Yoshioka, M., Kayo, T., Ikeda, T. & Koizumi, A. A novel locus, Mody4, distal to D7Mit189 on chromosome 7 determines early-onset NIDDM in nonobese C57BL/6 (Akita) mutant mice. *Diabetes* (1997). doi:10.2337/diab.46.5.887

155. Choeiri, C. *et al.* Longitudinal evaluation of memory performance and peripheral neuropathy in the Ins2 C96Y Akita mice. *Behav. Brain Res.* (2005). doi:10.1016/j.bbr.2004.06.005

156. Sullivan, K. A. *et al.* Mouse Models of Diabetic Neuropathy. *Neurobiol. Dis.* **28,** 276–285 (2007).

157. Schmidt, R. E. *et al.* Effect of insulin and an erythropoietin-derived peptide (ARA290) on established neuritic dystrophy and neuronopathy in Akita (Ins2 Akita) diabetic mouse sympathetic ganglia. *Exp. Neurol.* (2011). doi:10.1016/j.expneurol.2011.05.025

158. O'brien, P. D., Sakowski, S. A. & Feldman, E. L. Mouse models of diabetic neuropathy. *ILAR J.* (2014). doi:10.1093/ilar/ilt052

159. Sima, A. A. F. & Robertson, D. M. Peripheral neuropathy in mutant diabetic mouse [C57BL/Ks (db/db)]. *Acta Neuropathol.* (1978). doi:10.1007/BF00689757

160. Ingalls, A. M., Dickie, M. M. & Snell, G. D. Obese, a new mutation in the house mouse. *J. Hered.* (1950). doi:10.1093/oxfordjournals.jhered.a106072

161. Cheng, H. T., Dauch, J. R., Hayes, J. M., Hong, Y. & Feldman, E. L. Nerve growth factor mediates mechanical allodynia in a mouse model of type 2 diabetes. *J. Neuropathol. Exp. Neurol.* (2009). doi:10.1097/NEN.0b013e3181bef710

162. Kan, M., Guo, G., Singh, B., Singh, V. & Zochodne, D. W. Glucagon-like peptide 1, insulin, sensory neurons, and diabetic neuropathy. *J. Neuropathol. Exp. Neurol.* (2012). doi:10.1097/NEN.0b013e3182580673

163. Wang, L. *et al.* Phosphodiesterase-5 is a therapeutic target for peripheral

neuropathy in diabetic mice. *Neuroscience* (2011). doi:10.1016/j.neuroscience.2011.07.039

164. Dauch, J. R., Yanik, B. M., Hsieh, W., Oh, S. S. & Cheng, H. T. Neuron-astrocyte signaling network in spinal cord dorsal horn mediates painful neuropathy of type 2 diabetes. *Glia* (2012). doi:10.1002/glia.22349

165. Drel, V. R. *et al.* The leptin-deficient (ob/ob) mouse: A new animal model of peripheral neuropathy of type 2 diabetes and obesity. *Diabetes* (2006). doi:10.2337/db06-0885

166. Coppey, L., Davidson, E., Lu, B., Gerard, C. & Yorek, M. Vasopeptidase inhibitor ilepatril (AVE7688) prevents obesity- and diabetes-induced neuropathy in C57Bl/6J mice. *Neuropharmacology* (2011). doi:10.1016/j.neuropharm.2010.09.008

167. Guilford, B. L., Ryals, J. M. & Wright, D. E. Phenotypic Changes in Diabetic Neuropathy Induced by a High-Fat Diet in Diabetic C57Bl/6 Mice. *Exp. Diabetes Res.* (2011). doi:10.1155/2011/848307

168. Obrosova, I. G. *et al.* High-fat diet-induced neuropathy of pre-diabetes and obesity: Effects of 'healthy' diet and aldose reductase inhibition. *Diabetes* (2007). doi:10.2337/db06-1176

169. Robinson Singleton, J., Gordon Smith, A. & Bromberg, M. B. Painful sensory polyneuropathy associated with impaired glucose tolerance. *Muscle and Nerve* (2001). doi:10.1002/mus.1136

170. Obrosova, I. G., Watcho, P., Stavniichuk, R., Ribnicky, D. M. & Raskin, I. High-fat diet-induced neuropathy of prediabetes and obesity: Effect of PMI-5011, an ethanolic extract of artemisia dracunculus L. *Mediators Inflamm.* (2010). doi:10.1155/2010/268547

171. Surwit, R. S. *et al.* Diet-induced changes in uncoupling proteins in obesity-prone and obesity-resistant strains of mice. *Proc. Natl. Acad. Sci. U. S. A.* (1998). doi:10.1073/pnas.95.7.4061

172. Centers for Disease Control and Prevention (CDC). At A Glance 2016 Diabetes. 1–4 (2016).

173. Gordois, A., Scuffham, P., Shearer, A., Oglesby, A. & Tobian, J. A. The health care costs of diabetic peripheral neuropathy in the US. *Diabetes Care* **26,** 1790–1795 (2003).

174. Edwards, J. L. *et al.* Diabetic neuropathy: mechanisms to management. *Pharmacol. Ther.* **120,** 1–34 (2008).

175. Galer, B. S., Gianas, A. & Jensen, M. P. Painful diabetic polyneuropathy: Epidemiology, pain description, and quality of life. *Diabetes Res. Clin. Pract.* **47,** 123–128 (2000).

176. Pande, M. *et al.* Transcriptional profiling of diabetic neuropathy in the BKS db/db mouse: A model of type 2 diabetes. *Diabetes* **60,** 1981–1989 (2011).

177. O'Brien, P. D. *et al.* BTBR ob/ob mice as a novel diabetic neuropathy model: Neurological characterization and gene expression analyses. *Neurobiol. Dis.* **73,** 348–55 (2015).

178. Hur, J. *et al.* The Metabolic Syndrome and Microvascular Complications in a Murine Model of Type 2 Diabetes. *Diabetes* **64,** 3294–304 (2015).

179. Ma, J., Pan, P., Anyika, M., Blagg, B. S. J. & Dobrowsky, R. T. Modulating

Molecular Chaperones Improves Mitochondrial Bioenergetics and Decreases the Inflammatory Transcriptome in Diabetic Sensory Neurons. *ACS Chem. Neurosci.* **6,** 1637–1648 (2015).

180. Wiggin, T. D. *et al.* Rosiglitazone treatment reduces diabetic neuropathy in streptozotocin- treated DBA/2J mice. *Endocrinology* **149,** 4928–4937 (2008).

181. Hur, J. *et al.* The identification of gene expression profiles associated with progression of human diabetic neuropathy. *Brain* **134,** 3222–35 (2011).

182. Hur, J., Sullivan, K. A., Callaghan, B. C., Pop-Busui, R. & Feldman, E. L. Identification of factors associated with sural nerve regeneration and degeneration in diabetic neuropathy. *Diabetes Care* **36,** 4043–4049 (2013).

183. Hinder, L. M. *et al.* Transcriptional networks of progressive diabetic peripheral neuropathy in the db/db mouse model of type 2 diabetes: An inflammatory story. *Exp. Neurol.* **305,** 33–43 (2018).

184. O'Brien, P. D. *et al.* Gender-specific differences in diabetic neuropathy in BTBR ob/ob mice. *J. Diabetes Complications* **30,** 30–37 (2016).

185. Hur, J., Schuyler, A. D., States, D. J. & Feldman, E. L. SciMiner: web-based literature mining tool for target identification and functional enrichment analysis. *Bioinformatics* **25,** 838–40 (2009).

186. Kohl, M., Wiese, S. & Warscheid, B. Cytoscape: software for visualization and analysis of biological networks. *Methods Mol. Biol.* **696,** 291–303 (2011).

187. Tian, Y. & Patel, J. M. TALE: A Tool for Approximate Large Graph Matching. in *2008 IEEE 24th International Conference on Data Engineering* 963–972 (IEEE, 2008). doi:10.1109/ICDE.2008.4497505

188. Hur, J. *et al.* Transcriptional networks of murine diabetic peripheral neuropathy and nephropathy: common and distinct gene expression patterns. *Diabetologia* **59,** 1297–1306 (2016).

189. Hodgin, J. B. *et al.* Identification of cross-species shared transcriptional networks of diabetic nephropathy in human and mouse glomeruli. *Diabetes* **62,** 299–308 (2013).

190. Hur, J. *et al.* Identification of fever and vaccine-associated gene interaction networks using ontology-based literature mining. *J. Biomed. Semantics* **3,** 18 (2012).

191. Hur, J., Özgür, A. & He, Y. Ontology-based literature mining of E. coli vaccine-associated gene interaction networks. *J. Biomed. Semantics* **8,** 12 (2017).

192. Biessels, G. J. *et al.* Phenotyping animal models of diabetic neuropathy: A consensus statement of the diabetic neuropathy study group of the EASD (Neurodiab). *Journal of the Peripheral Nervous System* **19,** 77–87 (2014).

193. Skundric, D. S., Dai, R., James, J. & Lisak, R. P. Activation of IL-1 signaling pathway in Schwann cells during diabetic neuropathy. *Ann. N. Y. Acad. Sci.* **958,** 393–398 (2002).

194. Skundric, D. S. & Lisak, R. P. Role of neuropoietic cytokines in development and progression of diabetic polyneuropathy: From glucose metabolism to neurodegeneration. *Experimental Diabesity Research* **4,**

303–312 (2003).

195. Subramanian, M., Ozcan, L., Ghorpade, D. S., Ferrante, A. W. & Tabas, I. Suppression of adaptive immune cell activation does not alter innate immune adipose inflammation or insulin resistance in obesity. *PLoS One* **10,** (2015).

196. Lumeng, C. N., Bodzin, J. L. & Saltiel, A. R. Obesity induces a phenotypic switch in adipose tissue macrophage polarization. *J. Clin. Invest.* **117,** 175–184 (2007).

197. Lee, J. T. *et al.* Macrophage metalloelastase (MMP12) regulates adipose tissue expansion, insulin sensitivity, and expression of inducible nitric oxide synthase. *Endocrinology* **155,** 3409–3420 (2014).

198. O'Brien, P. D. *et al.* Dual CCR2/CCR5 antagonist treatment attenuates adipose inflammation, but not microvascular complications in *ob/ob* mice. *Diabetes, Obes. Metab.* **19,** 1468–1472 (2017).

199. Hinder, L. M. *et al.* Comparative RNA-Seq transcriptome analyses reveal distinct metabolic pathways in diabetic nerve and kidney disease. *Journal of Cellular and Molecular Medicine* (2017). doi:10.1111/jcmm.13136

200. Bae, E. J. DPP-4 inhibitors in diabetic complications : role of DPP-4 beyond glucose control. *Arch. Pharm. Res.* **39,** 1114–1128 (2016).

201. Jin, H. Y., Liu, W. J., Park, J. H., Baek, H. S. & Park, T. S. Effect of dipeptidyl peptidase-IV (DPP-IV) inhibitor (Vildagliptin) on peripheral nerves in streptozotocin-induced diabetic rats. *Arch. Med. Res.* **40,** 536–44 (2009).

202. Bianchi, R. *et al.* Beneficial Effects of PKF275-055 , a Novel , Selective , Orally Bioavailable , Long-Acting Dipeptidyl Peptidase IV Inhibitor in Streptozotocin-Induced Diabetic Peripheral Neuropathy. **340,** 64–72 (2012).

203. Alexander, G. M., Schwartzman, R. J., Nukes, T. A., Grothusen, J. R. & Hooker, M. D. Beta 2-adrenergic agonist as adjunct therapy to levodopa in Parkinson's disease. *Neurology* **44,** 1511–3 (1994).

204. Ben-Jonathan, N. & Hnasko, R. Dopamine as a prolactin (PRL) inhibitor. *Endocr. Rev.* **22,** 724–763 (2001).

205. Manocha, G. D. *et al.* APP regulates microglial phenotype in a mouse model of alzheimer's disease. *J. Neurosci.* **36,** (2016).

206. Bohlin, L., Edler, D., Lancichinetti, A. & Rosvall, M. in *Measuring Scholarly Impact: Methods and Practice* (eds. Ding, Y., Rousseau, R. & Wolfram, D.) 3–34 (Springer International Publishing, 2014). doi:10.1007/978-3-319-10377-8_1

207. Kautzky-Willer, A., Harreiter, J. & Pacini, G. Sex and Gender Differences in Risk, Pathophysiology and Complications of Type 2 Diabetes Mellitus. *Endocr. Rev.* **37,** 278–316 (2016).

208. Huffman, J., Hoffmann, C. & Taylor, G. T. Integrating insulin-like growth factor 1 and sex hormones into neuroprotection: Implications for diabetes. *World J. Diabetes* **8,** 45–55 (2017).

209. Zhang, H.-H. *et al.* Promoted Interaction of Nuclear Factor-κB With Demethylated Purinergic P2X3 Receptor Gene Contributes to Neuropathic

Pain in Rats With Diabetes. *Diabetes* **64,** 4272–84 (2015).

210. Chowdhury, S. R. *et al.* Ciliary neurotrophic factor reverses aberrant mitochondrial bioenergetics through the JAK/STAT pathway in cultured sensory neurons derived from streptozotocin-induced diabetic rodents. *Cell. Mol. Neurobiol.* **34,** 643–649 (2014).

211. Brosius, F. C. & Alpers, C. E. New targets for treatment of diabetic nephropathy. *Curr. Opin. Nephrol. Hypertens.* **22,** 1 (2012).

212. Vincent, A. M., Calabek, B., Roberts, L. & Feldman, E. L. Biology of diabetic neuropathy. *Handb. Clin. Neurol.* **115,** 591–606 (2013).

213. Butterfield, T. A., Best, T. M. & Merrick, M. A. The dual roles of neutrophils and macrophages in inflammation: a critical balance between tissue damage and repair. *J. Athl. Train.* **41,** 457–65

214. London, A. *et al.* Neuroprotection and progenitor cell renewal in the injured adult murine retina requires healing monocyte-derived macrophages. *J. Exp. Med.* **208,** 23–39 (2011).

215. Murdock, B. J., Bender, D. E., Segal, B. M. & Feldman, E. L. The dual roles of immunity in ALS: Injury overrides protection. *Neurobiol. Dis.* **77,** 1–12 (2015).

216. Yanai, H., Ban, T. & Taniguchi, T. High-mobility group box family of proteins: ligand and sensor for innate immunity. *Trends Immunol.* **33,** 633–40 (2012).

217. Ramasamy, R., Yan, S. F. & Schmidt, A. M. Advanced glycation endproducts: from precursors to RAGE: round and round we go. *Amino Acids* **42,** 1151–1161 (2012).

218. Stern, D. M., Yan, S. D., Yan, S. F. & Schmidt, A. M. Receptor for advanced glycation endproducts (RAGE) and the complications of diabetes. *Ageing Res. Rev.* **1,** 1–15 (2002).

219. Gonçalves, N. P. *et al.* Schwann cell interactions with axons and microvessels in diabetic neuropathy. *Nat. Rev. Neurol.* **13,** 135–147 (2017).

220. Nguyen, M. T. A. *et al.* A subpopulation of macrophages infiltrates hypertrophic adipose tissue and is activated by free fatty acids via Toll-like receptors 2 and 4 and JNK-dependent pathways. *J. Biol. Chem.* **282,** 35279–92 (2007).

221. Szatmari, I., Rajnavolgyi, E. & Nagy, L. PPAR-γ, a lipid-activated transcription factor as a regulator of dendritic cell function. *Ann. N. Y. Acad. Sci.* **1088,** 207–218 (2006).

222. Joseph, S. B., Castrillo, A., Laffitte, B. A., Mangelsdorf, D. J. & Tontonoz, P. Reciprocal regulation of inflammation and lipid metabolism by liver X receptors. *Nat. Med.* **9,** 213–219 (2003).

223. Baranowski, M. Biological role of liver X receptors. *J. Physiol. Pharmacol.* **59 Suppl 7,** 31–55 (2008).

224. Laffitte, B. A. *et al.* Activation of liver X receptor improves glucose tolerance through coordinate regulation of glucose metabolism in liver and adipose tissue. *Proc. Natl. Acad. Sci. U. S. A.* **100,** 5419–24 (2003).

225. Cermenati, G. *et al.* Diabetes-induced myelin abnormalities are associated

with an altered lipid pattern: protective effects of LXR activation. *J. Lipid Res.* **53,** 300–10 (2012).

226. Patel, M. *et al.* Liver X receptors preserve renal glomerular integrity under normoglycaemia and in diabetes in mice. *Diabetologia* **57,** 435–46 (2014).

227. Hazra, S. *et al.* Liver X receptor modulates diabetic retinopathy outcome in a mouse model of streptozotocin-induced diabetes. *Diabetes* **61,** 3270–9 (2012).

228. He, Q. *et al.* Liver X receptor agonist treatment attenuates cardiac dysfunction in type 2 diabetic db/db mice. *Cardiovasc. Diabetol.* **13,** 149 (2014).

229. Wang, L. *et al.* Liver X receptors in the central nervous system: from lipid homeostasis to neuronal degeneration. *Proc. Natl. Acad. Sci. U. S. A.* **99,** 13878–13883 (2002).

230. Callaghan, B. C. B. C., Little, A. A. A. A., Feldman, E. L. E. L. & Hughes, R. A. A. R. A. Enhanced glucose control for preventing and treating diabetic neuropathy. *Cochrane database Syst. Rev.* **6,** CD007543 (2012).

231. CDC. National Diabetes Fact Sheet. *Centers Dis. Control Prev. U.S. Dep. Heal. Hum. Serv.* **CS217080A,** 1–12 (2011).

232. Tesfaye, S. *et al.* Prevalence of diabetic peripheral neuropathy and its relation to glycaemic control and potential risk factors: The EURODIAB IDDM complications study. *Diabetologia* **39,** 1377–1384 (1996).

233. Maser, R. E. *et al.* Epidemiological correlates of diabetic neuropathy. Report from Pittsburgh epidemiology of diabetes complications study. *Diabetes* **38,** 1456–1461 (1989).

234. Martin, C. L., Albers, J. W. & Pop-Busui, R. Neuropathy and related findings in the diabetes control and complications trial/epidemiology of diabetes interventions and complications study. *Diabetes Care* **37,** 31–38 (2014).

235. Pop-Busui, R. *et al.* Diabetic neuropathy: A position statement by the American diabetes association. *Diabetes Care* (2017). doi:10.2337/dc16-2042

236. Ziegler-Graham, K., MacKenzie, E., Ephraim, P., Travison, T. & Brookmeyer, R. Estimating the prevalence of limb loss in the United States: 2005 to 2050. *Arch. Phys. Med. Rehabil.* **89,** 422–9 (2008).

237. Tuttle, K. R. *et al.* Diabetic kidney disease: A report from an ADA consensus conference. *Diabetes Care* **37,** 2864–2883 (2014).

238. Lim, B. J., Yang, H. C. & Fogo, A. B. Animal models of regression/progression of kidney disease. *Drug Discov. Today Dis. Model.* **11,** 45–51 (2014).

239. Bolzán, A. D. & Bianchi, M. S. Genotoxicity of streptozotocin. *Mutat. Res. Mutat. Res.* **512,** 121–134 (2002).

240. Leiter, E. H. Multiple low-dose streptozotocin-induced hyperglycemia and insulitis in C57BL mice:Influence of inbred background, sex, and thymus. *Proc. Natl. Acad. Sci. U. S. A.* **79,** 630–634 (1982).

241. Wilson, G. L. & Leiter, E. H. Streptozotocin interactions with pancreatic beta cells and the induction of insulin-dependent diabetes. *Curr. Top.*

Microbiol. Immunol. **156,** 27–54 (1990).

242. Johnson, M. S., Ryals, J. M. & Wright, D. E. Early loss of peptidergic intraepidermal nerve fibers in an STZ-induced mouse model of insensate diabetic neuropathy. *Pain* **140,** 35–47 (2008).

243. McEvoy, R. C., Andersson, J., Sandler, S. & Hellerstrom, C. Multiple low-dose streptozotocin-induced diabetes in the mouse. Evidence for stimulation of a cytotoxic cellular immune response against an insulin-producing beta cell line. *J. Clin. Invest.* **74,** 715–722 (1984).

244. Vincent, A. M. *et al.* SOD2 protects neurons from injury in cell culture and animal models of diabetic neuropathy. *Exp. Neurol.* **208,** 216–227 (2007).

245. Hodgin, J. B. *et al.* Identification of cross-species shared transcriptional networks of diabetic nephropathy in human and mouse glomeruli. *Diabetes* **62,** 299–308 (2013).

246. Hur, J. *et al.* Transcriptional networks of murine diabetic peripheral neuropathy and nephropathy: common and distinct gene expression patterns. *Diabetologia* **59,** 1297–1306 (2016).

247. Hinder, L. M. *et al.* Comparative RNA-Seq transcriptome analyses reveal distinct metabolic pathways in diabetic nerve and kidney disease. *J. Cell. Mol. Med.* **21,** 2140–2152 (2017).

248. Brosius Laboratory. Determination of podocyte number and density in rodent glomeruli. *Anim. Model. Diabet. Complicat. Consort.*

249. Biessels GJ, van der Heide LP, Kamal A, Bleys RL, G. W. Ageing and diabetes: implications for brain function. *Eur. J. Pharmacol.* (2002).

250. Bolger, A. M., Lohse, M. & Usadel, B. Trimmomatic: A flexible trimmer for Illumina sequence data. *Bioinformatics* **30,** 2114–2120 (2014).

251. Andrews, S. FastQC: A quality control tool for high throughput sequence data. *Http://www.Bioinformatics.Babraham.Ac.Uk/Projects/Fastqc/* http://www.bioinformatics.babraham.ac.uk/projects/ (2010). doi:citeulike-article-id:11583827

252. Sirén, J., Välimäki, N. & Mäkinen, V. HISAT2 - Fast and sensitive alignment against general human population. *IEEE/ACM Trans. Comput. Biol. Bioinforma.* **11,** 375–388 (2014).

253. Liao, Y., Smyth, G. K. & Shi, W. FeatureCounts: An efficient general purpose program for assigning sequence reads to genomic features. *Bioinformatics* **30,** 923–930 (2014).

254. Love, M. I., Huber, W. & Anders, S. Moderated estimation of fold change and dispersion for RNA-seq data with DESeq2. *Genome Biol.* **15,** (2014).

255. Krämer, A., Green, J., Pollard, J. & Tugendreich, S. Causal analysis approaches in ingenuity pathway analysis. *Bioinformatics* **30,** 523–530 (2014).

256. Rosvall, M., Axelsson, D. & Bergstrom, C. T. The map equation. *Eur. Phys. J. Spec. Top.* **178,** 13–23 (2009).

257. Fotopoulos, V., Sanmartin, M. & Kanellis, A. K. Effect of ascorbate oxidase over-expression on ascorbate recycling gene expression in response to agents imposing oxidative stress. *J. Exp. Bot.* **57,** 3933–3943 (2006).

258. Mohammedi, K. *et al.* Glutathione peroxidase-1 gene (GPX1) variants,

oxidative stress and risk of kidney complications in people with type 1 diabetes. *Metabolism.* **65,** 12–19 (2016).

259. Unanue, E. R. & Cerottini, J. C. Antigen presentation. *FASEB J* **3,** 2496–2502 (1989).

260. Ichikawa, A. & Tanaka, S. Histamine biosynthesis and function. *Encycl. Life Sci.* 1–8 (2012). doi:10.1002/9780470015902.a0001404.pub2

261. Dyck, P. J. *et al.* The prevalence by staged severity of various types of diabetic neuropathy, retinopathy, and nephropathy in a population-based cohort: The rochester diabetic neuropathy study. *Neurology* **43,** 817–817 (1993).

262. Klein, R., Klein, B. E. K. & Moss, S. E. Prevalence of microalbuminuria in older-onset diabetes. *Diabetes Care* **16,** 1325–1330 (1993).

263. Sima, A. A. Pathological mechanisms involved in diabetic neuropathy: can we slow the process? *Curr Opin Investig Drugs* **7,** 324–337 (2006).

264. Sima, a a *et al.* A comparison of diabetic polyneuropathy in type II diabetic BBZDR/Wor rats and in type I diabetic BB/Wor rats. *Diabetologia* **43,** 786–93 (2000).

265. Sima, A. A. *et al.* Regeneration and repair of myelinated fibers in sural-nerve biopsy specimens from patients with diabetic neuropathy treated with sorbinil. *N. Engl. J. Med.* **319,** 548–55 (1988).

266. Sima, A. A. F., Nathaniel, V., Bril, V., McEwen, T. A. J. & Greene, D. A. Histopathological heterogeneity of neuropathy in insulin-dependent and non-insulin-dependent diabetes, and demonstration of axo-glial dysjunction in human diabetic neuropathy. *J. Clin. Invest.* **81,** 349–364 (1988).

267. Vincent, A. M., Brownlee, M. & Russel, J. W. Oxidative stress and programmed cell death in diabetic neuropathy. *Ann. N. Y. Acad. Sci.* **959,** 368–383 (2002).

268. Thomasova, D. & Anders, H.-J. Cell cycle control in the kidney. *Nephrol. Dial. Transplant* **30,** 1622–1630 (2015).

269. Canaud, G. & Bonventre, J. V. Cell cycle arrest and the evolution of chronic kidney disease from acute kidney injury. *Nephrology Dialysis Transplantation* **30,** 575–583 (2015).

270. Müller, S. *et al.* Impaired glucose tolerance is associated with increased serum concentrations of interleukin 6 and co-regulated acute-phase proteins but not TNF-alpha or its receptors. *Diabetologia* **45,** 805–812 (2002).

271. Festa, A. *et al.* Chronic subclinical inflammation as part of the insulin resistance syndrome: The insulin resistance atherosclerosis study (IRAS). *Circulation* **102,** 42–7 (2000).

272. Brownlee, M. The pathobiology of diabetic complications: A unifying mechanism. in *Diabetes* **54,** 1615–1625 (2005).

273. Dodson, P. M., Galton, D. J. & Winder, A. F. Retinal vascular abnormalities in the hyperlipidaemias. *Trans. Ophthalmol. Soc. U. K.* **101,** 17–21 (1981).

274. Kwon, E. Y. *et al.* Time-course microarrays reveal early activation of the immune transcriptome and adipokine dysregulation leads to fibrosis in visceral adipose depots during diet-induced obesity. *BMC Genomics* **13,**

(2012).

275. Gill, D. S., Barradas, M. A., Fonseca, V. A. & Dandona, P. Plasma histamine concentrations are elevated in patients with diabetes mellitus and peripheral vascular disease. *Metabolism.* **38,** 243–7 (1989).

276. Bitar, M. S., Bajic, K. T., Farook, T., Thomas, M. I. & Pilcher, C. W. T. Spinal cord noradrenergic dynamics in diabetic and hypercortisolaemic states. *Brain Res.* **830,** 1–9 (1999).

277. Park, S.-W. *et al.* Thiazolidinedione class of peroxisome proliferator-activated receptor gamma agonists prevents neuronal damage, motor dysfunction, myelin loss, neuropathic pain, and inflammation after spinal cord injury in adult rats. *J. Pharmacol. Exp. Ther.* **320,** 1002–12 (2007).

278. Ko, G. J. *et al.* Pioglitazone attenuates diabetic nephropathy through an anti-inflammatory mechanism in type 2 diabetic rats. *Nephrol. Dial. Transplant.* **23,** 2750–2760 (2008).

279. Betteridge, D. J. Effects of pioglitazone on lipid and lipoprotein metabolism. *Diabetes. Obes. Metab.* **9,** 640–647 (2007).

280. Goldberg, R. B. *et al.* A comparison of lipid and glycemic effects of pioglitazone and rosiglitazone in patients with type 2 diabetes and dyslipidemia. *Diabetes Care* **28,** 1547–1554 (2005).

281. Lashuel, H. A., Overk, C. R., Oueslati, A. & Masliah, E. The many faces of α-synuclein: From structure and toxicity to therapeutic target. *Nature Reviews Neuroscience* (2013). doi:10.1038/nrn3406

282. Zhang, Q. S., Heng, Y., Yuan, Y. H. & Chen, N. H. Pathological α-synuclein exacerbates the progression of Parkinson's disease through microglial activation. *Toxicology Letters* (2017). doi:10.1016/j.toxlet.2016.11.002

283. Ammal Kaidery, N., Tarannum, S. & Thomas, B. Epigenetic Landscape of Parkinson's Disease: Emerging Role in Disease Mechanisms and Therapeutic Modalities. *Neurotherapeutics* (2013). doi:10.1007/s13311-013-0211-8

284. Doxakis, E. Post-transcriptional regulation of α-synuclein expression by mir-7 and mir-153. *J. Biol. Chem.* (2010). doi:10.1074/jbc.M109.086827

285. Kabaria, S., Choi, D. C., Chaudhuri, A. D., Mouradian, M. M. & Junn, E. Inhibition of miR-34b and miR-34c enhances α-synuclein expression in Parkinson's disease. *FEBS Lett.* (2015). doi:10.1016/j.febslet.2014.12.014

286. Villar-Menéndez, I. *et al.* Increased striatal adenosine A2A receptor levels is an early event in Parkinson's disease-related pathology and it is potentially regulated by miR-34b. *Neurobiol. Dis.* (2014). doi:10.1016/j.nbd.2014.05.030

287. Paolicelli, R. C. *et al.* Synaptic pruning by microglia is necessary for normal brain development. *Science (80-.).* (2011). doi:10.1126/science.1202529

288. Perry, V. H., Nicoll, J. A. R. & Holmes, C. Microglia in neurodegenerative disease. *Nature Reviews Neurology* (2010). doi:10.1038/nrneurol.2010.17

289. Aloisi, F. Immune function of microglia. *Glia* (2001). doi:10.1002/glia.1106

290. Nayak, D., Roth, T. L. & McGavern, D. B. Microglia Development and Function. *Annu. Rev. Immunol.* (2014). doi:10.1146/annurev-immunol-032713-120240

291. Halliday, G. M., Leverenz, J. B., Schneider, J. S. & Adler, C. H. The neurobiological basis of cognitive impairment in Parkinson's disease. *Movement Disorders* (2014). doi:10.1002/mds.25857

292. Spillantini, M. G., Crowther, R. A., Jakes, R., Hasegawa, M. & Goedert, M. alpha-Synuclein in filamentous inclusions of Lewy bodies from Parkinson's disease and dementia with lewy bodies. *Proc. Natl. Acad. Sci. U. S. A.* (1998). doi:10.1073/pnas.95.11.6469

293. Maroteaux, L., Campanelli, J. & Scheller, R. Synuclein: a neuron-specific protein localized to the nucleus and presynaptic nerve terminal. *J. Neurosci.* (2018). doi:10.1523/jneurosci.08-08-02804.1988

294. Withers, G. S., George, J. M., Banker, G. A. & Clayton, D. F. Delayed localization of synelfin (synuclein, NACP) to presynaptic terminals in cultured rat hippocampal neurons. *Dev. Brain Res.* (1997). doi:10.1016/S0165-3806(96)00210-6

295. Zhang, L. *et al.* Semi-quantitative analysis of α-synuclein in subcellular pools of rat brain neurons: An immunogold electron microscopic study using a C-terminal specific monoclonal antibody. *Brain Res.* (2008). doi:10.1016/j.brainres.2008.08.067

296. Goers, J. *et al.* Nuclear localization of α-synuclein and its interaction with histones. *Biochemistry* (2003). doi:10.1021/bi0341152

297. Liu, X. *et al.* Alpha-synuclein functions in the nucleus to protect against hydroxyurea-induced replication stress in yeast. *Hum. Mol. Genet.* (2011). doi:10.1093/hmg/ddr246

298. Bendor, J. T., Logan, T. P. & Edwards, R. H. The function of α-synuclein. *Neuron* (2013). doi:10.1016/j.neuron.2013.09.004

299. Vargas, K. J. *et al.* Synucleins Regulate the Kinetics of Synaptic Vesicle Endocytosis. *J. Neurosci.* (2014). doi:10.1523/JNEUROSCI.4787-13.2014

300. Desplats, P. *et al.* α-Synuclein induces alterations in adult neurogenesis in Parkinson disease models via p53-mediated repression of notch. *J. Biol. Chem.* (2012). doi:10.1074/jbc.M112.354522

301. Siddiqui, A. *et al.* Selective binding of nuclear alpha-synuclein to the PGC1alpha promoter under conditions of oxidative stress may contribute to losses in mitochondrial function: Implications for Parkinson's disease. *Free Radic. Biol. Med.* (2012). doi:10.1016/j.freeradbiomed.2012.05.024

302. Kontopoulos, E., Parvin, J. D. & Feany, M. B. α-synuclein acts in the nucleus to inhibit histone acetylation and promote neurotoxicity. *Hum. Mol. Genet.* (2006). doi:10.1093/hmg/ddl243

303. Desplats, P. *et al.* α-synuclein sequesters Dnmt1 from the nucleus: A novel mechanism for epigenetic alterations in Lewy body diseases. *J. Biol. Chem.* (2011). doi:10.1074/jbc.C110.212589

304. Matsumoto, L. *et al.* CpG demethylation enhances alpha-synuclein expression and affects the pathogenesis of Parkinson's disease. *PLoS One* (2010). doi:10.1371/journal.pone.0015522

305. Tagliafierro, L. & Chiba-Falek, O. Up-regulation of SNCA gene expression: implications to synucleinopathies. *Neurogenetics* (2016). doi:10.1007/s10048-016-0478-0

306. Karube, H. *et al.* N-terminal region of α-synuclein is essential for the fatty acid-induced oligomerization of the molecules. *FEBS Lett.* (2008). doi:10.1016/j.febslet.2008.10.001

307. Perrin, R. J., Woods, W. S., Clayton, D. F. & George, J. M. Exposure to Long Chain Polyunsaturated Fatty Acids Triggers Rapid Multimerization of Synucleins. *J. Biol. Chem.* (2001). doi:10.1074/jbc.M105022200

308. Sharon, R. *et al.* The formation of highly soluble oligomers of α-synuclein is regulated by fatty acids and enhanced in Parkinson's disease. *Neuron* (2003). doi:10.1016/S0896-6273(03)00024-2

309. Pletnikova, O. *et al.* Aggregation promoting C-terminal truncation of -synuclein is a normal cellular process and is enhanced by the familial Parkinson's disease-linked mutations. *Proc. Natl. Acad. Sci.* (2005). doi:10.1073/pnas.0406976102

310. Dufty, B. M. *et al.* Calpain-cleavage of α-synuclein: Connecting proteolytic processing to disease-linked aggregation. *Am. J. Pathol.* (2007). doi:10.2353/ajpath.2007.061232

311. Hashimoto, M. *et al.* Oxidative stress induces amyloid-like aggregate formation of NACP/α- synuclein in vitro. *Neuroreport* (1999). doi:10.1097/00001756-199903170-00011

312. Andringa, G. *et al.* Tissue transglutaminase catalyzes the formation of alpha-synuclein crosslinks in Parkinson's disease. *FASEB J.* (2004).

313. Fauvet, B. *et al.* α-Synuclein in central nervous system and from erythrocytes, mammalian cells, and Escherichia coli exists predominantly as disordered monomer. *J. Biol. Chem.* (2012). doi:10.1074/jbc.M111.318949

314. Garcia-Reitböck, P. *et al.* SNARE protein redistribution and synaptic failure in a transgenic mouse model of Parkinson's disease. *Brain* (2010). doi:10.1093/brain/awq132

315. Schulz-Schaeffer, W. J. The synaptic pathology of α-synuclein aggregation in dementia with Lewy bodies, Parkinson's disease and Parkinson's disease dementia. *Acta Neuropathologica* (2010). doi:10.1007/s00401-010-0711-0

316. Bellucci, A., Navarria, L., Zaltieri, M., Missale, C. & Spano, P. Alpha-synuclein synaptic pathology and its implications in the development of novel therapeutic approaches to cure Parkinson's disease. *Brain Research* (2012). doi:10.1016/j.brainres.2011.11.031

317. Lundblad, M., Decressac, M., Mattsson, B. & Bjorklund, A. Impaired neurotransmission caused by overexpression of alpha-synuclein in nigral dopamine neurons. *Proc. Natl. Acad. Sci.* (2012). doi:10.1073/pnas.1200575109

318. Nemani, V. M. *et al.* Increased Expression of α-Synuclein Reduces Neurotransmitter Release by Inhibiting Synaptic Vesicle Reclustering after Endocytosis. *Neuron* (2010). doi:10.1016/j.neuron.2009.12.023

319. Roy, S. *et al.* A Pathologic Cascade Leading to Synaptic Dysfunction in Alpha-Synuclein-Induced Neurodegeneration. *J. Neurosci.* (2010). doi:10.1523/jneurosci.1091-10.2010

320. Conway, K. A. *et al.* Acceleration of oligomerization, not fibrillization, is a shared property of both α-synuclein mutations linked to early-onset Parkinson's disease: Implications for pathogenesis and therapy. *Proc. Natl. Acad. Sci.* (2000). doi:10.1073/pnas.97.2.571

321. Conway, K. A., Harper, J. D. & Lansbury, P. T. Accelerated in vitro fibril formation by a mutant α-synuclein linked to early-onset Parkinson disease. *Nat. Med.* (1998). doi:10.1038/3311

322. Keller, M. F. *et al.* Using genome-wide complex trait analysis to quantify 'missing heritability' in Parkinson's disease. *Hum. Mol. Genet.* (2012). doi:10.1093/hmg/dds335

323. Tsigelny, I. F. *et al.* Role of α-synuclein penetration into the membrane in the mechanisms of oligomer pore formation. *FEBS J.* (2012). doi:10.1111/j.1742-4658.2012.08489.x

324. Kahle, P. J. *et al.* Subcellular Localization of Wild-Type and Parkinson's Disease-Associated Mutant α-Synuclein in Human and Transgenic Mouse Brain. *J. Neurosci.* (2000). doi:10.1523/JNEUROSCI.20-17-06365.2000

325. Tsigelny, I. F. *et al.* Mechanisms of hybrid oligomer formation in the pathogenesis of combined Alzheimer's and Parkinson's diseases. *PLoS One* (2008). doi:10.1371/journal.pone.0003135

326. Pradhan, S. & Andreasson, K. Commentary: Progressive inflammation as a contributing factor to early development of Parkinson's disease. *Experimental Neurology* (2013). doi:10.1016/j.expneurol.2012.12.008

327. Mahad, D. J. & Ransohoff, R. M. The role of MCP-1 (CCL2) and CCR2 in multiple sclerosis and experimental autoimmune encephalomyelitis (EAE). *Seminars in Immunology* (2003). doi:10.1016/S1044-5323(02)00125-2

328. Kawanokuchi, J. *et al.* Production of interferon-γ by microglia. *Mult. Scler.* (2006). doi:10.1177/1352458506070763

329. Loane, D. J. & Byrnes, K. R. Role of Microglia in Neurotrauma. *Neurotherapeutics* (2010). doi:10.1016/j.nurt.2010.07.002

330. Benarroch, E. E. Microglia: Multiple roles in surveillance, circuit shaping, and response to injury. *Neurology* (2013). doi:10.1212/WNL.0b013e3182a4a577

331. Nakagawa, Y. & Chiba, K. Diversity and plasticity of microglial cells in psychiatric and neurological disorders. *Pharmacology and Therapeutics* (2015). doi:10.1016/j.pharmthera.2015.06.010

332. Morgan, D., Gordon, M. N., Tan, J., Wilcock, D. & Rojiani, A. M. Dynamic complexity of the microglial activation response in transgenic models of amyloid deposition: Implications for Alzheimer therapeutics. *Journal of Neuropathology and Experimental Neurology* (2005). doi:10.1097/01.jnen.0000178444.33972.e0

333. Herber, D. L. *et al.* Diverse microglial responses after intrahippocampal administration of lipopolysaccharide. *Glia* (2006). doi:10.1002/glia.20272

334. Schwartz, M., Butovsky, O., Brück, W. & Hanisch, U. K. Microglial phenotype: Is the commitment reversible? *Trends Neurosci.* (2006). doi:10.1016/j.tins.2005.12.005

335. Becker, C., Jick, S. S. & Meier, C. R. NSAID use and risk of Parkinson

disease: A population-based case-control study. *Eur. J. Neurol.* (2011). doi:10.1111/j.1468-1331.2011.03399.x

336. Bornebroek, M. *et al.* Nonsteroidal anti-inflammatory drugs and the risk of Parkinson disease. *Neuroepidemiology* (2007). doi:10.1159/000108110

337. Gao, X., Chen, H., Schwarzschild, M. A. & Ascherio, A. Use of ibuprofen and risk of Parkinson disease. *Neurology* (2011). doi:10.1212/WNL.0b013e31820f2d79

338. Samii, A., Etminan, M., Wiens, M. O. & Jafari, S. NSAID use and the risk of parkinsons disease: Systematic review and meta-analysis of observational studies. *Drugs and Aging* (2009). doi:10.2165/11316780-000000000-00000

339. Shaunak, S., Brown, P. S. & Morgan-Hughes, J. A. Exacerbation of idiopathic Parkinson's disease by naproxen. *BMJ* (1995). doi:10.1136/bmj.311.7002.422b

340. Świątkiewicz, M., Zaremba, M., Joniec, I., Czonkowski, A. & Kurkowska-Jastrzêbska, I. Potential neuroprotective effect of ibuprofen, insights from the mice model of Parkinson's disease. *Pharmacol. Reports* (2013). doi:10.1016/S1734-1140(13)71480-4

341. Wahner, A. D., Bronstein, J. M., Bordelon, Y. M. & Ritz, B. Nonsteroidal anti-inflammatory drugs may protect against Parkinson disease. *Neurology* (2007). doi:10.1212/01.wnl.0000279519.99344.ad

342. Gagne, J. J. & Power, M. C. Anti-inflammatory drugs and risk of Parkinson disease: A meta-analysis. *Neurology* (2010). doi:10.1212/WNL.0b013e3181d5a4a3

343. Committee for the Update of the Guide for the Care and Use of Laboratory Animals; National Research Council. *Guide for the Care and Use of Laboratory Animals: Eighth Edition. Guide for the Care and Use of Laboratory Animals* (2010). doi:10.2307/1525495

344. Lee, J. K. & Tansey, M. G. Microglia isolation from adult mouse brain. *Methods Mol. Biol.* **1041,** 17–23 (2013).

345. Qiagen. AllPrep® DNA/RNA/Protein Mini Handbook. (2007). at <http://scholar.google.com/scholar?hl=en&btnG=Search&q=intitle:AllPrep+®+DNA/RNA/Protein+Mini+Handbook#0>

346. Garrett-Bakelman, F. E. *et al.* Enhanced Reduced Representation Bisulfite Sequencing for Assessment of DNA Methylation at Base Pair Resolution. *J. Vis. Exp.* (2015). doi:10.3791/52246

347. Krueger, F. Trim Galore!: A wrapper tool around Cutadapt and FastQC to consistently apply quality and adapter trimming to FastQ files. *Babraham Institute* (2015). doi:10.1002/maco.200603986

348. Krueger, F. & Andrews, S. R. Bismark: A flexible aligner and methylation caller for Bisulfite-Seq applications. *Bioinformatics* **27,** 1571–1572 (2011).

349. Langmead and Steven L Salzberg. Bowtie2. *Nat. Methods* (2013). doi:10.1038/nmeth.1923.Fast

350. Akalin, A. *et al.* MethylKit: a comprehensive R package for the analysis of genome-wide DNA methylation profiles. *Genome Biol.* (2012). doi:10.1186/gb-2012-13-10-R87

351. Akalin, A., Franke, V., Vlahoviček, K., Mason, C. E. & Schübeler, D.

Genomation: A toolkit to summarize, annotate and visualize genomic intervals. *Bioinformatics* (2015). doi:10.1093/bioinformatics/btu775

352. Zerbino, D. R. *et al.* Ensembl 2018. *Nucleic Acids Res.* (2018). doi:10.1093/nar/gkx1098

353. Maglott, D., Ostell, J., Pruitt, K. D. & Tatusova, T. Entrez gene: Gene-centered information at NCBI. *Nucleic Acids Res.* (2011). doi:10.1093/nar/gkq1237

354. Mi, H. *et al.* PANTHER version 11: Expanded annotation data from Gene Ontology and Reactome pathways, and data analysis tool enhancements. *Nucleic Acids Res.* (2017). doi:10.1093/nar/gkw1138

355. Ogata, H. *et al.* KEGG: Kyoto encyclopedia of genes and genomes. *Nucleic Acids Research* (1999). doi:10.1093/nar/27.1.29

356. Kanehisa, M., Furumichi, M., Tanabe, M., Sato, Y. & Morishima, K. KEGG : new perspectives on genomes , pathways , diseases and drugs. **45,** 353–361 (2017).

357. Fabregat, A. *et al.* The Reactome Pathway Knowledgebase. *Nucleic Acids Res.* (2018). doi:10.1093/nar/gkx1132

358. Fabregat, A. *et al.* Reactome pathway analysis: A high-performance in-memory approach. *BMC Bioinformatics* (2017). doi:10.1186/s12859-017-1559-2

359. Shannon, P. *et al.* Cytoscape: A software Environment for integrated models of biomolecular interaction networks. *Genome Res.* (2003). doi:10.1101/gr.1239303

360. Lam, H. A. *et al.* Elevated tonic extracellular dopamine concentration and altered dopamine modulation of synaptic activity precede dopamine loss in the striatum of mice overexpressing human α-synuclein. *J. Neurosci. Res.* (2011). doi:10.1002/jnr.22611

361. Fleming, S. M. *et al.* Behavioral effects of dopaminergic agonists in transgenic mice overexpressing human wildtype α-synuclein. *Neuroscience* **142,** 1245–1253 (2006).

362. Edgar, R., Tan, P. P. C., Portales-Casamar, E. & Pavlidis, P. Meta-analysis of human methylomes reveals stably methylated sequences surrounding CpG islands associated with high gene expression. *Epigenetics and Chromatin* (2014). doi:10.1186/1756-8935-7-28

363. Deaton, A. M. & Bird, A. CpG islands and the regulation of transcription. *Genes Dev.* (2011). doi:10.1101/gad.2037511

364. Hannink, M. & Donoghue, D. J. Structure and function of platelet-derived growth factor (PDGF) and related proteins. *BBA - Reviews on Cancer* (1989). doi:10.1016/0304-419X(89)90031-0

365. Robinson, D. R., Wu, Y. M. & Lin, S. F. The protein tyrosine kinase family of the human genome. *Oncogene* (2000). doi:10.1038/sj.onc.1203957

366. Östman, A. & Heldin, C. H. in *Molecular Oncology: Causes of Cancer and Targets for Treatment* (2015). doi:10.1017/CBO9781139046947.014

367. Kim, Y. S. & Joh, T. H. Microglia, major player in the brain inflammation: Their roles in the pathogenesis of Parkinson's disease. *Experimental and Molecular Medicine* (2006). doi:10.1038/emm.2006.40

368. Weinhard, L. *et al.* Microglia remodel synapses by presynaptic trogocytosis and spine head filopodia induction. *Nat. Commun.* (2018). doi:10.1038/s41467-018-03566-5

369. Gomez-Nicola, D., Fransen, N. L., Suzzi, S. & Perry, V. H. Regulation of Microglial Proliferation during Chronic Neurodegeneration. *J. Neurosci.* (2013). doi:10.1523/jneurosci.4440-12.2013

370. Martinelli, P. & Rugarli, E. I. Emerging roles of mitochondrial proteases in neurodegeneration. *Biochimica et Biophysica Acta - Bioenergetics* (2010). doi:10.1016/j.bbabio.2009.07.013

371. Abou-Sleiman, P. M., Muqit, M. M. K. & Wood, N. W. Expanding insights of mitochondrial dysfunction in Parkinson's disease. *Nature Reviews Neuroscience* (2006). doi:10.1038/nrn1868

372. López-Armada, M. J., Riveiro-Naveira, R. R., Vaamonde-García, C. & Valcárcel-Ares, M. N. Mitochondrial dysfunction and the inflammatory response. *Mitochondrion* (2013). doi:10.1016/j.mito.2013.01.003

373. Ordonez, D. G., Lee, M. K. & Feany, M. B. α-synuclein Induces Mitochondrial Dysfunction through Spectrin and the Actin Cytoskeleton. *Neuron* (2018). doi:10.1016/j.neuron.2017.11.036

374. Rocha, E. M., De Miranda, B. & Sanders, L. H. Alpha-synuclein: Pathology, mitochondrial dysfunction and neuroinflammation in Parkinson's disease. *Neurobiology of Disease* (2018). doi:10.1016/j.nbd.2017.04.004

375. Yoshio, T. & Okamoto, H. in *Neuropsychiatric Systemic Lupus Erythematosus: Pathogenesis, Clinical Aspects and Treatment* (2018). doi:10.1007/978-3-319-76496-2_6

376. Xavier-Elsas, P., Masid-de-Brito, D., Vieira, B. M. & Gaspar-Elsas, M. I. C. Odd couple: The unexpected partnership of glucocorticoid hormones and cysteinyl-leukotrienes in the extrinsic regulation of murine bone-marrow eosinopoiesis. *World J. Exp. Med.* (2017). doi:10.5493/wjem.v7.i1.11

377. Zhang, C. *et al.* Eosinophil-derived CCL-6 impairs hematopoietic stem cell homeostasis. *Cell Res.* (2018). doi:10.1038/cr.2018.2

378. Nesi, R. T. *et al.* Pharmacological modulation of reactive oxygen species (ROS) improves the airway hyperresponsiveness by shifting the Th1 response in allergic inflammation induced by ovalbumin. *Free Radic. Res.* (2017). doi:10.1080/10715762.2017.1364377

379. Magalhaes, G. S. *et al.* Angiotensin-(1-7) promotes resolution of eosinophilic inflammation in an experimental model of asthma. *Front. Immunol.* (2018). doi:10.3389/fimmu.2018.00058

380. Chapman, H. A., Riese, R. J. & Shi, G.-P. EMERGING ROLES FOR CYSTEINE PROTEASES IN HUMAN BIOLOGY. *Annu. Rev. Physiol.* (2002). doi:10.1146/annurev.physiol.59.1.63

381. Shebl, F. M. *et al.* Comparison of mRNA and protein measures of cytokines following vaccination with human papillomavirus-16 L1 virus-like particles. *Cancer Epidemiol. Biomarkers Prev.* (2010). doi:10.1158/1055-9965.EPI-10-0064

382. Mestas, J. & Hughes, C. C. W. Of Mice and Not Men: Differences between Mouse and Human Immunology. *J. Immunol.* (2014).

doi:10.4049/jimmunol.172.5.2731

383. Pande, M. *et al.* Transcriptional profiling of diabetic neuropathy in the BKS db/db mouse: A model of type 2 diabetes. *Diabetes* **60,** 1981–1989 (2011).

384. Hur, J. *et al.* The identification of gene expression profiles associated with progression of human diabetic neuropathy. *Brain* **134,** 3222–3235 (2011).

385. Hur, J. *et al.* The Metabolic Syndrome and Microvascular Complications in a Murine Model of Type 2 Diabetes. *Diabetes* (2015). doi:10.2337/db15-0133

386. Zhou, J. Y., Zhang, Z. & Qian, G. S. Mesenchymal stem cells to treat diabetic neuropathy: a long and strenuous way from bench to the clinic. *Cell Death Discov.* (2018). doi:10.1038/cddiscovery.2016.55

387. Mooradian, A. D. Dyslipidemia in type 2 diabetes mellitus. *Nature Clinical Practice Endocrinology and Metabolism* (2009). doi:10.1038/ncpendmet1066

388. Hur, J. *et al.* Transcriptional networks of murine diabetic peripheral neuropathy and nephropathy: common and distinct gene expression patterns. *Diabetologia* **59,** 1297–1306 (2016).

389. Domingueti, C. P. *et al.* Diabetes mellitus: The linkage between oxidative stress, inflammation, hypercoagulability and vascular complications. *Journal of Diabetes and its Complications* (2016). doi:10.1016/j.jdiacomp.2015.12.018

390. Taylor, C. T. & Colgan, S. P. Regulation of immunity and inflammation by hypoxia in immunological niches. *Nature Reviews Immunology* (2017). doi:10.1038/nri.2017.103

391. Mittal, M., Siddiqui, M. R., Tran, K., Reddy, S. P. & Malik, A. B. Reactive Oxygen Species in Inflammation and Tissue Injury. *Antioxid. Redox Signal.* (2014). doi:10.1089/ars.2012.5149

392. Klein, J. A. & Ackerman, S. L. Oxidative stress, cell cycle, and neurodegeneration. *J. Clin. Invest.* (2003). doi:10.1172/JCI18182

393. Holmes, C. *et al.* Systemic inflammation and disease progression in alzheimer disease. *Neurology* (2009). doi:10.1212/WNL.0b013e3181b6bb95

394. Exton, M. S. Infection-induced anorexia: Active host defence strategy. *Appetite* (1997). doi:10.1006/appe.1997.0116

395. Hart, B. L. Biological basis of the behavior of sick animals. *Neurosci. Biobehav. Rev.* (1988). doi:10.1016/S0149-7634(88)80004-6

396. Perry, V. H., Cunningham, C. & Boche, D. Atypical inflammation in the central nervous system in prion disease. *Current Opinion in Neurology* (2002). doi:10.1097/00019052-200206000-00020

397. Rankine, E. L., Hughes, P. M., Botham, M. S., Perry, V. H. & Felton, L. M. Brain cytokine synthesis induced by an intraparenchymal injection of LPS is reduced in MCP-1-deficient mice prior to leucocyte recruitment. *Eur. J. Neurosci.* (2006). doi:10.1111/j.1460-9568.2006.04891.x

398. Duncan, B. B. *et al.* Low-grade systemic inflammation and the development of type 2 diabetes: The atherosclerosis risk in communities study. *Diabetes* (2003). doi:10.2337/diabetes.52.7.1799

399. Hinder, L. M. *et al.* Transcriptional networks of progressive diabetic peripheral neuropathy in the db/db mouse model of type 2 diabetes: An inflammatory story. *Exp. Neurol.* **305,** 33–43 (2018).

400. Bongarzone, S., Savickas, V., Luzi, F. & Gee, A. D. Targeting the Receptor for Advanced Glycation Endproducts (RAGE): A Medicinal Chemistry Perspective. *J. Med. Chem.* **60,** 7213–7232 (2017).

401. Renee, M. *et al.* CSF1 receptor signaling is necessary for microglia viability, which unmasks a cell that rapidly repopulates the microglia-depleted adult brain. *Neuron* (2015). doi:10.1016/j.neuron.2014.02.040.CSF1

402. Rice, R. A. *et al.* Elimination of Microglia Improves Functional Outcomes Following Extensive Neuronal Loss in the Hippocampus. *J. Neurosci.* (2015). doi:10.1523/jneurosci.0336-15.2015

403. Gerber, Y. N. *et al.* CSF1R inhibition reduces microglia proliferation, promotes tissue preservation and improves motor recovery after spinal cord injury. *Front. Cell. Neurosci.* (2018). doi:10.3389/fncel.2018.00368

404. Toth, C. *et al.* Levodopa, methylmalonic acid, and neuropathy in idiopathic Parkinson disease. *Ann. Neurol.* (2010). doi:10.1002/ana.22021

405. Ferrari, C. C. & Tarelli, R. Parkinson's Disease and Systemic Inflammation. *Parkinsons. Dis.* (2011). doi:10.4061/2011/436813